
Two-Loop Corrections to Higgs Boson
Masses in the NMSSM

Zur Erlangung des akademischen Grades eines
DOKTORS DER NATURWISSENSCHAFTEN

von der KIT-Fakultät für Physik
des Karlsruher Instituts für Technologie (KIT)

genehmigte

DISSERTATION

von

M.Sc. Martin Gabelmann

aus Malsch

Referentin: Prof. Dr. M. M. Mühlleitner

Korreferent: Prof. Dr. D. Zeppenfeld

Tag der mündlichen Prüfung: 22. Oktober 2021



This document is licensed under a Creative Commons Attribution-ShareAlike 4.0 International License (CC BY-SA 4.0):

<https://creativecommons.org/licenses/by-sa/4.0/deed.en>

Eidesstattliche Versicherung gemäß § 13 Absatz 2 Ziffer 3 der Promotionsordnung des Karlsruher Instituts für Technologie (KIT) für die KIT-Fakultät für Physik:

1. Bei der eingereichten Dissertation zu dem Thema

Two-Loop Corrections to Higgs Boson Masses in the NMSSM

handelt es sich um meine eigenständig erbrachte Leistung.

2. Ich habe nur die angegebenen Quellen und Hilfsmittel benutzt und mich keiner unzulässigen Hilfe Dritter bedient. Insbesondere habe ich wörtlich oder sinngemäß aus anderen Werken übernommene Inhalte als solche kenntlich gemacht.
3. Die Arbeit oder Teile davon habe ich bislang nicht an einer Hochschule des In- oder Auslands als Bestandteil einer Prüfungs- oder Qualifikationsleistung vorgelegt.
4. Die Richtigkeit der vorstehenden Erklärungen bestätige ich.
5. Die Bedeutung der eidesstattlichen Versicherung und die strafrechtlichen Folgen einer unrichtigen oder unvollständigen eidesstattlichen Versicherung sind mir bekannt.

Ich versichere an Eides statt, dass ich nach bestem Wissen die reine Wahrheit erklärt und nichts verschwiegen habe.

Karlsruhe, den 6. Oktober 2021

.....
(Martin Gabelmann)

Abstract

We compute the quantum corrections to Higgs boson masses in the charge-parity violating Next-to-Minimal Supersymmetric Standard Model at second order in perturbation theory. The emphasis is on corrections that are specific to this model and not present in the Minimal Supersymmetric Standard Model. These corrections are interesting for two major reasons. First, they can considerably impact the mass spectrum and the resulting predictions for new phenomena studied at particle collider experiments. Therefore, they can change the discovery prospects of the investigated model depending on the considered point in parameter space. Second, the newly calculated corrections are subject to a technical difficulty, the appearance of (infra-red) divergences, which is not common to simple theories usually studied but appears in many non-minimal models beyond the Standard Model. The different solutions for the problem of infra-red divergences considered in this thesis can also impact future studies of different models.

Furthermore, we estimate the precision of the perturbative calculation using the methods of renormalization-scheme and renormalization-scale variation. In particular, we employ a mixed OS/ $\overline{\text{DR}}$ renormalization scheme in the Higgs boson and top/stop sector of the theory.

We show that the relative corrections calculated in this work can be as large as 6% but remain below 3% in the region compatible with perturbative unitarity below the Grand Unification scale. The overall size of the scheme- and scale-uncertainty varies between approximately 1-8% and 0-3%, respectively.

Zusammenfassung

In dieser Dissertation werden Quantenkorrekturen zu Higgs Boson Massen in dem ladungs- und paritätsverletzenden Nicht-Minimalen Supersymmetrischen Standardmodell auf Zweischleifenordnung berechnet. Der Fokus dieser Arbeit liegt auf jenen Korrekturen, welche ausschließlich im nicht-minimalen nicht aber im Minimalen Supersymmetrischen Standardmodell auftreten. Diese Beträge sind deshalb interessant, weil die korrigierten Higgs Boson Massen Einfluss auf Vorhersagen haben können, welche experimentell an Teilchenbeschleunigern getestet werden. Daher können die Higgsmassenkorrekturen die Aussicht auf eine Entdeckung des betrachteten Modells beeinflussen. Des Weiteren können die hier vorgestellten Korrekturen auch für zukünftige Untersuchungen anderer Modelle von Interesse sein. Der Grund dafür ist das Auftreten von (infra-rot) Divergenzen, welche nicht für derartige Berechnungen in minimalen Modellen üblich sind. Die verschiedenen Lösungen für dieses Problem, welche in dieser Arbeit studiert werden, können daher auch in anderen nicht-minimalen Modellrechnungen angewandt werden.

Darüber hinaus macht diese Arbeit Aussagen über die Genauigkeit der störungstheoretischen Resultate zu den Higgs Boson Massen unter Zuhilfenahme der Abhängigkeit derselbigen von der Wahl des Renormierungsschemata und der Renormierungsskala. Insbesondere werden gemischte OS/ $\overline{\text{DR}}$ Renormierungsschemata im Higgs Boson Sektor aber auch im top/stop Sektor der Theorie angewandt.

Es wird gezeigt, dass die relativen Korrekturen bis zu 6% groß werden können. In dem Bereich des Modells, welcher mit Unitarität unterhalb der Skala an der sich die Eichkopplungen

treffen kompatibel ist, sind die Korrekturen jedoch nicht größer als 3%. Des Weiteren beträgt die theoretische Unsicherheit abgeleitet aus der Variation des Renormierungsschematas in etwa 1-8% und die abgeleitet aus der Renormierungsskala in etwa 0-3%.

Contents

1. Introduction	1
I. The Standard Model	5
2. The Standard Model of Particle Physics	7
2.1. Gauge Symmetries and Field Content	7
2.2. Electroweak Symmetry Breaking	9
3. Higher-Order Corrections to Mass Parameters	11
3.1. Regularization and Renormalization	11
3.2. Scalar Mass Parameters	13
3.2.1. Scalar Two-Loop Corrections	17
3.3. Vector Boson Mass Parameters	19
3.4. Fermion Mass Parameters	20
4. The Hierarchy Problem	21
II. Supersymmetric Extensions of the Standard Model	23
5. Supersymmetry	25
5.1. The Minimal Supersymmetric Standard Model	26
5.2. The Next-To-Minimal Supersymmetric Standard Model	28
5.3. The NMSSM Tree-Level Spectrum	29
5.3.1. Higgs Boson Sector	30
5.3.2. The Top/Stop and Bottom/Sbottom Sector	31
5.3.3. Electroweakino (EW-ino) Sector	32
5.3.4. Summary	32
6. Previous Predictions for the MSSM and NMSSM	35
6.1. Higgs Boson Masses	35
6.2. Constraints from Higgs Boson Data	37
6.3. Constraints from CP Violation	38
III. The $\mathcal{O}((\alpha_t + \alpha_\kappa + \alpha_\lambda)^2)$ Corrections to Higgs Boson Masses in the CP-Violating NMSSM	39
7. Renormalization of the NMSSM Higgs Bosons at the Two-Loop Order	41
7.1. Employed Strategy of Renormalization	42
7.2. Derivation of all Two- and Sub-Loop Counterterms	43
7.2.1. Electroweak Gauge Bosons and the SM VEV	43
7.2.2. Fermion Sector	44
7.2.3. Scalar Sector	46
7.2.4. Independence of $\mathcal{O}(\epsilon^1)$ Counterterms	52
8. Two-Loop Corrections in the Gaugeless limit	55
8.1. The Goldstone Boson Catastrophe from a Diagrammatic Approach	56

8.2. Using only a Mass Regulator	57
8.3. Using Partial Momentum Dependence	59
8.4. Using Full Momentum Dependence	59
9. Phenomenological Impact of the $\mathcal{O}((\alpha_t + \alpha_\kappa + \alpha_\lambda)^2)$ Corrections	61
9.1. Setup of the Parameter Scan	61
9.2. Results	63
9.2.1. Impact of the $\mathcal{O}((\alpha_t + \alpha_\kappa + \alpha_\lambda)^2)$ Corrections	66
9.2.2. Renormalization Scheme Dependence	69
9.2.3. Renormalization Scale Dependence	70
9.2.4. Impact of the IR Regulator	71
9.2.5. Impact of the CP-Violating Phases	73
10. Final Conclusion and Outlook	75
A. Finite One-Loop Counterterm Contributions	79
B. Mass Regulated One- and Two-Loop Functions	81
C. IR-Divergent Topologies	85
D. Two-Loop Feynman Diagrams	87
D.1. Tadpoles	87
D.2. Selfenergies	88
D.2.1. Momentum Regulated Diagrams	89
References	91
Acknowledgements	105

The Standard Model of particle physics (SM) is one of the most successful theories describing fundamental interactions with a tremendous precision in an energy range spanning over multiple orders of magnitude. Despite its popularity, there is experimental and theoretical evidence for physics beyond the SM (BSM) such as for instance the naturalness of a small Higgs boson mass value. Supersymmetry (SUSY) is one promising candidate being able to address this problem [1–7].

In particular, supersymmetric Higgs boson masses are closely connected to the theories' gauge- and Yukawa-sector which reduces the number of independent parameters of the considered model. For instance, the Minimal Supersymmetric Standard Model (MSSM), *cf.* Refs. [8, 9], *predicts* the value m_h for the SM-like Higgs boson mass to be bounded from above by the Z -boson mass $m_h < m_Z$ at tree-level. This is in conflict with the experimental measured value for the Higgs boson mass $m_h \approx 125 \text{ GeV} > m_Z$ [10–12] and demands for the inclusion of higher-order corrections. On the other hand, SUSY cannot be an exact symmetry realized in nature but is at least softly broken [9]. As a consequence, the Higgs boson mass can be raised to its experimental value by increasing the soft-SUSY-breaking mass scale M_{SUSY} which enters the higher-order corrections to m_h . Even though the leading one-loop corrections to the Higgs boson mass in the MSSM are in addition proportional to the fourth power of the top-quark Yukawa coupling, rather large values of M_{SUSY} are required in order to achieve corrections which are large enough to obtain the measured Higgs boson mass. This in turn weakens motivations regarding naturalness of the MSSM. In contrast, the Next-to-MSSM (NMSSM), *cf.* Refs. [13–18], features additional F-term contributions from the superpotential parameters λ and κ raising the Higgs boson mass already at tree-level such that higher-order corrections become less important. Therefore, the NMSSM reduces the required amount of finetuning compared to the MSSM [19].

The experimental value of the SM-like Higgs boson mass has been measured at the Large Hadron Collider (LHC) to very high precision with an uncertainty of a few hundred MeV [20, 21]. Therefore, precise predictions for Higgs boson masses in SUSY models are necessary in order to comply with the experiment. In addition, the inclusion of higher-order corrections can be used to study the convergence of the perturbative calculation in different corners of the models parameter space. It is expected that the theoretical uncertainty of the Higgs boson mass prediction is reduced upon the inclusion of higher-orders. Thus, precise Higgs

boson mass predictions in SUSY models require the calculation of higher-order corrections. However, the occurrence of large mass gaps $M_{\text{SUSY}} \gg m_h$ can lead to large logarithmic corrections spoiling the perturbative series at any finite order. In these scenarios, effective field theory (EFT) techniques are required in order to resum these large logs. However, in contrast to the MSSM, the NMSSM is less constrained by the experimental measurements such that scenarios with top superpartners lighter than 1-2 TeV are still viable. Therefore fixed-order calculations utilized in this work, which incorporate the full logarithmic dependence at a given order, are still a useful tool for precision predictions in the NMSSM.

A further important ingredient of higher-order calculations is the choice of the renormalization conditions. The dependence on the renormalization prescription should ideally vanish in an all-orders calculations. Therefore, the variation of the renormalization scale as well as a comparison of results obtained using e.g. minimal subtraction (MS) or on-shell (OS) renormalization conditions can give an estimate of the size of missing higher-order terms.

Another aspect of the fixed-order calculation is the dependence on the electroweak (EW) gauge couplings (also known as the *D-term* corrections). State-of-the-art (two-loop) three-loop calculations in the (N)MSSM are performed in the limit of vanishing $U_Y(1)$ and $SU_L(2)$ gauge couplings g_1 and g_2 , also referred to as the *gaugeless limit*. This restriction reduces the number of Feynman diagrams to a smaller set of diagrams with relatively simple tensor structure.

Going beyond the gaugeless limit in the MSSM was for a long time avoided because of the appearance of infra-red (IR) divergences and imaginary parts in the loop-integration due to Goldstone bosons with a vanishing or negative squared mass [22, 23]. The gaugeless limit circumvents these divergences in the MSSM. However, they reappear in the NMSSM at the two-loop order when considering NMSSM-specific corrections proportional to λ and κ (also known as the *F-term* corrections), even in the gaugeless limit. With increasing interest in the MSSM D-term as well as NMSSM F-term contributions, solutions to the problem of IR divergences have been developed first for the MSSM two-loop effective potential based on resummation [24–26]. For general field theories, Ref. [27] developed the *generalised effective potential approach* based on OS counterterms for massless Goldstone bosons which has already been applied to the CP-conserving NMSSM [28] in a minimal subtraction scheme.

In addition to the gaugeless limit, the approximation of vanishing external momentum is often applied in the calculation of the Feynman diagrams, since the two kinds of corrections are estimated to be of similar size. Furthermore, vanishing external momentum simplifies the calculation of two- and three-loop integrals significantly. While in the MSSM, there exist studies about the momentum dependence of the two-loop QCD [29, 30] and leading top/stop [31] corrections, the momentum dependence in the NMSSM is not known beyond the one-loop order.

This work complements the diagrammatic two-loop calculations in the CP-violating NMSSM of Refs. [32] and [33] by taking into account all two-loop Feynman diagrams proportional to the NMSSM specific superpotential parameters λ and κ and the top-quark Yukawa coupling in the gaugeless limit. A mixed OS/ $\overline{\text{DR}}$ renormalization scheme for the top and stop sector, the charged Higgs boson mass and the EW vacuum expectation value (VEV) is employed. It is shown that a subset of the IR-divergences due to massless Goldstone bosons cancels in the final expression for the neutral Higgs boson selfenergy by using a mass regulator. The remaining IR-divergences are treated in three different ways: (i) using only a mass regulator, (ii) by expanding IR-divergent Feynman diagrams around small external momentum and (iii) by using arbitrary external momentum in all (even IR-finite) diagrams.

This thesis is organised as follows.

Part I introduces the SM at tree-level, focusing on the mechanism of electroweak symmetry

breaking in Chapter 2. Chapter 3 discusses the regularization of UV-divergences as well as the idea behind renormalization of scalar, vector boson and fermion masses at the one- and two-loop level. We give explicit examples for the SM Higgs boson, Z -boson and top-quark mass. The results of these examples lead to the main motivation for SUSY in this thesis, the hierarchy problem, which is discussed in Chapter 4.

The theoretical foundations for SUSY are discussed in Part II. The focus is set on the tree-level parts of the NMSSM that are important for the considered two-loop corrections. In addition, we shortly review previous works performed in this research field that are important for this thesis.

In Part III, we present the calculation conducted during this dissertation. Chapter 7 applies the renormalization techniques from Chapter 3 on the NMSSM and derives all counterterms necessary for the two-loop calculation. In Chapter 8, the method of calculating the two-loop selfenergy Feynman diagrams is explained while focusing on the different treatments of the appearing IR divergences and how they relate two previous works.

The impact of the two-loop corrections on the phenomenology of the NMSSM is discussed in Chapter 9. We draw conclusions in Chapter 10 as well as discuss open problems and ideas for future research.

Part I.

The Standard Model

The Standard Model of Particle Physics

Quantum field theory (QFT) is rooted in the foundations of quantum mechanics, field theory and special relativity. It incorporates a Lorentz invariant description of quantized field operators. Probability amplitudes can be calculated as functions of the field operators using perturbative expansions of time-ordered operator products. In momentum space, this prescription boils down to the computation of an infinite series of Feynman diagrams. Therefore, QFT provides a powerful framework which can be universally applied to calculate observable predictions. Gauge theories are QFTs that postulate Lagrangians which are invariant under certain local symmetry transformations. This leads to conservation laws, the connection between several classes of Feynman diagrams and further identities that simplify QFT calculations.

The Standard Model (SM) is a spontaneously broken gauge theory, that aims to explain a large fraction of observed physical phenomena. Many of its predictions have been evaluated very precisely up to multiple orders in perturbation theory while an enormous amount of experiments test it at a similar accuracy. For an overview on measurements and corresponding predictions of the SM, we refer to the Review of Particle Physics [34].

This chapter addresses several aspects of the gauge and matter sector of the SM. We focus on the mass generation in the Higgs- and gauge-boson as well as the top-quark sector since these are of particular importance for the calculations discussed in Part III of this thesis.

2.1. Gauge Symmetries and Field Content

The SM Lagrangian is invariant under local $SU_c(3) \otimes SU_L(2) \otimes U_Y(1)$ gauge transformations. The gauge fields transform according to the adjoint representation of the respective gauge group. That is, an octet representation for the eight Gluons g_μ^a , $a = 1, \dots, 8$, of $SU_c(3)$, a triplet representation for the three gauge bosons W_μ^i , $i = 1, 2, 3$, and a singlet representation for the gauge boson B_μ . The charges associated with the gauge transformations are color for the $SU_c(3)$, weak iso-spin I_3 for $SU_L(2)$, and hypercharge Y for the $U_Y(1)$. While the $SU_c(3)$, which mediates the strong interaction, remains unbroken the $SU_L(2) \otimes U_Y(1)$ is spontaneously broken to a $U_{\text{e.m.}}(1)$ with a massless photon, a massive neutral and two charged gauge bosons which are the mediators of the electromagnetic and electroweak forces, respectively.

Quarks and leptons are arranged in triplets, doublets and singlets of the $SU_c(3)$, $SU_L(2)$

gauge/matter field	generations	$(U_Y(1), SU_L(2), SU_c(3))$
B	1	$(0, \mathbf{1}, \mathbf{1})$
W	1	$(0, \mathbf{3}, \mathbf{1})$
G	1	$(0, \mathbf{1}, \mathbf{8})$
q	$\begin{pmatrix} u \\ d \end{pmatrix}_L, \begin{pmatrix} c \\ s \end{pmatrix}_L, \begin{pmatrix} t \\ b \end{pmatrix}_L$	$(1/6, \mathbf{2}, \mathbf{3})$
l	$\begin{pmatrix} \nu_\tau \\ \tau \end{pmatrix}_L, \begin{pmatrix} \nu_\mu \\ \mu \end{pmatrix}_L, \begin{pmatrix} \nu_e \\ e \end{pmatrix}_L$	$(-1/2, \mathbf{2}, \mathbf{1})$
d	d_R, s_R, b_R	$(1/3, \mathbf{1}, \mathbf{3})$
u	u_R, c_R, t_R	$(-2/3, \mathbf{1}, \mathbf{3})$
e	τ_R, μ_R, e_R	$(1, \mathbf{1}, \mathbf{1})$
Φ	1	$(1/2, \mathbf{2}, \mathbf{1})$

Table 2.1.: Field content of the SM categorized in gauge (upper) and matter (middle) fields. The Higgs doublet (lower part), containing the only scalar degree of freedom, plays a special role. The second column shows the number of generations and the notation used to distinguish the first, second and third generation of the fermions as well as the representation they belong to. The L stands for doublet and the R for singlet under $SU_L(2)$. The last column identifies all representations $(Y, \mathbf{n}, \mathbf{m})$ under the SM gauge groups. Here, Y is the $U_Y(1)$ hypercharge and $\mathbf{n}=\mathbf{1},\mathbf{2}$ refers to singlet and doublet representations of the $SU_L(2)$ gauge group. $\mathbf{m}=\mathbf{1},\mathbf{2}$ and $\mathbf{8}$ refers to the singlet, triplet and octet representation of the $SU_c(3)$ gauge group.

and $U_Y(1)$, i.e. they transform under the fundamental representations. In addition, the SM contains one complex Higgs doublet Φ with hypercharge $Y = 1/2$. The complete field content of the SM along with their representations is listed in Tab. 2.1.

The most general Lorentz- and gauge-invariant Lagrangian describing all fields of Tab. 2.1 reads

$$\begin{aligned}
\mathcal{L}_{\text{SM}} = & (D_\mu \Phi)^\dagger (D^\mu \Phi) \overbrace{-\mu^2 \Phi^\dagger \Phi - \frac{1}{2} \lambda |\Phi^\dagger \Phi|^2} = -V(\Phi) \\
& - \frac{1}{4} G_{\mu\nu} G^{\mu\nu} - \frac{1}{4} W_{\mu\nu} W^{\mu\nu} - \frac{1}{4} B_{\mu\nu} B^{\mu\nu} \\
& + i \bar{l} \not{D} l + i \bar{e} \not{D} e + i \bar{q} \not{D} q + i \bar{u} \not{D} u + i \bar{d} \not{D} d \\
& - \mathbf{Y}_d q \Phi d - \mathbf{Y}_u q \Phi^\dagger u - \mathbf{Y}_l l \Phi e \\
& + \mathcal{L}_{\text{ghosts}} + \mathcal{L}_{\text{gaugefix}},
\end{aligned} \tag{2.1}$$

where we have suppressed all generation and group indices. The first line in Eq. (2.1) describes the kinetic term and the scalar potential $V(\Phi)$ of the Higgs doublet Φ with a mass parameter μ^2 and a quartic self-coupling λ . The second line contains the gauge boson kinetic terms and self-interactions with the gluon, W and B boson field strength tensors $G_{\mu\nu}$, $W_{\mu\nu}$ and $B_{\mu\nu}$, respectively. The third and fourth lines are the kinetic fermion terms and Yukawa interactions of all fermion fields with the Higgs doublet. The last line consists of the *Faddeev-Popov* ghost-field Lagrangian, $\mathcal{L}_{\text{ghosts}}$, and the gauge-fixing Lagrangian, $\mathcal{L}_{\text{gaugefix}}$, which remove unphysical degrees of freedom from the gauge-boson sectors of the theory. We will not discuss them in more detail since they are not of relevance for this thesis. The covariant derivative D_μ ensures local gauge invariance and is given by

$$D_\mu = \partial_\mu - ig_1 Y B_\mu - ig_2 I_3 \sigma_i W_\mu^i + i \frac{g_3 \lambda_a}{2} g_\mu^a, \tag{2.2}$$

where σ_i , $i = 1, 2, 3$, are the Pauli- and λ_a , $a = 1, \dots, 8$, are the Gell-Mann matrices. The gauge couplings g_1 , g_2 and g_3 belong to the $U_Y(1)$, $SU_L(2)$ and $SU_c(3)$ gauge groups, respectively. Together with the complex 3×3 Yukawa matrices \mathbf{Y}_f , $f = d, u, l$, they are free input parameters of the theory. However, one can show that \mathbf{Y}_l can be assumed to be diagonal without loss of generality, since the kinetic terms in \mathcal{L}_{SM} are invariant under $U(3)$ transformations $U_{L,R}$ in generation space,

$$l \rightarrow U_L \hat{l} \quad \text{and} \quad e \rightarrow U_R \hat{e}. \quad (2.3)$$

Thus, the transformation (2.3) will only alter the Yukawa matrix $(U_L^l)^\dagger \mathbf{Y}_l U_R^l \equiv \hat{\mathbf{Y}}_l$ which breaks this $U(3)$ symmetry. Appropriate choices for U_L^l and U_R^l diagonalize \mathbf{Y}_l using a singular value decomposition. The states \hat{l} and \hat{e} are called *mass eigenstates* while e and l are the *interaction eigenstates*. Since the Lagrangian for the hatted and un-hatted lepton fields has the same form, we can relabel $\hat{l} = l$ and $\hat{e} = e$. Thus, mass and interaction basis for the leptons coincide.

The simultaneous diagonalization of \mathbf{Y}_d and \mathbf{Y}_u is more involved since we do not have enough $U(3)$ transformations. The resulting Lagrangian will depend on an additional $U(3)$ transformation V_{CKM} which is the Cabibbo-Kobayashi-Maskawa (CKM) matrix [35]. V_{CKM} is of particular importance for flavor physics. However, it does not play an important role in the context of the Higgs boson mass calculations performed in this thesis and is therefore set to unity. The motivation for this approximation is a large hierarchy between the top-quark Yukawa coupling to the Higgs boson compared to all other Yukawa couplings. Likewise, we neglect the presence of neutrino masses (i.e. right-handed neutrinos are missing in Tab. 2.1) since they do have a negligible small effect on the Higgs boson mass prediction.

The SM Lagrangian in Eq. (2.1) does not contain any explicit mass terms for fermions and gauge bosons since these would break the chiral- and gauge symmetries of the model. The description of massive fields is achieved using the mechanism of spontaneous symmetry breaking, discussed in the next chapter, which connects the free parameters $\mathbf{Y}_{l,d,u}$, μ^2 and $g_{1,2}$ to physical masses.

2.2. Electroweak Symmetry Breaking

In this section we briefly discuss electroweak symmetry breaking (EWSB) i.e. the dynamical generation of gauge boson and fermion masses without explicitly breaking local gauge invariance and chiral symmetries. This is also called *the Higgs mechanism* [36–38].

Consider the scalar potential $V(\Phi)$ in Eq. (2.1). If the squared mass parameter of the scalar field Φ is negative, $\mu^2 < 0$, the potential develops a minimum

$$\langle \Phi \rangle = \sqrt{-\frac{\mu^2}{\lambda}} \begin{pmatrix} 0 \\ 1 \end{pmatrix} \equiv \frac{v}{\sqrt{2}} \begin{pmatrix} 0 \\ 1 \end{pmatrix}, \quad (2.4)$$

with the vacuum expectation value (VEV) v . We can expand the scalar field Φ around this minimum

$$\Phi = \begin{pmatrix} G^+ \\ \frac{v + h + iG^0}{\sqrt{2}} \end{pmatrix}, \quad (2.5)$$

where h is *the* physical Higgs boson and $G^{0,+}$ are the neutral/charged Goldstone bosons discussed later. We rotate the four massless gauge bosons $W_\mu^{1,2,3}$ and B_μ into a diagonal basis

$$\begin{pmatrix} Z_\mu \\ A_\mu \end{pmatrix} = \begin{pmatrix} c_{\theta_w} & -s_{\theta_w} \\ s_{\theta_w} & c_{\theta_w} \end{pmatrix} \begin{pmatrix} W_\mu^3 \\ B_\mu \end{pmatrix} \quad \text{and} \quad W_\mu^\pm = \frac{1}{\sqrt{2}} (W_\mu^1 \mp iW_\mu^2), \quad (2.6)$$

with the Weinberg angle θ_w and the notation $s_x = \sin x$, $c_x = \cos x$, $t_x = \tan x$ which is used throughout this thesis¹. Using Eqs. (2.5) and (2.6) one can show that the kinetic term of Φ generates the gauge boson mass terms

$$(D^\mu \Phi)^\dagger D_\mu \Phi = \underbrace{\left(\frac{g_1 v}{2}\right)^2}_{M_W^2} W_\mu^+ W^{-\mu} + v^2 \underbrace{\frac{g_1^2 + g_2^2}{8}}_{\frac{1}{2}M_Z^2} Z_\mu Z^\mu + \text{interactions} \quad (2.7)$$

while the photon field A_μ remains massless. In accordance with the Goldstone theorem, *cf.* Ref. [39], the three Goldstone bosons $G^{\pm,0}$ remain massless and only the field h acquires a mass

$$V(\Phi) \supset \frac{v^2 \lambda}{2} h^2 \equiv \frac{m_h^2}{2} h^2. \quad (2.8)$$

In order to obtain the correct definition of the electrical charge e , it is useful to write the covariant derivative in the mass basis

$$D_\mu = \mathbb{1}_{2 \times 2} \partial_\mu - i \frac{2g_2 I_3}{\sqrt{2}} \begin{pmatrix} 0 & W_\mu^+ \\ W_\mu^- & 0 \end{pmatrix} - \mathbb{1}_{2 \times 2} i e Q A_\mu - \mathbb{1}_{2 \times 2} \frac{i e}{c_{\theta_w} s_{\theta_w}} Z_\mu (\mathbb{I}_3 - Q s_{\theta_w}^2), \quad (2.9)$$

using the Gell-Mann-Nishijima identity, $Y = 2(Q - I_3)$, and

$$e = \frac{g_1 g_2}{\sqrt{g_1^2 + g_2^2}} = \frac{2M_W}{v} s_{\theta_w} = \frac{2M_W}{v} \sqrt{1 - \frac{M_W^2}{M_Z^2}}. \quad (2.10)$$

Solving this equation for v , we can eliminate v as input parameter in favour of M_W , M_Z and e . At tree-level, this choice seems to be equivalent. However, in Part III we will exploit this relation at one- and two-loop order to construct an on-shell VEV counterterm which severely depends on the choice of input parameters.

We continue with the masses of the fermions. Using the expansion Eq. (2.5) in any Yukawa term of the type $\mathbf{Y}_f f_L \Phi f_R$, shows that the mass matrices of the fermions are

$$\mathbf{m}_f = \frac{v}{\sqrt{2}} \mathbf{Y}_f, \quad f = l, u, d. \quad (2.11)$$

Their experimentally measured values show a clear mass hierarchy, with the top quark mass $m_t \approx 173$ GeV being by far the heaviest fermion with a mass gap of several orders of magnitude [34]. Due to the tree-level relation, Eq. (2.11), this hierarchy is translated to a hierarchy in the Yukawa couplings. The proportionality between masses and coupling strengths to the Higgs boson is a very strong prediction of the EWSB mechanism. Due to this hierarchy, a common approximation in higher-order Higgs boson mass calculations is to neglect all Yukawa couplings $\mathbf{Y}_l = \mathbf{Y}_d = 0$ and only take into account the top quark Yukawa coupling, $(\mathbf{Y}_u)_{ij} = \delta_{i3} \delta_{j3} y_t$. Thus, the masses and couplings to the Higgs boson of all fermions other than the top-quark fermion are set to zero and the CKM matrix becomes unity.

It is important to note that the relations between masses and couplings, Eqs. (2.7), (2.8) and (2.11), are violated by higher-order corrections. Therefore, precision predictions that depend e.g. on m_t and y_t as an input, such as those of the Higgs boson mass, require to go beyond tree-level accuracy. The basic principles of such higher-order calculations are discussed in the next chapter.

¹Note that $t_x = \tan x$ clashes with the notation for the tadpole parameters $t_\Phi = \partial V / \partial \Phi$ defined in Sec. 5.3.1. However, in this thesis the tangens only appears as a function of mixing angles such that it is always clear from the context.

Higher-Order Corrections to Mass Parameters

This chapter introduces the notation and tools that are commonly used in the calculation of higher-order corrections to mass parameters.

Due to the quantum nature of higher-order calculations, they involve the summation and integration over all possible intermediate states, quantum numbers and momenta. The latter is called *loop* integration which can feature divergences at various places in the integration domain. A particular type of divergence is the ultra-violet (UV) divergence which can appear for very large loop momenta. The process of *regularization*, discussed in Sec. 3.1, isolates these divergences by introducing a regulator. Since physical observables need to be finite, UV divergences are a sign for a missing piece in the calculation. In fact, the quantities entering the SM Lagrangian discussed in Chapter 2 are not physical parameters since they can contain divergences at higher-orders. Therefore, it requires additional definitions of what we call physical parameters which are embedded into the theory by adding a minimal set of *counterterms* to the Lagrangian. This procedure is called *renormalization* and is briefly introduced in Sec. 3.1. The practical use of regularization and renormalization is explained at the example of one-loop corrections to scalar, vector boson and fermion masses in Sec. 3.2, 3.3 and 3.4, respectively. The basic tools for scalar two-loop mass corrections are discussed in Sec. 3.2.1.

3.1. Regularization and Renormalization

We consider the scalar one-loop two-point integral at vanishing external momenta which often appears in higher-order calculations

$$\text{Diagram} = \int \frac{dk^4}{(2\pi)^4} \frac{1}{(k^2 - m^2)^2}. \quad (3.1)$$

In the integration region with large loop momenta, $k^2 \gg m^2$, the integral scales with

$$\int_{m^2}^{\infty} \frac{dk}{k} \propto \lim_{\Lambda \rightarrow \infty} \log \Lambda^2 \quad (3.2)$$

which means that it diverges logarithmically in $D = 4$ dimensions. In Eq. (3.2) we intuitively introduced a mass regulator Λ which would enable us to proceed with the rest of the calculation and to employ renormalization conditions that cancel all $\log \Lambda^2$ terms before taking

the limit $\Lambda \rightarrow \infty$. However, the introduction of a mass regulator is in general not Lorentz invariant. A better way to deal with this kind of divergences is dimensional regularization which makes use of the fact, that integrals similar to Eq. (3.1) become UV finite if

$$\frac{dk^4}{(2\pi)^4} \rightarrow \mu_{\text{MS}}^{D-4} \frac{dk^D}{(2\pi)^D}, \quad (3.3)$$

with $D = 4 - 2\epsilon$ chosen small enough [40]. The resulting expression will be Lorentz invariant and involves inverse powers of ϵ parametrizing the divergence as ϵ goes to zero. This procedure is called dimensional regularization (DReg). The prefactor μ_{MS}^{D-4} is a dimensional quantity which ensures that the dimensions of all Lagrangian parameters in $D = 4$ stay the same in $D = 4 - 2\epsilon$ dimensions. At the n -loop order, we maximally encounter poles of $\mathcal{O}(\epsilon^{-n})$.

Once all divergent contributions have been isolated in ϵ^{-n} poles, a minimal set of counterterms and renormalization conditions is chosen to obtain a UV finite result. In practice, the *bare* (unrenormalized) quantities and fields, q_i^{bare} and Ψ_i^{bare} , in the classical Lagrangian are related to the physical (renormalized) quantities and fields, $q_i^{\text{ren.}}$ and $\Psi_i^{\text{ren.}}$, by

$$q_i^{\text{bare}} = q_i^{\text{ren.}} + \delta q_i \quad \text{and} \quad (3.4a)$$

$$\Psi_i^{\text{bare}} = \sqrt{Z_{\Psi_i}} \Psi_i^{\text{ren.}}. \quad (3.4b)$$

The counterterms δq_i are calculated perturbatively in terms of the physical parameters

$$\delta q_i = \sum_{n=1}^{\infty} \delta^{(n)} q_i (q_j^{\text{ren.}}) \quad (3.5)$$

where the $\delta^{(n)} q_i$'s will contain terms up to $\mathcal{O}(\epsilon^{-n})$. Depending on the chosen renormalization conditions, the $\delta^{(n)} q_i$'s may contain additional finite parts.

The wave function renormalization constants (Z -factors), ensure the proper normalization of the two-point correlator and can be similarly expanded:

$$\sqrt{Z_{\psi_i}} = \left(1 + \sum_{n=1}^{\infty} \delta^{(n)} Z_{\psi_i} \right)^{\frac{1}{2}} = 1 + \frac{\delta^{(1)} Z_{\psi_i}}{2} - \frac{1}{2} \left(\frac{\delta^{(1)} Z_{\psi_i}}{2} \right)^2 + \frac{\delta^{(2)} Z_{\psi_i}}{2} + \dots \quad (3.6a)$$

$$\equiv 1 + \frac{\Delta^{(1)} Z_{\psi_i}}{2} + \frac{\Delta^{(2)} Z_{\psi_i}}{2} + \dots \quad (3.6b)$$

where we introduced the Δ -notation used in this thesis. In the *minimal subtraction* (MS) scheme, the δq_i and Z -factors are chosen to only cancel all ϵ^{-n} terms

$$\delta q_i^{\text{MS}} = \sum_{n=1}^{\infty} \frac{1}{\epsilon^n} a_{q_i}^{(n)}, \quad (3.7)$$

where the $a_{q_i}^{(n)}$ can be determined by demanding UV-finite $q_i^{\text{ren.}}$. In the *modified minimal subtraction* ($\overline{\text{MS}}$) scheme, one also chooses to cancel constant factors,

$$\frac{1}{(4\pi)^{D/2}} \frac{\Gamma(1+\epsilon)}{\epsilon} = \frac{1}{(4\pi)^2} \left(\frac{1}{\epsilon} - \gamma_E + \log 4\pi + \mathcal{O}(\epsilon) \right), \quad (3.8)$$

which appear due to the D -dimensional phase space integral:

$$\delta q_i^{\overline{\text{MS}}} = \delta q_i^{\text{MS}} - \gamma_E + \log 4\pi, \quad (3.9)$$

where $\gamma_E \approx 0.577$ is the EulerMascheroni constant. In an equivalent way, one can make this cancellation manifest without modifying the MS counterterms but define the *renormalization*

scale $\mu_{\overline{\text{MS}}}$ in the $\overline{\text{MS}}$ scheme, which is closely connected to the *regularization scale* μ_{MS} used to regularize the loop integrals:

$$\mu_{\overline{\text{MS}}}^2 = 4\pi e^{-\gamma} \mu_{\text{MS}}^2. \quad (3.10)$$

Therefore, we do not explicitly mention the constant terms in analytic expressions of $\overline{\text{MS}}$ counterterms but only refer to the UV-divergent parts and to the renormalization scale $\mu_{\overline{\text{MS}}}$ as μ without the $\overline{\text{MS}}$ subscript.

However, DReg explicitly breaks SUSY as the number of degrees of freedom of gauge bosons changes in $D \neq 4$ dimensions while those of the corresponding fermionic superpartners remain constant. *Dimensional reduction* (DRed) treats all space-time indices in $D = 4$ dimensions except those of the four-momenta which intuitively should preserve SUSY. However, even in DRed no general proof for SUSY-preservation exists. Instead, various SUSY Ward identities have been explicitly shown to hold up to two- and three-loop order [41, 42]. The corresponding renormalization scheme of DRed is labeled $\overline{\text{DR}}$. While the SUSY-preservation of $\overline{\text{DR}}$ counterterms needs in general to be proven on a case-by-case basis, the two-loop calculation presented in this thesis does not require such a proof. We apply the approximation of vanishing gauge couplings, i.e. there are no internal gauge boson propagators, and therefore there is no issue with SUSY-breaking counterterms at the considered loop-level.

In addition to the $\overline{\text{MS}}/\overline{\text{DR}}$ schemes, it is also possible to include further finite parts in (some of) the counterterms. A popular choice is the OS scheme which employs conditions on the mass parameter counterterms in order to ensure that $m^{\text{ren.}}$ is given by the pole of the corresponding field propagator. If we calculate a physical observable $O(q_i^{\text{ren.}})$ perturbatively in terms of the input parameters $q_i^{\text{ren.}}$, the result will in general depend on the choice of the renormalization conditions for the parameters $q_i^{\text{ren.}}$. However, physical observables must not depend on the chosen renormalization scheme. Therefore, the results for O obtained from different renormalization conditions have to agree in an all-orders calculation. Thus, the freedom to choose different renormalization conditions for a set of input parameters $q_i^{\text{ren.}}$ can be used to estimate missing higher-order terms in the calculation of the observable $O(q_i^{\text{ren.}})$. In this thesis, the $q_i^{\text{ren.}}$'s are a set of dimensionful parameters renormalized in different renormalization schemes while O is the propagator-pole of the Higgs boson fields.

In the next section, we show how OS/ $\overline{\text{DR}}$ counterterms are calculated in practice for general scalar, vector boson and fermion mass terms. In addition, we list short example results for the SM Higgs boson, the top-quark and the Z -boson masses. Not only the corrections to the Higgs boson mass are going to be important for the calculation of the two-loop corrections in the NMSSM in this work, but also those to fermions and vector bosons since they contribute at the sub-loop level.

3.2. Scalar Mass Parameters

In an interacting QFT, the free-field tree-level propagator,

$$iS_s^{(0)} = \text{-----} = i(p^2 - m_s^2)^{-1}, \quad (3.11)$$

of a real scalar field with mass m_s receives quantum corrections characterized by an infinite series of Feynman diagrams. Collecting all *one-particle-irreducible* (1PI) diagrams one can write the all-orders propagator using a *Dyson* series,

$$iS_s(p) = \text{-----} + \text{---} \text{---} \text{---} \text{---} \text{---} \text{---} + \text{---} \text{---} \text{---} \text{---} \text{---} \text{---} \text{---} \text{---} + \dots \quad (3.12a)$$

$$= \frac{i}{p^2 - m_s^2 - \hat{\Sigma}_s(p^2)}, \quad (3.12b)$$

where $\hat{\Sigma}_s(p^2)$ is the renormalized scalar selfenergy given by the first 1PI blob in Eq. (3.12). At the one-loop order, $\hat{\Sigma}_s(p^2)$ in any renormalizable QFT is obtained by calculating the Feynman

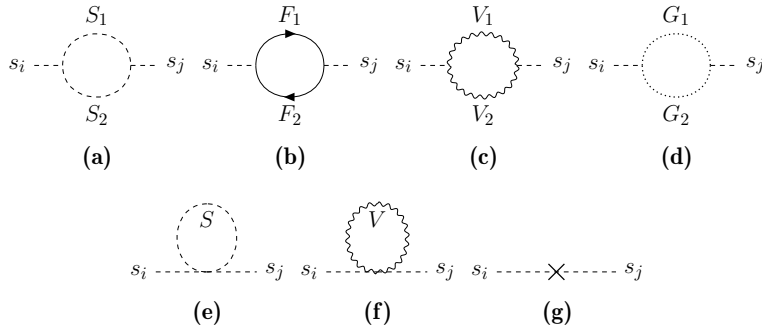


Figure 3.1.: All possible generic scalar (vector if s_{ij} are vectors) one-loop selfenergy diagrams.

diagrams shown in Fig. 3.4: Diagram (a) to (f) form the unrenormalized selfenergy $\Sigma_s(p^2)$. The diagrams schematically depict the contributions from arbitrary scalars (S), fermions (F), vectors bosons (V) and corresponding ghosts² (G). Diagram (g) is the counterterm contribution which renders the total selfenergy UV finite:

$$\hat{\Sigma}_s^{(1),Y}(p^2) = \Sigma_s^{(1),Y}(p^2) + (p^2 - m_s^{2,Y})\delta Z^Y - \delta m_s^{2,Y}, \quad (3.13)$$

where the superscript (1) denotes the number of loops and Y is a label for the chosen renormalization scheme. The tensor integrals contributing to $\Sigma_s^{(1),Y}(p^2)$ can be reduced to two common scalar integrals, the one-point integral \mathbf{A} and the two-point integral \mathbf{B} , using e.g. the Passarino-Veltman reduction formalism [43, 44]. They have been computed in Ref. [45] in terms of logarithms and di-logarithms. For completeness, we recall their definitions used in [46] here using the $(+, -, -, -)$ convention for the Minkowski metric:

$$\mathbf{A}(x) = (4\pi)^2 \mu^{4-D} \int \frac{dk^D}{(2\pi)^D} [k^2 - x]^{-1}, \quad (3.14a)$$

$$\mathbf{B}(x, y) = (4\pi)^2 \mu^{4-D} \int \frac{dk^D}{(2\pi)^D} [k^2 - x]^{-1} [(k+p)^2 - y]^{-1}, \quad (3.14b)$$

with the squared mass parameters x and y and the external momentum p . Both integrals feature a ϵ^{-1} pole and give additional UV-finite contributions. As discussed in the previous section, there are two common renormalization prescriptions. In the OS scheme, $Y = \text{OS}$, the conditions

$$\widetilde{\text{Re}} \hat{\Sigma}_s^{\text{OS}}(p^2 = m_s^{2,\text{OS}}) = 0 \quad \text{and} \quad \widetilde{\text{Re}} \left. \frac{\partial}{\partial p^2} \hat{\Sigma}_s^{\text{OS}}(p^2) \right|_{p^2 = m_s^{2,\text{OS}}} = 0 \quad (3.15)$$

are solved for δm_s^2 and δZ respectively:

$$\delta m_s^{2,\text{OS}} = \widetilde{\text{Re}} \Sigma_s^{\text{OS}}(p^2 = m_s^{2,\text{OS}}) \quad \text{and} \quad \delta Z^{\text{OS}} = -\widetilde{\text{Re}} \left. \frac{\partial}{\partial p^2} \Sigma_s^{\text{OS}}(p^2) \right|_{p^2 = m_s^{2,\text{OS}}}, \quad (3.16)$$

which ensures that m_s^{OS} entering the loop-corrected propagator

$$iS_s^{\text{OS}}(p^2) = i(p^2 - m_s^{2,\text{OS}})^{-1} \quad (3.17)$$

is the physical pole mass with a residue of one. Therefore, the OS scheme fulfils all requirements to be used in scattering and decay processes formulated using the standard *Lehmann-Symanzik-Zimmerman* (LSZ) formalism [47]. The parameter m_s^{OS} is an observable input of

²Diagrams with vector bosons and ghosts in the loop are not relevant for this work since we assume vanishing gauge couplings. However, for completeness we show the full set of generic one-loop diagrams including vectors and ghosts.

the theory while the loop corrections are absorbed into $\delta m_s^{2, \text{OS}}$. The symbol $\widetilde{\text{Re}}$ in Eqs. (3.15) and (3.16) ignores all absorptive contributions i.e. it uses the real value of all loop functions but otherwise takes into account imaginary parts of all complex parameters.

In the modified minimal subtraction scheme, $Y = \overline{\text{MS}}$, we only absorb the UV divergent parts (cf. the discussion of Eq. (3.10)) in δZ and δm_s^2 :

$$\widetilde{\text{Re}} \hat{\Sigma}_s^{\overline{\text{MS}}}(p^2)|_{\epsilon^{-n}} = 0 \quad \text{and} \quad \widetilde{\text{Re}} \frac{\partial}{\partial p^2} \hat{\Sigma}_s^{\overline{\text{MS}}}(p^2)|_{\epsilon^{-n}} = 0 \quad (3.18)$$

$$\Leftrightarrow \delta m_s^{2, \overline{\text{MS}}} = \widetilde{\text{Re}} \Sigma_s^{\overline{\text{MS}}}(p^2)|_{\epsilon^{-n}} \quad \text{and} \quad \delta Z^{\overline{\text{MS}}} = -\widetilde{\text{Re}} \frac{\partial}{\partial p^2} \Sigma_s^{\overline{\text{MS}}}(p^2)|_{\epsilon^{-n}}, \quad (3.19)$$

where $X|_{\epsilon^{-n}}$ takes the UV-divergent part of X into account. Therefore, the scalar propagator in the $\overline{\text{MS}}$ scheme is of the form

$$iS_s^{\overline{\text{MS}}}(p^2) = i \left(p^2 - m_s^{2, \overline{\text{MS}}} + \widetilde{\text{Re}} \hat{\Sigma}_s^{\overline{\text{MS}}}(p^2) \right)^{-1}, \quad (3.20)$$

where the tree-level mass $m_s^{\overline{\text{MS}}}$ and the UV-finite part of the selfenergy enter. In contrast to $m_s^{2, \text{OS}}$, the mass $m_s^{2, \overline{\text{MS}}}$ is not at the propagator pole, $iS_s^{\overline{\text{MS}}}(p^2 = m_s^{2, \overline{\text{MS}}}) \neq 0$. The actual pole of $S_s^{\overline{\text{MS}}}$ is the loop-corrected $\overline{\text{MS}}$ mass

$$\tilde{m}_s^{2, \overline{\text{MS}}} = m_s^{2, \overline{\text{MS}}} + \widetilde{\text{Re}} \Sigma_s^{\overline{\text{MS}}}(p^2 = \tilde{m}_s^{2, \overline{\text{MS}}}) \Big|_{\text{UV-finite part}} \quad (3.21)$$

which can be solved iteratively for $\tilde{m}_s^{2, \overline{\text{MS}}}$. It should be noted that the iterative solution mixes contributions from different orders in perturbation theory. Furthermore, $\tilde{m}_s^{2, \overline{\text{MS}}}$ seems to depend on the chosen renormalization scale μ . However, physics must be independent of the artificial parameter μ . Therefore, the μ -dependence of the renormalized parameters which enter $\tilde{m}_s^{2, \overline{\text{MS}}}$ must be such that the overall μ -dependence of $\tilde{m}_s^{2, \overline{\text{MS}}}$ vanishes. Demanding that $\tilde{m}_s^{2, \overline{\text{MS}}}$ cannot depend on μ

$$\mu \frac{\partial \tilde{m}_s^{2, \overline{\text{MS}}}}{\partial \mu} = 0, \quad (3.22)$$

can be used to derive a differential equation for $m_s^{2, \overline{\text{MS}}}(\mu)$ which depends on the other theory parameters entering Σ_s^3 . In phenomenologically relevant models, with many mass and coupling parameters q_i , this procedure leads to a system of coupled equations

$$\frac{\partial q_i^{\overline{\text{MS}}}}{\partial \log \mu} \equiv \beta_{q_i}(q_i^{\overline{\text{MS}}}, q_j^{\overline{\text{MS}}}, \dots) \quad (3.23)$$

which are called the *Renormalization Group Equations* (RGEs). The expressions on the right hand side of Eq. (3.23) are called *beta functions*. The RGEs are known for arbitrary renormalizable QFTs up to two-loop order [49–51] and are an important tool to study the behavior of higher-order corrections. They have been implemented in the computer program SARAH [52–55] which can calculate the RGEs for any renormalizable gauge theory. In particular, the RGEs can be used to study the residual dependence of e.g. $\tilde{m}_s^{2, \overline{\text{MS}}}$ on μ as a further estimate of the size of missing higher-orders. In Ref. [49] it was shown that the RGEs are inevitably connected to the UV-structure of the theory. More specifically, the coefficient of the n -loop RGE for a coupling q_i is fully determined by the single-pole of the corresponding n -loop $\overline{\text{MS}}$ counterterm. This gives a convenient and effective possibility to construct $\overline{\text{MS}}$ counterterms without actually calculating Feynman diagrams. Likewise, one can partially

³A more elegant but equivalent way of obtaining differential equations for the renormalized parameters is to demand that the bare parameters and fields are independent of μ . For a detailed discussion, we refer to Ref. [48].

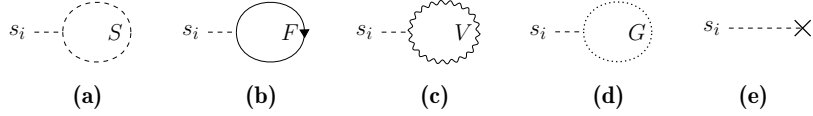


Figure 3.2.: All possible generic scalar one-loop tadpole diagrams.

double-check analytic results for higher-order corrections to a parameter q_i by comparing the pole-structure with generic results for the beta function from the literature (such as for instance $\Sigma_s^{(1), \overline{\text{MS}}}|_{\epsilon^{-1}}$ and $\beta_{m_s^2}^{(1)}$). This strategy is also applied in this thesis to cross-check the required counterterms for the two-loop Higgs boson mass calculation.

Unlike the squared mass parameter m_s^2 of the hypothetical scalar from our previous discussion, the squared mass parameter μ^2 in the SM, and in general in any spontaneously broken theory, is replaced by the VEV and the quartic Higgs self-coupling by making use of the minimum condition

$$\left. \frac{\partial}{\partial \Phi} V(\Phi) \right|_{\Phi=\langle \Phi \rangle} \equiv t_{\Phi}^{(0)} \stackrel{\text{tree-level}}{=} 0 \quad (3.24)$$

$$\Leftrightarrow -\mu^2 = \frac{v^2 \lambda}{2} - \frac{t_{\Phi}^{(0)}}{v} \equiv \frac{m_h^2}{2}, \quad (3.25)$$

where we explicitly kept the dependence on the position of the tree-level minimum $t_{\Phi}^{(0)} = 0$. Thus, the $\overline{\text{MS}}/\overline{\text{DR}}$ counterterm for the squared scalar mass of the Higgs boson is derived from the $\overline{\text{MS}}/\overline{\text{DR}}$ counterterm of the VEV (δv), the quartic coupling ($\delta \lambda$) as well as the tadpole counterterm (δt_{Φ})

$$\delta m_h^2(q_1, \dots, q_n) = \sum_{x=q_1}^{q_n} \frac{\partial m_h^2}{\partial x} \delta x = \frac{\partial m_h^2}{\partial v} \delta v + \frac{\partial m_h^2}{\partial \lambda} \delta \lambda + \frac{\partial m_h^2}{\partial t_{\Phi}} \delta t_{\Phi}. \quad (3.26)$$

Therefore, the treatment of the loop-corrected vacuum is of particular importance in spontaneously broken theories. In practice, this means that the tree-level minimum condition $t_{s_i}^{(0)} = 0$ of the scalar potential $V(s_1, \dots, s_n)$ of any spontaneously broken theory w.r.t. a field s_i is shifted by quantum corrections to yield the renormalized all-orders minimum \hat{t}_{s_i} . At the one-loop level, all possible types of corrections to $\hat{t}_{s_i}^{(1)}$ are shown in Fig. 3.2. Diagrams (a) to (d) are all proportional to trilinear couplings of s_i to scalars (a), fermions (b), vector bosons (c) and ghosts (d). Diagram (e) shows the one-loop counterterm contribution. A convenient tadpole renormalization prescription is to choose

$$\hat{t}_{s_i} = t_{s_i}^{(0)} = 0 \quad (3.27)$$

$$\Leftrightarrow \delta t_{s_i} = t_{s_i} \quad (3.28)$$

such that diagram (e) in Fig. 3.2 effectively cancels all other tadpole diagrams. Therefore, the tree-level minimum $t_{s_i}^{(0)}$ stays at the physical minimum \hat{t}_{s_i} at each order in perturbation theory.

For demonstration purposes, we end this section by considering the top quark contribution to the SM Higgs boson mass, i.e. Fig. 3.1 (b) with $s_{i,j} = h$ and $F_{1,2} = t, \bar{t}$, in the limit of vanishing external momentum:

$$\Sigma_h^{(1)}(p^2) = \frac{3m_t^2}{8\pi^2 v^2} (2\mathbf{A}(m_t^2) + (p^2 - 4m_t^2)\mathbf{B}(m_t^2, m_t^2)) \quad (3.29)$$

$$\stackrel{p^2=0}{=} -\frac{3m_t^4}{4\pi^2 v^2} \left(-1 + \log \frac{m_t^2}{\mu^2} - \frac{3}{\epsilon} \right) + \mathcal{O}(\epsilon) \quad (3.30)$$

which contains UV-divergent and UV-finite parts. The tadpole contribution, Fig. 3.2 (b) with $s_i = h$ and $F = t$, reads:

$$t_h^{(1)} = -\frac{3m_t^2}{4\pi^2 v} \mathbf{A}(m_t^2) \quad (3.31)$$

$$= -\frac{3m_t^4}{4\pi^2 v} \left(-1 + \log \frac{m_t^2}{\mu^2} - \frac{1}{\epsilon} \right) + \mathcal{O}(\epsilon) \quad (3.32)$$

Thus, the one-loop corrected $\overline{\text{MS}}$ mass is given by

$$m_h^{2(1),\overline{\text{MS}}} \approx m_h^{2(0)} + \hat{\Sigma}^{(1),\overline{\text{MS}}}(p^2 = 0) - \frac{1}{v} \hat{t}_h^{(1),\overline{\text{MS}}} \quad (3.33)$$

$$= \lambda v^2 + \frac{3m_t^4}{2\pi^2 v^2} \log \frac{m_t^2}{\mu^2} \quad (3.34)$$

which is a crucial result for the discussion of the hierarchy problem in Chapter 4.

3.2.1. Scalar Two-Loop Corrections

The renormalization of two-loop corrections to scalar mass parameters works similar to the one-loop case. In addition to the two-loop counterterm, which has the same structure as the one-loop counterterm, there are also contributions from products of two one-loop counterterms

$$\begin{aligned} \text{---}\overline{\times}\text{---}^{\text{two-loop}} &= (p^2 - m_s^2) \Delta^{(2)} Z_s - \delta^{(2)} m_s^2 \\ &+ (p^2 - m_s^2) \frac{1}{4} \left(\Delta^{(1)} Z_s \right)^2 - \delta^{(1)} m_s^2 \Delta^{(1)} Z_s, \end{aligned} \quad (3.35)$$

and similarly for the tadpole counterterm

$$\text{-----}\overline{\times}\text{-----}^{\text{two-loop}} = \delta^{(2)} t_s - \frac{1}{2} \Delta^{(1)} Z_s \delta^{(1)} t_s. \quad (3.36)$$

The full set of all generic two-loop selfenergy and tadpole diagrams with internal scalars and fermions is shown in the Appendix in Fig. D.2 and Fig. D.1, respectively. For the sake of readability, we show here five sample two-loop selfenergy diagrams in Fig. 3.3 discussed in the following. The diagram in Fig. 3.3 (a) consists of two closed internal lines and is therefore called a *genuine* two-loop diagram. Diagrams (b)-(e) can be interpreted in two ways: they consist of only one closed internal loop and therefore contribute with the one-loop integrals defined in Eqs. (3.14a) and (3.14b). However, since they also contain a one-loop counterterm, they are formally a two-loop contribution of $\mathcal{O}(\epsilon^{-2})$. Therefore, we call them *counterterm-inserted* two-loop diagrams. Diagrams (b) and (c) contribute with a one-loop mass counterterm while diagrams (d) and (e) contribute with a vertex counterterm. In this thesis, we take into account Z -factor contributions from scalar mass- and vertex counterterm diagrams. However, for fermion mass counterterm insertions, such as Fig. 3.3 (c), we only

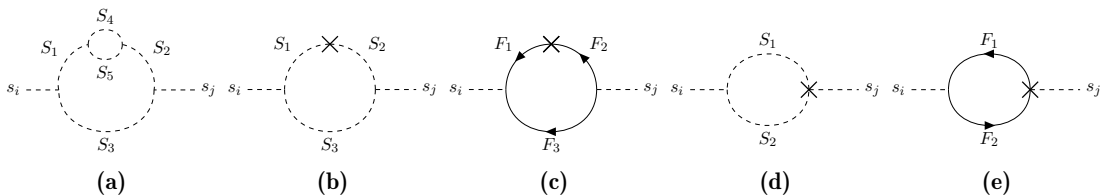


Figure 3.3.: Example scalar selfenergy diagrams. Shown are a genuine two-loop diagram (a) and counterterm-inserted diagrams (b-d).

require the $\delta^{(1)}m_F$ contributions but not $\delta^{(1)}Z_F$ since we do not calculate any two-loop diagrams with fermions on the external lines.

Therefore, a full-fledged two-loop calculation that takes into account the contributions from certain scalar and fermion degrees of freedom (as we do in this work), requires a one-loop renormalization of the corresponding sectors. In order to consistently cancel all UV-divergences, the sub-loop renormalization must consider the same approximations as in the genuine two-loop diagrams (e.g. if certain parameters are assumed to vanish or not).

The loop integrals appearing along the evaluation of all considered two-loop diagrams can be reduced to a set of master integrals using the recurrence algorithm proposed in Ref. [56] which was implemented in the computer program TARCER [57]. The two-loop master integrals required in this work are [46]

$$\mathbf{S}(x, y, z) = \int_2 \frac{1}{[k^2 - x][q^2 - y][(k + q - p)^2 - z]} \quad (3.37a)$$

$$\mathbf{T}(x, y, z) = -\frac{\partial}{\partial x} \mathbf{S}(x, y, z) \quad (3.37b)$$

$$\mathbf{U}(x, y, z, u) = \int_2 \frac{1}{[k^2 - x][(k - p)^2 - y][q^2 - z][(q + k - p)^2 - u]} \quad (3.37c)$$

$$\mathbf{V}(x, y, z, u) = -\frac{\partial}{\partial y} \mathbf{U}(x, y, z, u) \quad (3.37d)$$

$$\mathbf{M}(x, y, z, u, v) = \int_2 \frac{1}{[k^2 - x][q^2 - y][(k - p)^2 - z][(q - p)^2 - u][(k - q)^2 - v]}, \quad (3.37e)$$

with

$$\int_2 = ((4\pi)^2 \mu^{4-D})^2 \int \frac{d^D k}{(2\pi)^D} \int \frac{d^D q}{(2\pi)^D}. \quad (3.38)$$

In the limit of vanishing external momentum, all integrals reduce to the tadpole integral $\mathbf{I}(x, y, z) \equiv \mathbf{S}(x, y, z)|_{p^2=0}$ and derivatives thereof which are known analytically [58]. For arbitrary external momentum and mass parameters, one can rely on numerical techniques such as implemented in the computer program TSIL [59] which numerically solves differential equations involving the master integrals. For the evaluation of the mass counterterm-inserted diagrams, Fig. 3.3(b-c), it is useful to define a special case of the one-loop three-point integral

$$\mathbf{C}(x, y, z) = \frac{\mathbf{B}(y, x) - \mathbf{B}(z, x)}{y - z}. \quad (3.39)$$

The one- and two-loop integrals are further discussed in Chapter 8 and Appendix B.

In Sec. 2.2 we discussed that, due to the Higgs mechanism, all couplings between the SM Higgs boson and the fermions are connected to the VEV of the Higgs boson. Furthermore, the VEV also enters the tree-level mass of the Higgs boson. As a consequence, the one- and two-loop VEV counterterms, $\delta^{(1)}v$ and $\delta^{(2)}v$, are required for the calculation of Fig. 3.3(b-e) and for the determination of the two-loop Higgs mass counterterm in Eq. (3.26). Furthermore, the Higgs mechanism predicts a close connection between the SM VEV and the W^\pm - and Z -boson masses, *cf.* Eq. (2.10). Thus, a two-loop Higgs boson mass calculation, which relies on vector boson masses as input, also requires the one- and two-loop SM vector boson mass counterterms in order to construct the VEV counterterm.

Therefore, we briefly discuss the renormalization of vector boson and fermion mass parameters in Secs. 3.3 and 3.4 while focusing on the construction of mass counterterms. The calculation of wave-function renormalization constants for fermions and vector bosons is not required for this thesis.

3.3. Vector Boson Mass Parameters

The discussion about higher-order corrections to vector boson masses goes along the same lines as the one of the scalar masses, *cf.* Sec. 3.2. However, the tree-level propagator

$$iS_V^{(0)} = \text{wavy} = -i \left[\frac{g^{\mu\nu}}{p^2 - m_V^2} + (\xi_V - 1) \frac{p^\mu p^\nu / (p^2 - m_V^2)}{p^2 - \xi M_V^2} \right] \quad (3.40)$$

of a vector boson V with mass m_V and gauge-fixing parameter ξ_V involves non-trivial Lorentz structures. For simplicity, we work in the Feynman gauge, $\xi_V = 1$, which eliminates the second term in the propagator $\propto p^\mu p^\nu$. If one considers an on-shell decay of a heavy vector $V = W^\pm, Z$ into a pair of fermions with mass m_f , the $p^\mu p^\nu$ are contracted with the 4-momenta of the fermions which yields an overall suppression⁴ m_f^2/m_V^2 such that only the transverse part is of relevance. The Dyson series for the all-orders selfenergy works as in Eq. (3.12) for the scalar field:

$$i\hat{S}_V(p) = \frac{-ig^{\mu\nu}}{p^2 - m_V^2 - \hat{\Pi}_V^T(p^2)}, \quad (3.41)$$

with the transverse part of the renormalized vacuum polarisation tensor which is determined using an appropriate projector,

$$\hat{\Pi}_V^T(p^2) = \frac{1}{D-1} \left(g^{\mu\nu} - \frac{p^\mu p^\nu}{p^2} \right) \left(\text{wavy} \text{ with loop } \right)_{\mu\nu}, \quad (3.42)$$

leading to the following OS counterterm for the squared mass parameter

$$\delta m_V^{2,\text{OS}} = \widetilde{\text{Re}} [\Pi_V^T(p^2 = m_V^2)]. \quad (3.43)$$

Using a loop-expansion of the tree-level relation, Eq. (2.10), between the vector boson masses and the VEV v , one can then connect the counterterms δm_V , $V = W^\pm, Z$, δe and δv with each other. This procedure is discussed in more detail in Sec. 7.2.2 for the complex NMSSM.

The diagrams contributing to the vector boson selfenergy look very similar to the scalar case: replacing the external scalar propagators in Fig. 3.1 with those of the vectors $s_i \rightarrow V_i$ yields all possible generic one-loop diagrams for Π_V^T .

For instance, the leading one-loop corrections from the top-quark to the squared Z -boson mass in the limit of vanishing external momentum in the $\overline{\text{MS}}$ scheme, i.e. Fig. 3.1 (b) with $s_i = Z$ and $F_{1,2} = t, \bar{t}$, reads in the SM

$$\begin{aligned} m_Z^{2(1), \overline{\text{MS}}} &= m_Z^{2(0)} + \hat{\Pi}_Z^T(p^2 = 0) \\ &= m_Z^{2(0)} \left(1 + \frac{3m_t^2}{8\pi^2 v^2} \overline{\log} m_t^2 \right), \quad \text{with } m_Z^{2(0)} = \frac{g_1^2 + g_2^2}{4} v^2, \end{aligned} \quad (3.44)$$

where we have introduced the notation

$$\overline{\log} x = \log \frac{x}{\mu^2}. \quad (3.45)$$

⁴It was shown in Ref. [60], that the one-loop corrections to the longitudinal components indeed vanish in the limit $m_f \rightarrow 0$.

3.4. Fermion Mass Parameters

The propagator

$$iS_F^{(0)} = \longrightarrow = i(\not{p} - m_F)^{-1}, \quad (3.46)$$

of a fermion with mass m_F also receives selfenergy corrections from 1PI diagrams

$$i\hat{S}_F(\not{p}) = \frac{i}{\not{p} - m_F - \hat{\Sigma}_F(\not{p})}, \quad (3.47)$$

with the renormalized selfenergy $\hat{\Sigma}_F(\not{p})$ defined in spinor space. It is convenient to split the selfenergy into vector left/right-handed (VL/VR) and scalar left/right-handed (L/R) parts:

$$\Sigma_F(\not{p}) = [m_F \Sigma_F^L(p^2) + \not{p} \Sigma_F^{VL}(p^2)] P_L + [m_F \Sigma_F^R(p^2) + \not{p} \Sigma_F^{VR}(p^2)] P_R, \quad P_{L/R} = \frac{1 \mp \gamma_5}{2} \quad (3.48)$$

which can be found with the help of appropriate projectors

$$\Sigma_F^{L/R}(p^2) = \frac{\text{Tr} [\Sigma_F(\not{p}) P_{L/R}]}{m_F}, \quad \Sigma_F^{VL/VR}(p^2) = \frac{\text{Tr} [\not{p} \Sigma_F(\not{p}) P_{L/R}]}{p^2}. \quad (3.49)$$

Since $\Sigma_F(\not{p})$ acts in the spinor space, the on-shell condition for the fermion propagator [61] is slightly different from the one for scalar fields:

$$\widetilde{\text{Re}} [\Sigma_F(\not{p}) u(p)|_{\not{p}=m_F}] = 0 \quad \text{and} \quad \widetilde{\text{Re}} [\bar{u}(p) \Sigma_F(\not{p})|_{\not{p}=m_F}] = 0 \quad (3.50)$$

which is used to derive the OS fermion mass counterterm [61]

$$\delta m_F^{\text{OS}} = \frac{m_F}{2} \widetilde{\text{Re}} [\Sigma_F^{VL}(m_F) + \Sigma_F^{VR}(m_F) + \Sigma_F^L(m_F) + \Sigma_F^R(m_F)]. \quad (3.51)$$

In the SM, the leading one-loop contribution to the renormalized top-quark selfenergy originates from Fig. 3.4 (a) and (b) with $\{S, F\} = \{h, t\}$ and $\{V, F\} = \{g, \bar{t}\}$ respectively. Using general statements about the involved dimensions of the couplings, the one-loop corrected top-quark mass in the $\overline{\text{MS}}$ scheme has to scale like

$$m_t^{(1), \overline{\text{MS}}} = m_t^{(0)} + \hat{\Sigma}_t(\not{p} = m_t) \quad (3.52)$$

$$\propto m_t^{(0)} [1 + \mathcal{O}(\alpha_s) + \mathcal{O}(\alpha_t)], \quad \text{with } m_t^{(0)} = \frac{v y_t}{\sqrt{2}}, \quad (3.53)$$

where $\mathcal{O}(\alpha_s)$ with $\alpha_s = g_s^2/4\pi$ are the QCD corrections and $\mathcal{O}(\alpha_t)$ with $\alpha_t = y_t^2/4\pi$ are top-quark Yukawa corrections. The powers of α_X are conventionally used to denote the number of loops originating from a certain sector X of a theory. For instance $\mathcal{O}(\alpha_s \alpha_t)$ denotes two-loop corrections with mixed QCD and Yukawa couplings.

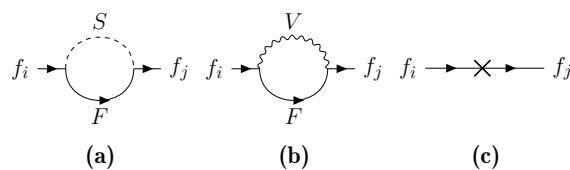


Figure 3.4.: All possible generic fermion one-loop selfenergy diagrams.

The Hierarchy Problem

This chapter briefly discusses one of the major theoretical issues of the SM, the *hierarchy problem*, based on the results of the previous chapters.

We summarize the behavior of the one-loop corrected SM Higgs boson, top-quark and Z -boson masses:

$$m_h^{2(1),\overline{\text{MS}}} \approx m_h^{2(0)} + \frac{3m_t^4}{2\pi^2 v^2} \overline{\log m_t^2}, \quad (4.1)$$

$$m_t^{(1),\overline{\text{MS}}} \approx m_t^{(0)} [1 + \mathcal{O}(\alpha_s) + \mathcal{O}(\alpha_t)] \quad \text{and} \quad (4.2)$$

$$m_Z^{2(1),\overline{\text{MS}}} \approx m_Z^{2(0)} \left[1 + \frac{3m_t^2}{8\pi^2 v^2} \overline{\log m_t^2} \right], \quad (4.3)$$

which have been discussed in Sec. 3.1. A special property of the Z -boson and top-quark masses is that the loop corrections vanish once we set their corresponding tree-level masses to zero

$$\begin{aligned} m_t^{(1),\overline{\text{MS}}} &\xrightarrow{m_t^{(0)} \rightarrow 0} 0, \\ m_Z^{2(1),\overline{\text{MS}}} &\xrightarrow{m_Z^{(0)} \rightarrow 0} 0. \end{aligned} \quad (4.4)$$

This is a consequence of the gauge and chiral symmetries which *protect* the masses of gauge bosons and fermions, respectively. Therefore, Eq. (4.4) also holds to all orders in perturbation theory in any model that preserves the gauge and chiral symmetries. However, the Higgs boson mass $m_h^{2(1)}$ is non-zero even for very small or vanishing tree-level Higgs boson masses. Thus, there is no ad-hoc mechanism in the SM that can protect m_h from receiving very large quantum corrections. Such corrections should appear at latest at the scale where gravity is becoming a strong force, i.e. at the Planck scale $m_{\text{Planck}} \approx 10^{19}$ GeV. Since $m_h \ll m_{\text{Planck}}$, a very large counterterm would be required in order to cancel these corrections. A cancellation in many orders of magnitude can be seen as a sign for a hidden symmetry of the theory which makes this cancellation manifest. The absence of such a symmetry within the SM is called the *hierarchy problem*.

The problem of a light Higgs boson mass in the presence of heavy new physics becomes even more pronounced when considering a UV cut-off Λ to regulate the loop integral $\mathbf{A}(x)$ that contributes to the Higgs boson mass through diagrams like Fig. 3.1 (a). In this scheme, Λ is interpreted as the scale of new physics where the description of particle interactions in the SM breaks down.

While the two-point integral was shown to diverge only logarithmically with Λ , *cf.* Eq. (3.1), the tadpole integral diverges quadratically

$$\mathbf{A}(x) \propto \Lambda^2 + \mathcal{O}(x \log \Lambda^2), \quad (4.5)$$

which yields a much stronger dependence of m_h on the new physics scale Λ than e.g. those of chiral fermions which depend only logarithmically on Λ . Using the mass-regularization scheme, it was shown in Ref. [62] that the one-loop contribution to the Higgs boson mass indeed contains a quadratically divergent component

$$\delta m_h^{2(1),\text{mass-reg.}} = \frac{3\Lambda^2}{v^2(4\pi)^2} \underbrace{(m_Z^2 + 2m_W^2 + m_h^2 - 4m_t^2)}_{\stackrel{!}{=} 0 \text{ (Veltman condition)}} + \mathcal{O}(\log \Lambda^2). \quad (4.6)$$

Postulating a cancellation between the different contributions in Eq. (4.6), also known as the *Veltman condition* [63], had interesting consequences at the time the top-quark mass and the Higgs boson mass were still unknown. Today it is out of question that the Veltman condition can be satisfied within the SM. This can be seen as another manifestation of the hierarchy problem. However, even if not applicable in the SM, it is important to note that the Veltman condition is satisfied for

$$m_Z = m_W = m_h = m_t \quad (4.7)$$

which implies a symmetry among the bosons and fermions. Supersymmetry is such a symmetry. In fact, it was shown in Ref. [64] that supersymmetric theories are free of quadratic divergences. Likewise, it was argued in Ref. [65], that soft-SUSY-breaking contributions (which are discussed later) do not influence the Veltman condition and therefore do not spoil the cancellation of quadratic divergences. Thus, softly broken SUSY, discussed in the next chapter, is a promising candidate for the solution to the hierarchy problem.

Part II.

**Supersymmetric Extensions of the
Standard Model**

In Chapter 4 we introduced supersymmetry as one of the most promising candidates for the solution of the hierarchy problem which is the main motivation for SUSY in this thesis. In this chapter we will provide the basic notation used to describe softly-broken supersymmetric models.

However, SUSY has a long tradition in particle physics since the first supersymmetric QFTs were already formulated in the early 70's [2–7]. Therefore, we refer to the literature [9, 13, 17, 18, 66, 67] for a rigorous introduction into the field.

Supersymmetric gauge theories require the same number of boson and fermion degrees of freedom, $n_B = n_F$, within the individual representations of all gauge groups. For instance, a gauge boson A_μ^a charged under the gauge group G^a with gauge coupling g_a and generators T^a requires the existence of a Weyl spinor λ_a which is usually referred to as the *gaugino* of G_a . The gauge boson and gaugino are combined in one vector *Superfield* $\hat{A}_a = (A_\mu^a, \lambda_a)$ transforming under the adjoint representation of G_a . Likewise, we can define a chiral superfield $\hat{\Phi}_i = (\Phi_i, \Psi_i)$ consisting of a complex scalar field Φ_i and a Weyl spinor Ψ_i (here i is a group index for the fields charged under a specific representation R of G_a). The most general scalar potential V_Φ invariant under SUSY transformations is constructed as follows [9]

$$V_\Phi = \underbrace{\mathcal{W}_i^* \mathcal{W}^i}_{\text{F-Terms}} + \underbrace{\frac{1}{2} g_a^2 \left(\Phi^{i*} T_{ij}^a \Phi^j \right)^2}_{\text{D-Terms}} + \text{soft-breaking terms}, \quad (5.1)$$

where summation over repeated indices is implicit. For our calculation we further require the recipe for the construction of SUSY-invariant interactions between the scalars and Weyl spinors [9]:

$$\mathcal{L}_{\Phi, \Psi, \lambda} = \frac{1}{2} (\mathcal{W}^{ij} \Psi_i \Psi_j + \text{h.c.}) + \sqrt{2} g_a \left((\Phi^{i*} T_{ij}^a \Psi^j) \lambda_a + \text{h.c.} \right) + \text{soft-breaking terms} \quad (5.2)$$

with

$$\mathcal{W}^{i_1, \dots, i_n} = \frac{\delta^n \mathcal{W}}{\delta \Phi_{i_1} \dots \delta \Phi_{i_n}}. \quad (5.3)$$

Superfield	fermion	scalar	generations	$(U_Y(1), SU_L(2), SU_C(3))$
\hat{B}	\tilde{B}	B	1	$(0, \mathbf{1}, \mathbf{1})$
\hat{W}	\tilde{W}	W	1	$(0, \mathbf{3}, \mathbf{1})$
\hat{G}	\tilde{G}	G	1	$(0, \mathbf{1}, \mathbf{8})$
\hat{q}	q	\tilde{q}	3	$(1/6, \mathbf{2}, \mathbf{3})$
\hat{l}	l	\tilde{l}	3	$(-1/2, \mathbf{2}, \mathbf{1})$
\hat{d}	\bar{d}	\tilde{d}^*	3	$(1/3, \mathbf{1}, \bar{\mathbf{3}})$
\hat{u}	\bar{u}	\tilde{u}^*	3	$(-2/3, \mathbf{1}, \bar{\mathbf{3}})$
\hat{e}	\bar{e}	\tilde{e}^*	3	$(1, \mathbf{1}, \mathbf{1})$
\hat{H}_u	\tilde{H}_u	H_u	1	$(1/2, \mathbf{2}, \mathbf{1})$
\hat{H}_d	\tilde{H}_d	H_d	1	$(-1/2, \mathbf{2}, \mathbf{1})$

Table 5.1.: Field content of the MSSM categorized in vector (upper cell) and chiral (two lower cells) superfields. The second and third columns show the notation used for the scalar and fermionic degrees of freedom. The generations and representations in the fourth and fifth column are as in the SM, *cf.* Tab. 2.1.

The *superpotential* $\mathcal{W}(\hat{\Phi}_n)$ is a holomorphic function of the superfields and has mass dimension 3 [9]. It is the central object of the theory and can be constrained by imposing additional symmetries on it. The soft-breaking terms in Eqs. (5.1) and (5.2) break SUSY softly which means that SUSY is only broken by dimensionful parameters. Without specifying the SUSY-breaking mechanism, the most general soft-SUSY-breaking Lagrangian $\mathcal{L}_{\text{soft}}$ consists of all operators with dimension $D < 4$ which obey the gauge symmetries of the model and the discrete symmetries of \mathcal{W} .

In summary, the Lagrangian of a SUSY invariant theory is fully determined by the gauge group, the superpotential and the (super)field content. Sec. 5.1 introduces the MSSM field content and the resulting Lagrangian based on Eqs. (5.1) and (5.2) as well as discusses a selection of theoretical problems of the MSSM. These problems are used as the main motivation for the NMSSM introduced in Sec. 5.2. Section 5.3 discusses the resulting NMSSM tree-level spectrum in more detail while focusing on the parts relevant for the two-loop calculation.

5.1. The Minimal Supersymmetric Standard Model

The field content of the minimal SUSY extension of the SM, the MSSM, is shown in Tab. 5.1 in the same manner as for the SM (all gauge and Lorentz indices are suppressed), *cf.* Tab. 2.1. The MSSM gauge group, shown in the first block, is identical to the SM. Therefore, there are eight additional *gluinos*, three *winos* and one *bino* with spin 1/2 which transform identically to the gluons, W bosons and B boson, respectively. Chiral vector fields are added in the second block such that their fermionic components resemble the field content of the SM lepton and quark sectors. In the last block two additional chiral doublets are added for the sake of electroweak symmetry breaking. The most general lepton- and baryon-number conserving superpotential with the field content of Tab. 5.1 reads:

$$\mathcal{W}_{\text{MSSM}} = -\mathbf{Y}_e \hat{H}_d \cdot \hat{l} \hat{e} - \mathbf{Y}_d \hat{H}_d \cdot \hat{q} \hat{d} + \mathbf{Y}_u \hat{H}_u \cdot \hat{q} \hat{u} + \mu \hat{H}_d \cdot \hat{H}_u, \quad (5.4)$$

where $\mathbf{Y}_{e,d,u}$ are the usual Yukawa matrices and μ is a dimensionful parameter (not to be confused with the μ^2 -parameter of the SM). Color- and generation-indices have been suppressed.

The symplectic product "·" consists of the anti-symmetric tensor $\epsilon_{12} = \epsilon^{12} = 1$. In contrast to the SM, the MSSM requires two Higgs doublets because of the additional constraint of a holomorphic superpotential, since the term which couples \hat{H}_d with \hat{u} would require a complex conjugate. The soft-breaking Lagrangian reads

$$\begin{aligned} \mathcal{L}_{\text{MSSM}}^{\text{soft}} = & -m_{H_d}^2 H_d^\dagger H_d - m_{H_u}^2 H_u^\dagger H_u - \mathbf{m}_{\tilde{q}}^2 \tilde{q}^\dagger \tilde{q} - \mathbf{m}_{\tilde{l}}^2 \tilde{l}^\dagger \tilde{l} \\ & - \mathbf{m}_{\tilde{u}_R}^2 \tilde{u}_R^* \tilde{u}_R - \mathbf{m}_{\tilde{d}_R}^2 \tilde{d}_R^* \tilde{d}_R - \mathbf{m}_{\tilde{e}_R}^2 \tilde{e}_R^* \tilde{e}_R \\ & - \left[B_\mu H_u \cdot H_d - \mathbf{T}_e H_d \cdot \tilde{L} \tilde{e}_R^* - \mathbf{T}_d H_d \cdot \tilde{q} \tilde{d}_R^* + \mathbf{T}_u H_u \cdot \tilde{q} \tilde{u}_R^* \right. \\ & \left. + \frac{M_1}{2} \tilde{B} \tilde{B} + \frac{M_2}{2} \tilde{W}_i \tilde{W}_i + \frac{M_3}{2} \tilde{G} \tilde{G} + \text{h.c.} \right], \end{aligned} \quad (5.5)$$

with the soft gaugino mass parameters $M_{1,2,3}$, the soft trilinear Higgs-sfermion-sfermion coupling matrices $\mathbf{T}_{e,d,u}$, the squared soft bilinear masses B_μ and m_i^2 for the Higgs bosons $i = H_u, H_d$ as well as the soft-breaking mass matrices \mathbf{m}_i^2 for the sfermions, with $i = \tilde{q}, \tilde{u}_R, \tilde{d}_R, \tilde{l}, \tilde{e}_R$ (left- and right-handed squarks as well as sleptons). In general, all mentioned parameters can be complex except for the soft squared mass parameters. With the superfield content given in Tab. 5.1, the superpotential in Eq. (5.5) and the recipes in Eqs. (5.1) and (5.2), all ingredients are available to determine the MSSM Lagrangian. However, the result is rather lengthy and not important for this thesis. Instead, we continue with the discussion of two shortcomings of the MSSM as a motivation for the NMSSM and later derive the NMSSM Lagrangian.

In analogy to EWSB in the SM, the two Higgs doublets are expanded around their minima

$$H_d = \begin{pmatrix} H_d^0 \\ H_d^- \end{pmatrix} = \begin{pmatrix} \frac{v_d + h_d + ia_d}{\sqrt{2}} \\ h_d^- \end{pmatrix} \quad \text{and} \quad H_u = \begin{pmatrix} H_u^+ \\ H_u^0 \end{pmatrix} = e^{i\varphi_u} \begin{pmatrix} \frac{h_u^+}{v_u + h_u + ia_u} \\ \frac{v_u + h_u + ia_u}{\sqrt{2}} \end{pmatrix}, \quad (5.6)$$

with the complex phase φ_u and the ratio of the two VEVs

$$\tan \beta \equiv t_\beta \equiv \frac{v_u}{v_d}, \quad (5.7)$$

such that

$$v^2 = v_u^2 + v_d^2 \approx (246 \text{ GeV})^2 \quad (5.8)$$

coincides with the SM VEV at tree-level. Similarly to the μ^2 -parameter of the SM, one can eliminate $m_{H_u}^2$ and $m_{H_d}^2$ in the MSSM by making use of the tadpole conditions for h_u and h_d . For instance, the tadpole condition for h_u yields

$$\frac{\partial}{\partial v_u} V_{\text{MSSM}} = 0 \quad \Leftrightarrow \quad m_{H_u}^2 = B_\mu t_\beta^{-1} + \frac{m_Z^2}{2} \cos 2\beta - \mu^2, \quad (5.9)$$

which inevitably connects μ with the EWSB and the SUSY-breaking scales. While m_Z and B_μ are connected through some SUSY-breaking mechanism to solve the hierarchy problem, there is no obvious reason why μ should be of the order of the electroweak scale rather than, for instance, at the Plank scale. The lack of an explanation for the size of μ is called the *μ -problem* [68], and is one motivation for considering the NMSSM, which naturally connects μ to the soft-SUSY-breaking scale. Another theoretical problem of the MSSM is the upper bound on the lightest tree-level Higgs boson mass,

$$(m_h^{\text{MSSM}})^2 \leq m_Z^2 \cos^2 2\beta, \quad (5.10)$$

Super field	fermion	scalar	generations	$(U_Y(1), SU_L(2), SU_c(3))$
\hat{S}	\tilde{S}	S	1	$(0, \mathbf{1}, \mathbf{1})$

Table 5.2.: Additional degrees of freedom of the NMSSM compared to the MSSM, *cf.* Tab. 5.1.

which requires very large quantum corrections in order to agree with the experimental value of $m_h \approx 125$ GeV. To achieve higher-order corrections of the order of 40%, the masses of the scalar superpartners need to be above the TeV scale which reintroduces a small hierarchy between the MSSM and the SM. This is called the *little hierarchy problem* and is a further motivation for studying non-minimal SUSY extensions that modify the tree-level prediction for m_h and therefore require smaller loop corrections and soft-SUSY-breaking scales.

5.2. The Next-To-Minimal Supersymmetric Standard Model

There exist several versions of the NMSSM [18]. In this thesis, we focus on a minimal extension which adds one additional singlet superfield, \hat{S} , to the MSSM. The associated components and their transformation under the SM gauge group are listed in Tab. 5.2. The considered superpotential,

$$\mathcal{W}_{\text{NMSSM}} = \mathcal{W}_{\text{MSSM}}|_{\mu=0} + \lambda \hat{S} \hat{H}_d \cdot \hat{H}_u + \frac{1}{3} \kappa \hat{S}^3, \quad (5.11)$$

is identical to the MSSM with a vanishing μ -term and additional singlet couplings. Equation (5.11) exhibits a \mathbb{Z}_3 -symmetry which forbids all scale-dependent terms in the superpotential. The soft-SUSY-breaking Lagrangian is also very similar to the MSSM,

$$\mathcal{L}_{\text{NMSSM}}^{\text{soft}} = \mathcal{L}_{\text{MSSM}}^{\text{soft}}|_{B\mu=0} - m_S^2 |S|^2 + \left(T_\lambda S H_d \cdot H_u - \frac{1}{3} T_\kappa S^3 + \text{h.c.} \right), \quad (5.12)$$

with the soft trilinear couplings $T_{\lambda,\kappa}$ and the soft squared mass parameter m_S^2 . Once the scalar singlet field acquires a VEV,

$$\langle S \rangle = \frac{v_s e^{i\varphi_s}}{\sqrt{2}}, \quad S = \frac{e^{i\varphi_s}}{\sqrt{2}} (v_s + h_s + i a_s), \quad (5.13)$$

with the complex phase φ_s , one can define an effective μ -term:

$$\mathcal{W}_{\text{NMSSM}} \supset \lambda \langle S \rangle H_u \cdot H_d \xrightarrow{\text{SSB}} \frac{\lambda v_s e^{i\varphi_s}}{\sqrt{2}} H_u \cdot H_d \equiv \mu_{\text{eff}} H_u \cdot H_d, \quad (5.14)$$

which plays the very same role as the μ -parameter in the MSSM. However, μ_{eff} is dynamically generated and has its origin in the symmetry-breaking scale of the new scalar singlet mass since one can relate the soft-SUSY-breaking parameter m_S^2 with the singlet VEV v_s by making use of the tadpole equation $\partial V_{\text{NMSSM}} / \partial v_s = 0$. Thus, also $\mu_{\text{eff}}(v_s)$ is now naturally connected to the soft-SUSY-breaking scale which solves the μ -problem of the MSSM discussed in Sec. 5.1. Furthermore, the tree-level prediction for the lightest Higgs boson mass, *cf.* Eq. (5.10), receives an additional contribution from the F-terms

$$(m_h^{\text{NMSSM}})^2 \leq m_Z^2 \cos^2 2\beta + \frac{v^2}{2} \lambda^2 \sin^2 2\beta, \quad (5.15)$$

which can relax the little hierarchy problem discussed in Sec. 5.1.

In summary, the \mathbb{Z}_3 -symmetric NMSSM is a natural extension of the MSSM which does not only solve the little-hierarchy- and the μ -problem, but also features a richer phenomenology due to the additional singlet states.

5.3. The NMSSM Tree-Level Spectrum

We parametrize all trilinear soft-breaking couplings with their superpotential counterparts

$$T_\alpha = \alpha A_\alpha, \quad \alpha = \lambda, \kappa, \quad (5.16a)$$

$$\mathbf{T}_i = \alpha_i \mathbf{A}_i, \quad \alpha_i = \mathbf{Y}_d, \mathbf{Y}_e, \mathbf{Y}_u \quad (5.16b)$$

and use the A_α 's and \mathbf{A}_i 's as input parameters. This parametrization allows us to study the MSSM-limit of the NMSSM

$$\lambda, \kappa \rightarrow 0, \quad v_s \rightarrow \infty \quad \text{and} \quad \mu_{\text{eff}} = \text{constant} \quad (5.17)$$

which decouples the singlet and recovers all couplings of the MSSM. Comparing with the MSSM limit is particularly useful for studying effects that are exclusive to the NMSSM.

In this thesis, we are interested in the two-loop corrections that are proportional to linear combinations of $y_t, \lambda, \kappa, A_t, A_\lambda$ and A_κ . The latter three are by construction always multiplied with y_t, λ and κ , respectively. Therefore, we denote the two-loop corrections studied in this work as $\mathcal{O}((\alpha_t + \alpha_\kappa + \alpha_\lambda)^2)$ corrections. These corrections are the successors of the $\mathcal{O}(\alpha_t^2)$ and $\mathcal{O}(\alpha_t \alpha_s)$ corrections which have been calculated in Refs. [32,33]. The sum of all two-loop contributions as well as the NMSSM-specific contributions are abbreviated as

$$\mathcal{O}(\alpha_{\text{new}}^2) = \mathcal{O}((\alpha_t + \alpha_\kappa + \alpha_\lambda)^2) + \mathcal{O}(\alpha_t \alpha_s), \quad (5.18a)$$

$$\Delta\mathcal{O}(\alpha_{\text{new}}^2) = \mathcal{O}(\alpha_{\text{new}}^2) - \mathcal{O}(\alpha_t \alpha_s) - \mathcal{O}(\alpha_t^2). \quad (5.18b)$$

The complete interaction Lagrangian relevant for the $\mathcal{O}((\alpha_t + \alpha_\kappa + \alpha_\lambda)^2)$ calculation takes a rather simple form

$$V_{\text{NMSSM}}|_{\mathcal{O}((\alpha_t + \alpha_\kappa + \alpha_\lambda)^2)} = V_H + V_{\tilde{t}} + V_{\text{Yukawa}}, \quad (5.19)$$

with the Higgs boson potential

$$V_H = (|\lambda S|^2 + m_{H_d}^2) H_d^\dagger H_d + (|\lambda S|^2 + m_{H_u}^2) H_u^\dagger H_u + m_S^2 |S|^2 + |\kappa S^2 - \lambda H_d \cdot H_u|^2 + \left(\frac{1}{3} \kappa A_\kappa S^3 - \lambda A_\lambda S H_d \cdot H_u + \text{h.c.} \right), \quad (5.20)$$

the stop/sbottom potential

$$V_{\tilde{t}/\tilde{b}} = m_{\tilde{q}_3}^2 \left(|\tilde{t}_L|^2 + |\tilde{b}_R|^2 \right) + m_{\tilde{t}_R}^2 |\tilde{t}_R|^2 + |y_t|^2 \left[|\tilde{t}_R|^2 \left(|\tilde{t}_L|^2 + |\tilde{b}_L|^2 \right) + |H_u^0|^2 \left(|\tilde{t}_R|^2 + |\tilde{t}_L|^2 \right) \right] - y_t \left[A_t \left(\tilde{t}_L \tilde{t}_R^* H_u^0 - \tilde{d}_L \tilde{t}_R^* H_u^+ \right) + (\lambda S)^* \tilde{t}_R^* \tilde{t}_L (H_d^0)^* + \text{h.c.} \right], \quad (5.21)$$

and the fermion-scalar interactions

$$V_{\text{Yukawa}} = \kappa \tilde{S} \tilde{S} S + \lambda \tilde{S} \left(\tilde{H}_u \cdot H_d + \tilde{H}_d \cdot H_u \right) + \lambda S \tilde{H}_d \cdot \tilde{H}_u + y_t \left(t_L \bar{t}_R H_u^0 - d_L \bar{t}_R H_u^+ + d_L \tilde{t}_R^* \tilde{H}_u^+ + t_L \tilde{d}_R^* \tilde{H}_d^- + t_L \tilde{t}_R^* \tilde{H}_d^0 \right) + \text{h.c.}, \quad (5.22)$$

where $t_{L/R}$ and $\tilde{t}_{L/R}$ are the left/right-handed top and stop⁵ fields, $b_{L/R}$ and $\tilde{b}_{L/R}$ are the left/right-handed bottom and sbottom fields, $\tilde{H}_{u/d}$ are the up/down-type higgsinos with the components

$$\tilde{H}_d = \begin{pmatrix} \tilde{H}_d^0 \\ \tilde{H}_d^- \end{pmatrix} \quad \text{and} \quad \tilde{H}_u = \begin{pmatrix} \tilde{H}_u^+ \\ \tilde{H}_u^0 \end{pmatrix}, \quad (5.23)$$

and \tilde{S} is the singlino. From this Lagrangian, we derive all mass matrices and couplings that are generated after the scalar fields develop their VEVs. Note that all contributions from the gauge couplings $g_{1,2,3}$ are set to zero since they do not contribute at the considered order $\Delta\mathcal{O}(\alpha_{\text{new}}^2)$.

⁵Note that scalar superpartners have no chirality but we refer to the chirality of their fermion superpartners.

5.3.1. Higgs Boson Sector

After spontaneous symmetry breaking and expanding the Higgs boson fields around their vacuum expectation values, *cf.* Eqs. (5.6) and (5.13), we parametrize the scalar potential in the broken phase according to

$$V_H \supset \mathbf{t}\mathbf{h} + \mathbf{h}^T \mathcal{M}_{\phi\phi} \mathbf{h} + \mathbf{h}^{+\dagger} \mathcal{M}_{h^+h^-} \mathbf{h}^-, \quad (5.24)$$

with

$$\mathbf{h} = (h_d, h_u, h_s, a_d, a_u, a_s)^T, \quad \mathbf{h}^+ = (h_d^{-,*}, h_u^+)^T,$$

and the tadpole coefficients

$$(\mathbf{t})_\Phi = t_\Phi = \frac{\partial V_H}{\partial \Phi}, \quad \Phi = h_d, h_u, h_s, a_d, a_u, a_s. \quad (5.25)$$

Analytic results for the neutral and charged squared mass matrices \mathcal{M}_{hh} and $\mathcal{M}_{h^+h^-}$ in the most general (CP-violating) case are rather lengthy and given in Appendix F of Ref. [33] using the same notation as in this thesis. Therefore, we refrain from showing them here in full detail. The diagonalization of $\mathcal{M}_{\phi\phi}$ is carried out using a two-fold rotation into the mass basis while $\mathcal{M}_{h^+h^-}$ is diagonalized with one single rotation,

$$\mathcal{M}_{hh} = \mathcal{R}^G(\beta_n) \mathcal{M}_{\phi\phi} (\mathcal{R}^G(\beta_n))^T, \quad (5.26a)$$

$$\text{diag}(m_{h_1}^2, m_{h_2}^2, m_{h_3}^2, m_{h_4}^2, m_{h_5}^2, m_{G^0}^2) = \mathcal{M}'_{hh} = \mathcal{R} \mathcal{M}_{hh} \mathcal{R}^T, \quad (5.26b)$$

$$\text{diag}(M_{H^\pm}^2, m_{G^\pm}^2) = \mathcal{R}^{G^-}(\beta_c) \mathcal{M}_{h^+h^-} (\mathcal{R}^{G^-}(\beta_c))^T, \quad (5.26c)$$

which results in five physical neutral Higgs bosons ordered in mass $m_{h_1} < \dots < m_{h_5}$, two charged Higgs bosons with mass M_{H^\pm} and neutral/charged Goldstone bosons with vanishing masses, $m_{G^{0/\pm}} \equiv m_G = 0$, due to the gaugeless limit $g_{1,2} = 0$.

The rotation \mathcal{R}^G (\mathcal{R}^{G^-}) projects onto the neutral (charged) Goldstone mode. In case of the charged Higgs/Goldstone bosons, the resulting tree-level matrix is already diagonal. The neutral Higgs boson mass matrix is diagonalized by a further rotation \mathcal{R} ,

$$\underbrace{(h_d, h_u, h_s, a_d, a_u, a_s)}_{\substack{\text{gauge basis} \\ \mathcal{M}_{\phi\phi}}} \xrightarrow{\mathcal{R}^G(\beta_n)} \underbrace{(h_d, h_u, h_s, a, a_s, G^0)}_{\substack{\text{Goldstone separated} \\ \mathcal{M}_{hh}}} \xrightarrow{\mathcal{R}} \underbrace{(h_1, h_2, h_3, h_4, h_5, G^0)}_{\substack{\text{mass basis} \\ \mathcal{M}'_{hh}}, \quad (5.27a)$$

$$\underbrace{(h_d^{-,*}, h_u^+)}_{\substack{\text{gauge basis} \\ \mathcal{M}_{h^+h^-}}} \xrightarrow{\mathcal{R}^{G^-}(\beta_c)} \underbrace{(h^+, G^+)}_{\substack{\text{Goldstone separated} \\ \text{diag}(M_{H^\pm}^2, m_{G^\pm}^2)}} = \text{mass basis}. \quad (5.27b)$$

At tree-level all three mixing angles coincide, $\beta_c = \beta_n = \beta$. However, it is still necessary to distinguish between them since β_c and β_n are mixing angles and do not receive a counterterm. Only the counterterm of $\tan \beta = v_u/v_d$ is non-zero. This means that the counterterm δf of any tree-level quantity $f(\beta, \beta_c, \beta_n)$ is calculated from $f(\beta + \delta\beta, \beta_c, \beta_n)|_{\beta_c=\beta_n=\beta}$. Likewise, we keep the dependence on the tree-level tadpole parameters for the construction of the mass counterterms, as discussed in Sec. 3.2, Eq. (3.26). The tadpole dependence introduces many non-zero contributions on diagonal and off-diagonal elements of \mathcal{M}'_{hh} . Of special interest are the Goldstone components in the gaugeless limit which are entirely given by the tadpoles

$$m_{G^0}^2 = m_{G^\pm}^2 \equiv m_G^2 = \frac{s_\beta t_{h_u} + c_\beta t_{h_d}}{v}, \quad (5.28)$$

i.e. the Goldstone boson masses vanish if the tadpoles t_{h_u} and t_{h_d} vanish. This is a crucial result for the discussion in Chapter 8 about the infra-red divergences appearing in the two-loop integrals.

In alignment with the SUSY Les Houches Accord (SLHA) [69, 70], we define the absolute values $|\lambda|$ and $|\kappa|$ as well as the phases φ_λ and φ_κ of λ and κ as independent input parameters. Furthermore, we write $A_{\lambda,\kappa} = \text{Re}A_{\lambda,\kappa} + i\text{Im}A_{\lambda,\kappa}$ and eliminate $\text{Im}A_{\lambda,\kappa}$, as well as the soft-SUSY-breaking masses $m_{H_{u,d},S}^2$, by making use of the tadpole conditions for t_{a_d,a_s} , as well as $t_{h_d,u,s}$, given in Eqs. (2.9)-(2.14) of Ref. [33]. Common linear combinations of CP-violating phases entering the tree-level mass matrices and counterterms are

$$\varphi_y = \varphi_\kappa - \varphi_\lambda + 2\varphi_s - \varphi_u \quad \text{and} \quad (5.29a)$$

$$\varphi_w = \varphi_\kappa + 3\varphi_s. \quad (5.29b)$$

Using these conventions, the massive eigenvalue of \mathcal{M}_{h+h^-} is given by

$$M_{H^\pm}^2 = \frac{|\lambda|c_{\beta-\beta_c}^2 v_s (|\kappa|v_s \cos(\varphi_w) + \sqrt{2}\text{Re}A_\lambda)}{s_{2\beta} \cos(\varphi_y - \varphi_w)} - \frac{1}{2}|\lambda|^2 c_{\beta-\beta_c}^2 v^2 + \frac{s_\beta (c_\beta c_{\beta_c}^2 t_{h_u} + s_\beta s_{\beta_c}^2 t_{h_d}) + c_{\beta-\beta_c}^2 t_{a_d} \tan(\varphi_y - \varphi_w)}{c_\beta s_\beta^2 v}. \quad (5.30)$$

We can also choose to solve Eq. (5.30) for the parameter $\text{Re}A_\lambda$ and therefore replace the dependence on $\text{Re}A_\lambda$ with the dependence on M_{H^\pm} in all Feynman rules and the neutral Higgs boson mass matrix. Thus, we are able to choose between the input parameters M_{H^\pm} and $\text{Re}A_\lambda$ which has interesting implications on the renormalization procedure discussed in Chapter 7.

5.3.2. The Top/Stop and Bottom/Sbottom Sector

If the up-type Higgs boson H_u acquires a VEV, the top quark mass can be read-off from the Yukawa potential in Eq. (5.22). To this point, the top-quark mass is a complex number

$$m_t = \frac{v_u y_t}{\sqrt{2}} e^{i(\varphi_u + \varphi_L - \varphi_R)}, \quad (5.31)$$

where φ_u is the phase of the field H_u and $e^{\varphi_{L/R}}$ are arbitrary $U(1)$ field transformations of the left/right handed quark fields. Therefore, we choose $\varphi_L = -\varphi_R = -\varphi_u/2$ to achieve a real top-quark mass.

The squared mass matrix of the left/right handed scalar top partners $\tilde{t}_{L/R}$ can be derived from the quadratic terms in $V_{\tilde{t}/\tilde{b}}$ with $\sqrt{2}H_u \rightarrow v_u = v \sin \beta$:

$$\mathcal{M}_{\tilde{t}} = \text{diag}(m_{\tilde{t}_1}^2, m_{\tilde{t}_2}^2) = \mathcal{U}^{\tilde{t}} \begin{pmatrix} m_{\tilde{q}_3}^2 + m_t^2 & m_t \left(A_t^* e^{-i\varphi_u} - \frac{\mu_{\text{eff}}}{\tan \beta} \right) \\ m_t \left(A_t e^{i\varphi_u} - \frac{\mu_{\text{eff}}^*}{\tan \beta} \right) & m_{\tilde{t}_R}^2 + m_t^2 \end{pmatrix} \mathcal{U}^{\tilde{t}\dagger}, \quad (5.32)$$

where $\mathcal{U}^{\tilde{t}}$ rotates the left- and right-handed stop fields $\tilde{t}_{L,R}$ into the mass eigenbasis $\tilde{t}_{1,2}$.

There is no mass term for the bottom quark in $V_{\tilde{t}/\tilde{b}}$, since we assume $\mathbf{Y}_d = 0$, and therefore there is no neutral current that would couple the bottom quark to the Higgs boson fields. However, the (massless) bottom quark can still contribute to the diagrammatic calculation through the charged currents in Eq. (5.22) which are proportional to y_t .

The only squared term for the sbottom fields is the squared soft-SUSY-breaking mass for

the superpartners of the left-handed bottom component, $m_{\tilde{q}_3}^2$. Therefore, the gauge- and mass-eigenstate of the sbottom entering the $\mathcal{O}((\alpha_t + \alpha_\kappa + \alpha_\lambda)^2)$ corrections coincide and has a mass

$$m_{\tilde{b}_1}^2 = m_{\tilde{q}_3}^2, \quad (5.33)$$

while the superpartner of the right-handed bottom, \tilde{b}_R , does not contribute in this approximation.

While the tree-level masses for the top/stop and bottom/sbottom fields do not change between $\mathcal{O}(\alpha_t^2)$ and $\Delta\mathcal{O}(\alpha_{\text{new}}^2)$ (i.e. there are no new tree-level contributions to $m_t/m_{\tilde{t}_{1/2}}$ which are proportional to λ or κ), the stop/sbottom potential, $V_{\tilde{t}/\tilde{b}}$ in Eq. (5.21), introduces a new contribution to the quartic Higgs-Stop coupling which is proportional to λ . This means that the results for the two-loop diagrams of $\mathcal{O}(\alpha_t^2)$, previously calculated in Ref. [33], cannot be disentangled and need to be reevaluated at $\mathcal{O}((\alpha_t + \alpha_\kappa + \alpha_\lambda)^2)$ since these diagrams contain mixed contributions of $\mathcal{O}(\alpha_t\alpha_\lambda)$. However, one can still rely on results of the $\mathcal{O}(\alpha_t^2)$ calculation when doing a consistency check in the MSSM limit

$$\lim_{\lambda, \kappa \rightarrow 0} \mathcal{O}((\alpha_t + \alpha_\kappa + \alpha_\lambda)^2) - \mathcal{O}(\alpha_t^2) = 0, \quad (5.34)$$

which was used to cross-check intermediate tree-level, one- and two-loop results that have been obtained analytically.

5.3.3. Electroweakino (EW-ino) Sector

The mass generation for wino, bino, higgsino and singlino interaction states is entirely determined by the Yukawa potential, Eq. (5.22). Since we are applying the limit of vanishing gauge couplings, the gauginos \tilde{B} and \tilde{W} fully decouple. Therefore, we only consider the symmetric 3×3 sub-matrix for the neutral higgsinos and the singlino,

$$\text{diag}(m_{\tilde{\chi}_3^0}, m_{\tilde{\chi}_5^0}, m_{\tilde{\chi}_5^0}) = N^* \begin{pmatrix} 0 & -\mu_{\text{eff}} & -\frac{\lambda}{\sqrt{2}} v_s s_\beta e^{i\varphi_u} \\ -\mu_{\text{eff}} & -\frac{\lambda}{\sqrt{2}} v_s s_\beta e^{i\varphi_u} & -\frac{\lambda}{\sqrt{2}} v c_\beta \\ 0 & -\frac{\lambda}{\sqrt{2}} v c_\beta & \sqrt{2}\kappa v_s e^{i\varphi_s} \end{pmatrix} N^\dagger, \quad (5.35)$$

with the mixing matrix N . Therefore, the singlino and neutral higgsinos ($\tilde{S}, \tilde{H}_u^0, \tilde{H}_d^0$) mix to form the neutralinos ($\tilde{\chi}_3, \tilde{\chi}_4, \tilde{\chi}_5$) in the mass eigenbasis with mass ordering $m_{\tilde{\chi}_3^0} < \dots < m_{\tilde{\chi}_5^0}$. The 1×1 sub-matrix for the chargino (charged higgsino) reads

$$m_{\chi_2^\pm} = m_{\tilde{h}^\pm} = \mu_{\text{eff}} V_{22}^* U_{22}^* \equiv |\mu_{\text{eff}}|, \quad (5.36)$$

where U and V are unitary 2×2 mixing matrices. We absorb the phase of μ_{eff} into the unitary 2×2 chargino mixing matrix V . As a consequence, the higgsino couplings entering the two-loop diagrams will depend on $e^{i\varphi\mu_{\text{eff}}}$.

5.3.4. Summary

Let us shortly summarize the tree-level mass spectrum which is relevant for the two-loop $\mathcal{O}((\alpha_t + \alpha_\kappa + \alpha_\lambda)^2)$ corrections. An overview of the mass and gauge eigenstates is given in Tab. 5.3. The scalar sector consists of five neutral and one charged Higgs boson which have non-zero masses and cubic as well as quartic self-couplings. In the CP-conserving case, there are three CP-even and two CP-odd Higgs bosons. Furthermore, there are two color-charged stop and one sbottom scalars with distinct masses. They couple linearly with all

Gauge basis	mass basis	new couplings
Higgs bosons $H_u^0, H_d^0, S, H_u^+, H_d^-$	$h_1, \dots, h_5, h^\pm, G^0, G^\pm$ $m_{h_1} \leq \dots \leq m_{h_5}, M_{H^\pm},$ $m_{G^0} = m_{G^\pm} = 0$	all cubic and quartic couplings
left-/right-handed stops \tilde{t}_L, \tilde{t}_R	\tilde{t}_1, \tilde{t}_2 $m_{\tilde{t}_1} \leq m_{\tilde{t}_2}$	$y_t \lambda^* S^* \tilde{t}_R \tilde{t}_L H_d^0 + h.c.$
left-handed sbottom \tilde{b}_L	\tilde{b}_1 $m_{\tilde{b}} = m_{\tilde{q}_3}$	-
higgsinos, singlino $\tilde{H}_u^0, \tilde{H}_d^0, \tilde{S}, \tilde{H}_u^+, \tilde{H}_d^-$	$\tilde{\chi}_3, \dots, \tilde{\chi}_5, \tilde{\chi}_2^\pm$ $m_{\tilde{\chi}_3} \leq \dots \leq m_{\tilde{\chi}_5}, m_{\tilde{\chi}_2^\pm}$	all singlino/singlet couplings (first line in Eq. (5.22))
top / bottom $t_{L/R}, b_{L/R}$	t, b $m_t \neq 0, m_b = 0$	-

Table 5.3.: Summary of the gauge and mass eigenstates contributing at $\mathcal{O}((\alpha_t + \alpha_\kappa + \alpha_\lambda)^2)$. The last column lists the couplings which are new compared to the $\mathcal{O}(\alpha_t(\alpha_t + \alpha_s))$ calculations.

considered fermions (top/bottom quark) and Higgs bosons. Furthermore, they feature squark-squark-Higgs-Higgs couplings as well as quartic self-couplings. In the fermion sector three neutral (two higgsinos and one singlino) and one charged $SU_L(2) \otimes U_Y(1)$ fermion (higgsino) contribute with distinct masses as well as the massive top quark and massless bottom quark. The W - and Z -bosons as well as the corresponding Goldstone modes are massless due to the approximation of vanishing gauge couplings. While the W - and Z -bosons do not contribute in loop-propagators, the Goldstone modes have non-zero couplings to the Higgs bosons which are proportional to λ and κ .

One of the main difficulties compared to the $\mathcal{O}(\alpha_t^2)$ corrections is the presence of cubic and quartic Higgs self-couplings which vanish at $\mathcal{O}(\alpha_t^2)$. This leads to an increased number of two-loop diagrams with up to five different mass scales. Moreover, the couplings between the massless Goldstone bosons and the massive Higgs bosons (proportional to λ, κ and g_1, g_2 and therefore absent in the gaugeless limit at $\mathcal{O}(\alpha_t(\alpha_t + \alpha_s))$) generate Feynman diagrams which can be IR divergent due to multiple massless loop propagators. Chapter 8 discusses this issue in detail.

Previous Predictions for the MSSM and NMSSM

In this chapter, we review the higher-order calculations to the Higgs bosons masses in the MSSM and NMSSM as well as discuss how the calculation performed in this thesis relates to previous works. In particular, the numerical analysis of the two-loop $\mathcal{O}((\alpha_t + \alpha_\kappa + \alpha_\lambda)^2)$ corrections to the Higgs boson masses presented in Chapter 9 relies on tree-level, one- and two-loop results previously calculated in the literature. Note, however, that a phenomenologically viable analysis also needs to confront the considered parameter space with available experimental data other than only the SM Higgs boson mass constraint. Higgs search data and exclusion limits are important experimental constraints that also need to be taken into account [8]. Furthermore, the NMSSM can have multiple sources of CP-violating phases which predict the presence of sizeable anomalous electric dipole moments (EDMs) of e.g. the electron or neutron. Therefore, this thesis also makes use of previous results on Higgs signals rates and EDMs which are briefly discussed in Sec. 6.2 and Sec. 6.3.

In the past years, there also have been major improvements in the treatment of IR divergences caused by massless Goldstone bosons which influenced this work. Since these divergences are a crucial part of the calculation performed in this thesis, there is a dedicated discussion about this issue in Chapter 8.

6.1. Higgs Boson Masses

Higher-order corrections to Higgs boson masses can be obtained using three different methods that are based on fixed-order (FO), effective field theory (EFT) or hybrid techniques. In this thesis, FO calculations are defined by calculations which include all corrections of the considered theory at a single renormalization scale while the EFT approach separates the hierarchies in the calculation by making use of RGEs. Hybrid approaches try to combine results of both methods. In the following, we briefly review the progress in the MSSM and NMSSM regarding the three techniques to obtain Higgs boson mass predictions and show how previous works feed into the calculation of this thesis. The focus is on the FO approach in the NMSSM since it concerns the calculation performed in this thesis. For a complete review on Higgs boson mass calculations in SUSY models we refer to Ref. [71].

Concerning the MSSM, FO calculations enjoy a 30-year old tradition with major developments within the last years that range from leading logarithmic to full one- and two-loop

results including CP-violation up to three-loop accuracy in the strong gauge coupling at vanishing external momentum [22, 23, 29, 30, 42, 72–110].

Resummation techniques assume the SM or an extension of it as low-energy EFT of the MSSM and make use of RGEs and threshold corrections by integrating out all heavy degrees of freedom [31, 99, 111–132]. For a more detailed review about the different FO as well as EFT techniques we refer to Ref. [71]. Notably, the FO and EFT calculations have been implemented in a variety of public available computer tools such as `FeynHiggs` [113, 117, 120, 125, 133], `SARAH/SPheno` [134–136], `Flexible SUSY` [119, 137, 138], `SusyHD` [115] or `MhEFT` [116]. This allows us to precisely calculate the MSSM Higgs boson masses at both low and high soft-SUSY breaking scales. Furthermore, generic spectrum generator generators such as `SARAH` [52–54, 139–141] and `FlexibleSUSY` [119, 137, 138] are based on two-loop effective potential [23, 142] and diagrammatic [143–146] results for arbitrary renormalizable field theories in the $\overline{\text{MS}}/\overline{\text{DR}}$ scheme. This allows us to also study the NMSSM at fixed-order with high precision using the $\overline{\text{DR}}$ renormalization scheme which is discussed in the next paragraph.

The NMSSM Higgs boson mass spectrum at fixed-order was first calculated in the CP-conserving case using the one-loop effective potential approach [147–149]. The one-loop corrections including the full external momentum dependence have been calculated in Refs. [103, 141] using a pure $\overline{\text{DR}}$ scheme and in Refs. [150–153] using mixed $\text{OS}/\overline{\text{DR}}$ schemes. The two-loop $\mathcal{O}(\alpha_s(\alpha_t + \alpha_b))$ corrections in the $\overline{\text{DR}}$ scheme have been calculated in Ref. [103] using the effective potential approach. The first effective potential results which include the leading QCD and the full two-loop contributions from all superpotential parameters in the gaugeless limit (i.e. including the NMSSM-specific parameters) have been calculated in Ref. [140] in the $\overline{\text{DR}}$ scheme.

In the CP-violating version of the NMSSM, the one-loop effective potential corrections have been calculated in Refs. [154–157] in the $\overline{\text{DR}}$ scheme. Diagrammatic calculations which incorporate the full external momentum dependence at the one-loop order have been performed in Refs. [103, 141, 158] in the $\overline{\text{DR}}$ and in Ref. [159] in a mixed $\text{OS}/\overline{\text{DR}}$ renormalization scheme. Two-loop effective potential corrections which include the $\mathcal{O}(\alpha_t\alpha_s)$ as well as all contributions from the MSSM and NMSSM superpotential parameters have been calculated in Ref. [160] using the $\overline{\text{DR}}$ scheme. The direct predecessor calculations of this thesis calculated the two-loop $\mathcal{O}(\alpha_t\alpha_s)$ [161] and two-loop $\mathcal{O}(\alpha_t^2)$ [33] corrections using a mixed $\text{OS}/\overline{\text{DR}}$ renormalization scheme in the Feynman diagrammatic approach in the approximation of vanishing external momentum for the CP-violating as well as CP-conserving case. This renormalization scheme is also pursued in this thesis. It uses an OS condition for the SM VEV and gives the possibility to choose between $\text{OS}/\overline{\text{DR}}$ conditions for the charged Higgs boson mass as well as the top/stop sector.

In the discussion of the MSSM, we already mentioned the generic spectrum generators which are also able to study the NMSSM using a $\overline{\text{DR}}$ renormalization scheme. However, NMSSM-specific computer packages exist which go beyond the $\overline{\text{DR}}$ renormalization scheme by implementing the calculations mentioned above. Furthermore, these tools also calculate observables within the NMSSM other than the Higgs boson masses such as for instance various decay widths, EDMs or the Dark Matter (DM) relic density. The program `NMSSMTools` is a consortium of the codes `NMHDECAY` [162, 163], `NMHDECAY_CPV` [158], `NMSDECAY` [164], `NMSPEC` [165], `NMGMSB` [166] and `micrOMEGAS` [167] which can be used to calculate the NMSSM Higgs boson mass spectrum using the two-loop QCD corrections [103] as well as Higgs boson and sfermion decay widths and the dark matter relic density for various SUSY-breaking scenarios in the CP-conserving and CP-violating case. For detailed informations, we refer to the author’s website [168]. The computer code `Next-to-Minimal SOFTSUSY` [169] can calculate the Higgs boson mass spectrum in the case of a \mathbb{Z}_3 -breaking superpotential at the one-loop order and further implements the two-loop QCD corrections from Ref. [103]. The code `NMSSM-FeynHiggs`

calculates the one-loop corrected Higgs boson masses using a mixed OS/ $\overline{\text{DR}}$ scheme (which differs from the scheme employed in this thesis) but combines them with two-loop corrections calculated in the in the MSSM-limit using known analytic MSSM results available in **FeynHiggs**. Furthermore, the program package **NMSSMCALC** [33, 150, 159, 161, 170–173] implements the neutral and charged Higgs boson mass corrections at the full one-loop order and two-loop $\mathcal{O}(\alpha_t(\alpha_t + \alpha_s))$ based on the mixed OS/ $\overline{\text{DR}}$ renormalization which is also pursued in this thesis. The results obtained with **NMSSMCALC** and **NMSSM-FeynHiggs** at $\mathcal{O}(\alpha_t\alpha_s)$ in the CP-conserving case have been compared in detail in Ref. [174] which focused on the differences between their mixed OS/ $\overline{\text{DR}}$ renormalization conditions. In addition, the two-loop $\mathcal{O}(\alpha_t\alpha_s)$ corrections in the CP-violating version of **NMSSMCALC** obtained using the $\overline{\text{DR}}$ scheme in the top/stop sector have been cross-checked with **SARAH** in Ref. [160] which found excellent agreement. **NMSSMCALC** also calculates the decay widths of all Higgs bosons as well as the EDMs which is described in the next sections. A detailed comparison between various spectrum generators for the CP-conserving NMSSM was performed in Ref. [175].

Among all these two-loop corrections, the $\mathcal{O}(\alpha_t(\alpha_t + \alpha_s))$ corrections implemented in **NMSSMCALC** are the only available two-loop results that can take into account NMSSM-specific contributions from OS counterterms of the top/stop sector, electroweak VEV and the charged Higgs boson in the CP-violating and CP-conserving case. However, in Ref. [140] it was shown in the $\overline{\text{DR}}$ context that the two-loop contributions involving the superpotential parameters λ and κ can be as sizeable as the QCD corrections. In order to estimate the uncertainty due to the scheme ambiguity introduced by the $\mathcal{O}((\alpha_t + \alpha_\kappa + \alpha_\lambda)^2)$ corrections, a mixed OS/ $\overline{\text{DR}}$ calculation can be performed. The calculation of these corrections and the implementation in the computer code **NMSSMCALC** is performed in this thesis.

EFT Higgs boson mass predictions for the NMSSM can be obtained by combining tree-level (one-loop) NMSSM results with one-loop (two-loop) MSSM results as it was done in Refs. [119, 153] (Ref. [176]) by assuming only the SM as EFT and performing a pole-mass matching of the SM-like Higgs boson mass. Generic one-loop results based on diagrammatic matchings [136, 177] as well as the effective action [178, 179] can be used to study more complex split-SUSY scenarios with additional light degrees of freedom such as a singlet extended SM in the EFT [180].

6.2. Constraints from Higgs Boson Data

NMSSMCALC is a computer program specifically designed for computing predictions related to the Higgs boson sector of the (CP-violating) NMSSM. It does not only calculate the Higgs boson masses at two-loop $\mathcal{O}(\alpha_t(\alpha_t + \alpha_s))$, which are complemented by the $\mathcal{O}((\alpha_t + \alpha_\kappa + \alpha_\lambda)^2)$ corrections in this work, but also calculates the decay widths of the charged and neutral Higgs bosons including leading QCD and full one-loop electroweak corrections [171–173]. In addition, **NMSSMCALC** calculates effective couplings of the Higgs bosons to gluons, photons, W^\pm/Z -bosons and the top/bottom quark as well as the tau lepton normalized to the value of the respective SM coupling. Using the program packages **HiggsSignals/HiggsBounds** [181–185] this information can be turned into signal strengths which are compared against current collider searches. The return value of **HiggsSignals** is the result of a χ -squared test based on the signal rates and masses showing how compatible the Higgs data collected at collider experiments is with a given parameter point. The precise values of the Higgs boson masses can have an impact on the kinematics of the decays but can also change the mixing between the Higgs boson mass eigenstates and therefore we also expect a different χ -squared value when including the new $\mathcal{O}((\alpha_t + \alpha_\kappa + \alpha_\lambda)^2)$ corrections to the Higgs boson masses.

6.3. Constraints from CP Violation

The current experimental upper bound on e.g. the electron EDM is [186]

$$d_e < 1.1 \times 10^{-29} \text{ ecm}, \quad (6.1)$$

which strongly constrains the CP-violating phases of the NMSSM [187]. The calculation of the electron, neutron, thallium and mercury EDM has been implemented in `NMSSMCALC` in Ref. [187]. It is used in this thesis to study the influence of the CP-violating phases in the new two-loop Higgs boson mass corrections within the range that is compatible with the EDMs.

Part III.

**The $\mathcal{O}((\alpha_t + \alpha_\kappa + \alpha_\lambda)^2)$ Corrections to
Higgs Boson Masses
in the CP-Violating NMSSM**

Renormalization of the NMSSM Higgs Bosons at the Two-Loop Order

In this chapter, we generalize the renormalization prescription discussed in Sec. 3.1 to the Higgs sector of the complex NMSSM. In case of the neutral Higgs bosons, the five mass eigenstates $h_{1,\dots,5}$, which have been diagonalized in Sec. 5.3 at tree-level, mix upon the inclusion of higher-order corrections. Therefore, the pole of the inverse of the propagator is determined by iteratively solving

$$\text{Det} \left(\mathbb{1}_{5 \times 5} p^2 - \mathcal{M}'_{hh} + \hat{\Sigma}_{hh}(p^2) \right) = 0 \quad (7.1)$$

where, $\left(\hat{\Sigma}_{hh} \right)_{ij}$ is the renormalized selfenergy i.e. incorporates the 1PI diagrammatic corrections to the $h_i \rightarrow h_j$ transition. Since also the loop-corrected charged Higgs boson mass is required in our calculation, we omit the hh suffix for the moment as the following definitions also apply for the 2×2 dimensional selfenergy of the charged Higgs/Goldstone bosons $\hat{\Sigma}_{H^+H^-}$. We approximate $\hat{\Sigma}$ to one- and two-loop order as

$$\hat{\Sigma}_{ij}(p^2) = \hat{\Sigma}_{ij}^{(1)}(p^2) + \hat{\Sigma}_{ij}^{(2)}(p^2), \quad (7.2)$$

using the Feynman-diagrammatic approach. The generalization of the renormalized selfenergy to a complex $n \times n$ matrix at the one-loop order is given by

$$\hat{\Sigma}^{(1)}(p^2) = \Sigma^{(1)}(p^2) + \frac{1}{2} \left[\delta^{(1)} \mathcal{Z}^\dagger (\mathbb{1} p^2 - \mathcal{M}) + (\mathbb{1} p^2 - \mathcal{M}) \delta^{(1)} \mathcal{Z} \right] + \delta^{(1)} \mathcal{M}, \quad (7.3)$$

and has already been studied for the complex NMSSM in Ref. [159] including all possible one-loop contributions. The two-loop approximation reads

$$\begin{aligned} \hat{\Sigma}^{(2)}(p^2) = \Sigma^{(2)}(p^2) + \frac{1}{2} \left[\delta^{(2)} \mathcal{Z}^\dagger (\mathbb{1} p^2 - \mathcal{M}) + (\mathbb{1} p^2 - \mathcal{M}) \delta^{(2)} \mathcal{Z} \right. \\ \left. + \frac{1}{2} \delta^{(1)} \mathcal{Z}^\dagger (\mathbb{1} p^2 - \mathcal{M}) \delta^{(1)} \mathcal{Z} - \delta^{(1)} \mathcal{Z}^\dagger \delta^{(1)} \mathcal{M} - \delta^{(1)} \mathcal{M} \delta^{(1)} \mathcal{Z} \right] \\ - \delta^{(2)} \mathcal{M} \end{aligned} \quad (7.4)$$

and was calculated at $\mathcal{O}(\alpha_t \alpha_s)$ and $\mathcal{O}(\alpha_t^2)$ in Refs. [32] and [33] in the gaugeless limit at vanishing external momenta using a mixed OS/ $\overline{\text{DR}}$ renormalization scheme. In order to consistently combine the new corrections with the $\mathcal{O}(\alpha_t \alpha_s)$ corrections from Ref. [32], we

	$v, \sin \theta_w$	$M_{H^\pm}^2 (\text{Re}A_\lambda)$	$m_t, m_{\tilde{t}}, A_t$	t_{h_i, a_i}	$ \lambda , \kappa , v_S,$ $\text{Re}A_\kappa, \tan \beta$	$m_{\tilde{\chi}_i^{0,\pm}}$	$m_{h_i}^2$
OS	×	×	×	×			
$\overline{\text{DR}}$		(×)	×		×	×	×
required CT	$\mathcal{O}(\epsilon^{-2})$	$\mathcal{O}(\epsilon^{-2})$	$\mathcal{O}(\epsilon^{-1})$	$\mathcal{O}(\epsilon^{-2})$	$\mathcal{O}(\epsilon^{-2})$	$\mathcal{O}(\epsilon^{-1})$	$\mathcal{O}(\epsilon^{-2})$

Table 7.1.: The input parameters entering the two-loop selfenergies. The crosses (×) mark whether the parameters are OS and/or $\overline{\text{DR}}$ renormalized (in case of two crosses the user can choose between both, in case of $M_{H^\pm}^2/\text{Re}A_\lambda$ either M_{H^\pm} is chosen as OS input or $\text{Re}A_\lambda$ as $\overline{\text{DR}}$ input). The last row tells up to which order the counterterms are required. The masses of the neutral Higgs boson m_{h_i} (last column) and their counterterms are no input parameters but dependent on the other quantities in the middle part.

apply the same renormalization scheme in this work at the order $\mathcal{O}((\alpha_t + \alpha_\kappa + \alpha_\lambda)^2)$. The total two-loop selfenergy reads:

$$\hat{\Sigma}_{\mathcal{O}(\alpha_{\text{new}}^2)}(p^2) = \hat{\Sigma}_{\mathcal{O}(\alpha_t \alpha_s)}^{(2)}(p^2 = 0) + \hat{\Sigma}_{\mathcal{O}((\alpha_t + \alpha_\kappa + \alpha_\lambda)^2)}^{(2)}(p^2). \quad (7.5)$$

While in Ref. [32] the momentum dependence was neglected at $\mathcal{O}(\alpha_t \alpha_s)$ in the calculation of $\hat{\Sigma}_{\mathcal{O}(\alpha_t \alpha_s)}^{(2)}$, the new selfenergy corrections, $\hat{\Sigma}_{\mathcal{O}((\alpha_t + \alpha_\kappa + \alpha_\lambda)^2)}^{(2)}$, to the neutral Higgs bosons are optionally calculated with finite p^2 to cure the appearance of IR divergences (see Chapter 8 for a detailed discussion). We will later show that the charged Higgs selfenergy is found to be manifestly IR-finite, regardless of the value of p^2 , and therefore is always computed at vanishing external momentum. The same also applies to the calculation of the W -boson and Z -boson selfenergies discussed later.

In the following chapter, we discuss the renormalization schemes and derive all required OS and $\overline{\text{DR}}$ counterterms which enter the two-loop Higgs boson mass counterterm matrices, the two-loop selfenergies and the two-loop Z -factors.

7.1. Employed Strategy of Renormalization

To achieve UV-finite renormalized selfenergies, we have to renormalize all tree-level parameters discussed in Sec. 5.3 to either one- or two-loop order. If the tree-level Higgs boson mass matrix explicitly depends on a parameter, the corresponding counterterm needs to be determined at the two-loop order. If the parameter only starts to contribute to the Higgs boson mass at the one-loop level at $\mathcal{O}(\alpha_\lambda + \alpha_\kappa + \alpha_t)$, then we only need to renormalize it at the one-loop level. This means that the top/stop and electroweakino masses only need to be renormalized at one-loop order while all other parameters that contribute to the tree-level mass matrix have to be evaluated up to $\mathcal{O}(\epsilon^{-2})$.

In Tab. 7.1 we give an overview of the different input parameters and whether they are renormalized in an OS or $\overline{\text{DR}}$ scheme (second row) as well as up to which loop order the corresponding counterterms are evaluated (third row). In addition to the parameters in Tab. 7.1, the phases $\varphi_\alpha, \alpha = s, u, \kappa, \lambda$ are independent input parameters. It turns out, that the phases do not develop a UV-divergence and all counterterms are chosen to identically vanish. According to Tab. 7.1 the renormalization scheme of all parameters is fixed to either $\overline{\text{DR}}$ or OS. However, for the charged Higgs boson (or $\text{Re}A_\lambda$ respectively) and the top/stop sector we leave it open to choose between OS or $\overline{\text{DR}}$ which will allow us to estimate the size of missing higher-order corrections by varying the renormalization scheme. While the top/stop sector can be entirely defined in the OS or $\overline{\text{DR}}$ scheme, the scalar sector will always consist of a mixed OS/ $\overline{\text{DR}}$ combination of counterterms.

7.2. Derivation of all Two- and Sub-Loop Counterterms

In the subsequent sections, we introduce the calculation of the various parameter counterterms at one- and two-loop order in the OS/ $\overline{\text{DR}}$ schemes. If the OS scheme is chosen, the counterterms are calculated from selfenergies which can be expanded up to $\mathcal{O}(\epsilon^1)$. The $\mathcal{O}(\epsilon^1)$ -terms would in principle vanish after taking the limit $\epsilon \rightarrow 0$. However, a strict expansion in ϵ potentially multiplies $\mathcal{O}(\epsilon^{-1})$ and $\mathcal{O}(\epsilon^1)$ terms, thereby the $\mathcal{O}(\epsilon^1\epsilon^{-1})$ -terms yield additional finite parts in intermediate results that do not vanish for $\epsilon \rightarrow 0$. In Sec. 7.2.4 we show that a consistent expansion in ϵ , including $\mathcal{O}(\epsilon^1)$ -contributions in *all* (OS as well as $\overline{\text{DR}}$) counterterms, leads to the cancellation of these additional finite parts and yields the same result for the renormalized selfenergy as if we were ignoring all $\mathcal{O}(\epsilon^1)$ contributions in the first place. Since UV-divergences are universal, we also partially cross-check all OS counterterms by comparing the UV-divergent parts with the corresponding $\overline{\text{DR}}$ counterterms.

The complete renormalization of the NMSSM at the one-loop order has already been worked out in Refs. [151, 152, 159, 171, 188]. Thus, we only give the explicit expressions for all needed one-loop counterterms after applying our approximations discussed in Sec. 5.2. The one-loop OS counterterms are of particular importance as they enter counterterm-inserted diagrams as well as two-loop mass counter terms thereby generating additional finite contributions which are not present in a pure $\overline{\text{DR}}$ calculation.

7.2.1. Electroweak Gauge Bosons and the SM VEV

According to the first column in Tab. 7.1, the electroweak VEV counterterm is defined as OS parameter and required at one- and two-loop order. In Sec. 3.3 we have shown the possibility to relate the SM VEV with the W - and Z -boson masses. The tree-level relation between the VEV and the electroweak sector, *cf.* Eq. (2.10), also holds in the NMSSM:

$$v = \frac{2M_W}{e} s_{\theta_w} = \frac{2M_W}{e} \sqrt{1 - \frac{M_W^2}{M_Z^2}} \quad (7.6)$$

and is expanded using one- and two-loop counterterms

$$x \rightarrow x + \delta^{(1)}x + \delta^{(2)}x, \quad x = e, v, M_W^2, M_Z^2, s_{\theta_w}, \quad (7.7)$$

which yields (using $\delta^{(n)}e = 0$):

$$\frac{\delta^{(n)}v}{v} = \frac{\cos \theta_w^2}{2 \sin \theta_w^2} \left(\frac{\delta^{(n)}M_Z^2}{M_Z^2} - \frac{\delta^{(n)}M_W^2}{M_W^2} \right) + \frac{\delta^{(n)}M_W^2}{2M_W^2} + \delta_{n2}\delta^{(2)}\bar{v}, \quad n = 1, 2, \quad (7.8a)$$

$$\delta^{(2)}\bar{v} = -\frac{1}{8 \sin^4 \theta_w} \left[\left(\frac{\delta^{(1)}M_W^2}{M_W^2} \right)^2 - 2 \cos^2 \theta_w (1 + 2 \sin^2 \theta_w) \frac{\delta^{(1)}M_W^2}{M_W^2} \frac{\delta^{(1)}M_Z^2}{M_Z^2} + \cos^2 \theta_w (1 + 3 \sin^2 \theta_w) \left(\frac{\delta^{(1)}M_Z^2}{M_Z^2} \right)^2 \right], \quad (7.8b)$$

where δ_{nm} is the Kronecker delta. Using OS conditions for the W and Z bosons as described in Sec. 3.3,

$$\delta^{(n)}M_V^2, \text{OS} = \Sigma_V^{(n)T}(p^2 = m_V^2 = 0), \quad V = W, Z, \quad (7.9)$$

yields an OS VEV counterterm $\delta^{(n)}v^{\text{OS}}$. While the transverse part of the vector boson self-energies and their tree-level masses vanish in the gaugeless limit, $\Sigma_{W,Z}^{(n)T} = 0$ and $M_{W,Z}^2 = 0$,

their ratio contributing to the VEV counterterms is non-zero. However, the counterterm for the electric charge, *i.e.* $\delta^{(n)}e$, is given by the photon selfenergy which vanishes in the gaugeless limit. The vector boson selfenergies are calculated at vanishing external momentum using the procedure described in Chapter 8.

In order to cross-validate our result, we compare the UV-divergent part obtained from the diagrammatic calculation with the $\overline{\text{DR}}$ counterterm which can be constructed using results from the literature. In the $\overline{\text{DR}}$ scheme one can make use of the general relation [189, 190]

$$\frac{\delta^{(n)}v_i^{\overline{\text{DR}}}}{v_i^{\overline{\text{DR}}}} = \frac{1}{2}\Delta^{(n)}Z_{\phi_i}^{\overline{\text{DR}}} \quad (7.10)$$

which connects the counterterm of the VEV v_i to the field renormalization constant of the respective field ϕ_i of any renormalizable QFT. Expanding the tree-level relation $v^2 = v_u^2 + v_d^2$ up to two-loop order, we can express the SM VEV counterterm through the Z -factors of the gauge eigenstates $H_{u,d}$:

$$\frac{\delta^{(n)}v^{\overline{\text{DR}}}}{v^{\overline{\text{DR}}}} = \frac{s_\beta^2}{2}\Delta^{(n)}Z_{H_u}^{\overline{\text{DR}}} + \frac{c_\beta^2}{2}\Delta^{(n)}Z_{H_d}^{\overline{\text{DR}}} + \delta_{2n}\frac{s_{2\beta}^2}{32}\left(\delta^{(1)}Z_{H_d}^{\overline{\text{DR}}} - \delta^{(1)}Z_{H_u}^{\overline{\text{DR}}}\right)^2 \quad n = 1, 2. \quad (7.11)$$

We find full agreement between the UV-divergent part of our diagrammatic approach for the OS VEV, Eq. (7.8), and the $\overline{\text{DR}}$ counterterm Eq. (7.11). The derivation of the Z -factors at one- and two-loop order which are required for this cross-check is discussed in Sec. 7.2.3.

The one-loop counterterm of the weak mixing angle, $\delta^{(1)}\sin\theta_w$, is required since it enters the diagrammatic calculation via vertex-counterterm diagrams. We derive $\delta^{(1)}\sin\theta_w$ by solving Eq. (7.6) for $\sin\theta_w$ and proceeding in the same way as for $\delta^{(1)}v$:

$$\delta^{(1)}\sin\theta_w = \frac{c_{\theta_w}^2}{2s_{\theta_w}}\left(\frac{\delta^{(1)}M_Z^2}{M_Z^2} - \frac{\delta^{(1)}M_W^2}{M_W^2}\right). \quad (7.12)$$

The linear combination $(\Sigma_Z^{(n)}/M_Z^2 - \Sigma_W^{(n)}/M_W^2)$ is proportional to the oblique T parameter [191] and therefore UV-finite. We explicitly verified that $\delta^{(1)}s_{\theta_w}^{\overline{\text{DR}}}$ vanishes while $\delta^{(1)}s_{\theta_w}^{\text{OS}}$ is UV-finite. It is useful to write the one-loop OS counterterms in the following form

$$\delta^{(1)}v^{\text{OS}} = \delta^{(1)}v^{\text{OS}}|_{\text{fin}} + \frac{1}{\epsilon}\delta^{(1)}v^{\text{OS}}|_{\epsilon^{-1}} + \epsilon\delta^{(1)}v^{\text{OS}}|_{\epsilon} \quad (7.13)$$

and similarly for all other one-loop OS counterterms derived in the following.

7.2.2. Fermion Sector

The fermion masses do not enter the tree-level Higgs boson mass matrix but only contribute as internal loop propagators of one- and two-loop Higgs boson selfenergies. At the two-loop level, we therefore have to calculate the one-loop mass counterterms as well as the Yukawa coupling counterterms of all contributing fermions.

Top-Quark Mass and Yukawa Coupling

If the top-quark mass is defined as OS input parameter, we calculate its counterterm from the vector and scalar components of the top selfenergy, *cf.* Sec. 3.4:

$$\delta^{(1)}m_t^{\text{OS}} = \frac{m_t^{\text{OS}}}{2}\widetilde{\text{Re}}\left[\Sigma_t^{(1),VL} + \Sigma_t^{(1),VR} + \Sigma_t^{(1),L} + \Sigma_t^{(1),R}\right] \quad (7.14)$$

evaluated at $p^2 = (m_t^{\text{OS}})^2$ in the gaugeless limit $g_{1,2,3} \rightarrow 0$. The counterterm of the top-Higgs Yukawa coupling, which contributes in one-loop diagrams with a vertex counterterm, can be derived by expanding the expression for the tree-level top mass Eq. (5.31):

$$\delta^{(1)}y_t^{\text{OS}} = \frac{\sqrt{2}}{s_\beta v^{\text{OS}2}} \left(v^{\text{OS}}\delta^{(1)}m_t^{\text{OS}} - m_t^{\text{OS}}\delta^{(1)}v^{\text{OS}} - v^{\text{OS}}m_t^{\text{OS}}c_\beta^2 t_\beta^{-1}\delta^{(1)}t_\beta \right), \quad (7.15)$$

where the counterterm δt_β of $\tan\beta$ is derived in the next section.

If the top quark is defined as $\overline{\text{DR}}$ parameter, we can simply set $\delta^{(1)}y_t^{\text{OS}}|_{\text{fin}} = \delta^{(1)}y_t^{\text{OS}}|_\epsilon = 0$ and similarly for the mass counterterm. As a further cross-check, we can compare against the $\overline{\text{DR}}$ counterterm which we get from the renormalization group equations for y_t calculated with the help of the computer package **SARAH**:

$$\delta^{(1)}m_t^{\overline{\text{DR}}} = \frac{1}{\epsilon}\delta^{(1)}m_t^{\text{OS}}|_{\epsilon^{-1}} \quad (7.16)$$

$$= \frac{1}{\sqrt{2}} \left[v^{\overline{\text{DR}}}s_\beta\delta^{(1)}y_t^{\overline{\text{DR}}} + y_t^{\overline{\text{DR}}} \left(s_\beta\delta^{(1)}v^{\overline{\text{DR}}} + c_\beta^3 v^{\overline{\text{DR}}}\delta^{(1)}\tan\beta \right) \right] \quad (7.17)$$

$$\delta^{(1)}y_t^{\overline{\text{DR}}} = \frac{1}{2\epsilon}\beta_{y_t}^{(1)} = y_t^{\overline{\text{DR}}}\frac{k}{2} \left(|\lambda|^2 + 6y_t^{\overline{\text{DR}2}} \right), \quad (7.18)$$

where $\beta_{y_t}^{(1)}$ is the beta function of the top-quark Yukawa coupling y_t in the NMSSM and

$$k = (4\pi)^{-2}. \quad (7.19)$$

We explicitly verified that using Eq. (7.18) in Eq. (7.17) yields the same result for $\delta^{(1)}m_t^{\overline{\text{DR}}}$ as using our diagrammatic result in Eq. (7.16). Likewise, the single pole of the diagrammatic result in Eq. (7.15) is identical to Eq. (7.18).

Chargino and Neutralino Masses

The electroweakino masses are defined in the $\overline{\text{DR}}$ scheme and are dependent on the other input parameters discussed in this chapter. Therefore, it is sufficient to replace all parameters x in the chargino/neutralino mass matrices by $x \rightarrow x + \delta^{(1)}x$ and to consistently expand them up to one-loop order.

In Sec. 5.3.3 we found that the tree-level mass of the chargino is given by the absolute value of the effective μ_{eff} parameter. Thus, the corresponding counterterm reads

$$\delta^{(1)}m_{\chi_2^\pm} = \delta|\mu_{\text{eff}}| = \frac{1}{\sqrt{2}} \left(v_s\delta^{(1)}|\lambda| + |\lambda|\delta^{(1)}v_s \right), \quad (7.20)$$

where the counterterms $\delta^{(1)}|\lambda|$ and $\delta^{(1)}v_s$ are derived in the next section.

The symmetric neutralino counterterm mass matrix reads in the gauge basis:

$$\left(\delta^{(1)}m_{\chi^0} \right)_{34} = -e^{i(\varphi_\lambda + \varphi_s)}\delta^{(1)}m_{\chi_2^\pm} \quad (7.21a)$$

$$\left(\delta^{(1)}m_{\chi^0} \right)_{35} = -\frac{e^{i\varphi_u}v\lambda}{\sqrt{2}} \left(c_\beta^3\delta^{(1)}\tan\beta + s_\beta\frac{\delta^{(1)}|\lambda|}{|\lambda|} + s_\beta\frac{\delta^{(1)}v}{v} \right) \quad (7.21b)$$

$$\left(\delta^{(1)}m_{\chi^0} \right)_{45} = -\frac{c_\beta v\lambda}{\sqrt{2}} \left(\frac{\delta^{(1)}|\lambda|}{|\lambda|} + \frac{\delta^{(1)}v}{v} - c_\beta s_\beta\delta^{(1)}\tan\beta \right) \quad (7.21c)$$

$$\left(\delta^{(1)}m_{\chi^0} \right)_{55} = \sqrt{2}e^{i\varphi_s}|\kappa|v_s \left(\frac{\delta^{(1)}|\kappa|}{|\kappa|} + \frac{\delta^{(1)}v_s}{v_s} \right), \quad (7.21d)$$

while the upper 2×2 matrix for the gaugino mass counterterms vanishes. The rotation into the mass basis (*cf.* Eq. (5.35))

$$\delta^{(1)} M_{\chi^0} = N^* \delta^{(1)} m_{\chi^0} N^\dagger, \quad (7.22)$$

diagonalizes the tree-level mass matrix m_{χ^0} but not necessarily the counterterm mass matrix $\delta^{(1)} M_{\chi^0}$ which is in general not diagonal.

In order to cross-validate the electroweakino mass counterterms, we verified that they lead to UV-finite chargino/neutralino selfenergies.

7.2.3. Scalar Sector

The scalar sector requires the renormalization at the one- and two-loop level of the superpotential parameters which are connected to the field renormalization constants. Furthermore, the one- and two-loop counterterms of the charged Higgs boson mass and soft-SUSY-breaking parameters are required. The stop sector is, however, only needed at the one-loop order.

Squark Masses and Soft-SUSY-Breaking Quark Yukawa Couplings

The renormalization of the squark sector at the one-loop level using OS conditions has been formulated in Ref. [192]. For completeness we repeat the basic ingredients here. Without further specification of a renormalization scheme, we can derive relations between the counterterms of the Lagrangian parameters $m_{\tilde{t}_R}^2$, $m_{\tilde{q}_3}^2$, A_t and the counterterms of the stop masses $m_{\tilde{t}_{1,2}}^2$. In order to do so, we consider the one-loop expansion of Eq. (5.32) in the gauge basis:

$$U_{\tilde{t}}^\dagger \begin{pmatrix} \delta m_{\tilde{t}_1}^2 & \delta Y_{\tilde{t}} \\ \delta Y_{\tilde{t}}^* & \delta m_{\tilde{t}_2}^2 \end{pmatrix} U_{\tilde{t}} = \delta \begin{pmatrix} m_{\tilde{q}_3}^2 + m_t^2 & m_t \left(A_t^* e^{-i\varphi_u} - \frac{\mu_{\text{eff}}}{\tan \beta} \right) \\ m_t \left(A_t^* e^{-i\varphi_u} - \frac{\mu_{\text{eff}}}{\tan \beta} \right)^* & m_{\tilde{t}_R}^2 + m_t^2 \end{pmatrix} \quad (7.23)$$

where $\delta Y_{\tilde{t}}$ is used to render the off-diagonal elements of the stop quark selfenergy UV-finite. Solving the diagonal and off-diagonal elements for $\delta m_{\tilde{q}_3}^2$, $\delta m_{\tilde{t}_R}^2$ and δA_t yields:

$$\delta m_{\tilde{q}_3}^2 = |\mathcal{U}_{11}^{\tilde{t}}|^2 \delta m_{\tilde{t}_1}^2 + |\mathcal{U}_{12}^{\tilde{t}}|^2 \delta m_{\tilde{t}_2}^2 \mathcal{U}_{21}^{\tilde{t}} \mathcal{U}_{11}^{\tilde{t}*} \delta Y_{\tilde{t}} + \mathcal{U}_{11}^{\tilde{t}} \mathcal{U}_{21}^{\tilde{t}*} \delta Y_{\tilde{t}}^* - 2m_t \delta m_t, \quad (7.24a)$$

$$\delta m_{\tilde{t}_R}^2 = |\mathcal{U}_{12}^{\tilde{t}}|^2 \delta m_{\tilde{t}_1}^2 + |\mathcal{U}_{22}^{\tilde{t}}|^2 \delta m_{\tilde{t}_2}^2 \mathcal{U}_{22}^{\tilde{t}} \mathcal{U}_{12}^{\tilde{t}*} \delta Y_{\tilde{t}} + \mathcal{U}_{12}^{\tilde{t}} \mathcal{U}_{22}^{\tilde{t}*} \delta Y_{\tilde{t}}^* - 2m_t \delta m_t \quad (7.24b)$$

and

$$\delta A_t = \frac{e^{-i\varphi_u}}{m_t} \left[\mathcal{U}_{11}^{\tilde{t}} \mathcal{U}_{11}^{\tilde{t}*} \left(\delta m_{\tilde{t}_1}^2 - \delta m_{\tilde{t}_2}^2 \right) + \mathcal{U}_{11}^{\tilde{t}} \mathcal{U}_{22}^{\tilde{t}*} \delta Y_{\tilde{t}}^* + \mathcal{U}_{21}^{\tilde{t}} \mathcal{U}_{12}^{\tilde{t}*} \delta Y_{\tilde{t}} - \delta m_t \left(A_t e^{i\varphi_u} - \frac{\mu_{\text{eff}}^*}{t_\beta} \right) - \frac{m_t \mu_{\text{eff}}^*}{t_\beta^2} \delta^{(1)} \tan \beta + \frac{m_t}{t_\beta} \delta^{(1)} \mu_{\text{eff}}^* \right]. \quad (7.25)$$

Since the top/stop sector is only needed at one-loop order, we omit the (1)-suffix on all corresponding loop-quantities for simplicity. The counterterm for A_t is of particular interest since it also enters Feynman diagrams with a vertex counterterm insertion. If the squark sector is renormalized on-shell, we use the conditions

$$0 = \widetilde{\text{Re}} \Sigma_{\tilde{t}_i \tilde{t}_i} (m_{\tilde{t}_i}^2) - \delta m_{\tilde{t}_i}^{2, \text{OS}}, \quad i = 1, 2 \quad \text{and} \quad (7.26a)$$

$$0 = \frac{1}{2} \widetilde{\text{Re}} \left(\Sigma_{\tilde{t}_1^* \tilde{t}_2} (m_{\tilde{t}_1}^2) + \Sigma_{\tilde{t}_1^* \tilde{t}_2^*} (m_{\tilde{t}_2}^2) \right) - \delta Y_{\tilde{t}}^{\text{OS}}, \quad (7.26b)$$

to obtain $\delta m_{\tilde{t}_i}^{2, \text{OS}}$ and $\delta Y_{\tilde{t}}^{\text{OS}}$, which enter the mass counterterm-inserted diagrams. Using Eqs. (7.24) and (7.25) leads to the on-shell counterterms $\delta m_{\tilde{q}_3}^{2, \text{OS}}$, $\delta m_{\tilde{t}_R}^{2, \text{OS}}$ and δA_t^{OS} .

In the $\overline{\text{DR}}$ scheme we again utilize the beta functions (note that we parameterized $T_{y_t} = y_t A_t$) calculated with SARAH:

$$\delta A_t^{\overline{\text{DR}}} = \frac{1}{2\epsilon} \frac{\beta_{T_{y_t}} - A_t \beta_{y_t}}{y_t} \quad (7.27a)$$

$$= k (|\lambda|^2 A_\lambda + 6 A_t y_t^2), \quad (7.27b)$$

$$\delta m_{\tilde{q}_3}^{2, \overline{\text{DR}}} = \frac{1}{2\epsilon} \beta_{m_{\tilde{q}_3}^2} = \frac{k}{\epsilon} y_t^2 \left(|A_t|^2 + m_{\tilde{q}_3}^2 + m_{\tilde{t}_R}^2 + c_\beta^2 M_{H^\pm}^2 - \frac{1}{2} |\lambda|^2 v_s^2 \right), \quad (7.27c)$$

$$\delta m_{\tilde{t}_R}^{2, \overline{\text{DR}}} = 2 \delta m_{\tilde{q}_3}^{2, \overline{\text{DR}}}, \quad (7.27d)$$

which have been verified to agree with the single-poles of the corresponding OS counterterms.

Higgs Boson Wave-Function Renormalization Constants

The fields of the Higgs boson gauge eigenstates are renormalized multiplicatively as described in Sec. 3.1, Eq. (3.6b):

$$\Phi \rightarrow \left(1 + \frac{1}{2} \Delta^{(1)} Z_\Phi + \frac{1}{2} \Delta^{(2)} Z_\Phi \right) \Phi, \quad \Phi = H_{u,d}, S. \quad (7.28)$$

The Z -factors are defined in the $\overline{\text{DR}}$ scheme. In Sec. 3.1, we discussed, that they are connected to the derivatives of the selfenergies

$$\delta^{(n)} Z_\Phi = - \left. \frac{\partial \Sigma_{\Phi\Phi}^{(n)}(p^2)}{\partial p^2} \right|_{\text{UV-div}}, \quad (7.29)$$

where only the UV-divergent parts are taken into account due to the $\overline{\text{DR}}$ nature. In the $\overline{\text{DR}}$ scheme, it is also possible to derive the Z -factors using generic results for the anomalous dimension γ_Φ of the Higgs bosons in general QFTs [189, 190]:

$$\delta^{(1)} Z_\Phi = \frac{1}{\epsilon} \gamma_\Phi^{(1)}, \quad (7.30a)$$

$$\delta^{(2)} Z_\Phi = \frac{1}{2\epsilon} \gamma_\Phi^{(2)} + \frac{1}{2\epsilon^2} \left[(\gamma_\Phi^{(1)})^2 + \sum_x \beta_x^{(1)} \frac{\partial \gamma_\Phi^{(1)}}{\partial x} \right], \quad (7.30b)$$

with $x = \{y_t, \lambda, \kappa\}$. The γ_Φ 's have been derived with the help of SARAH and cross-checked against explicit results given in Refs. [189, 190]. This is a further cross-check for the calculation of the selfenergies.

However, there is a subtle difference between Eq. (7.29) and Eq. (7.30): the parameters entering the anomalous dimension matrix as well as the beta functions are defined in a pure $\overline{\text{DR}}$ scheme while the quantities entering the selfenergies can be defined in a different renormalization scheme. Thus, a scheme change in e.g. the top sector from $\overline{\text{DR}}$ to OS will lead to a different result when using the method of computing the derivative of the selfenergies. Therefore, we label the Z -factors with OS/ $\overline{\text{DR}}$ which fixes the renormalization of the top/stop sector entering the Z -factors (while the Z -factors are always defined in the $\overline{\text{DR}}$ scheme). At one-loop order only tree-level quantities enter (which are identical in all schemes). Therefore, the Z -factors agree in both schemes:

$$\delta^{(1)} Z_{H_d}^{\overline{\text{DR}}} = \delta^{(1)} Z_{H_d}^{\text{OS}} = -k |\lambda|^2 \quad (7.31a)$$

$$\delta^{(1)} Z_{H_u}^{\overline{\text{DR}}} (y_t^{\overline{\text{DR}}} = y_t^{\text{OS}}) = \delta^{(1)} Z_{H_u}^{\text{OS}} = -k (|\lambda|^2 - 3 y_t^{\text{OS}2}) \quad (7.31b)$$

$$\delta^{(1)} Z_{H_s}^{\overline{\text{DR}}} = \delta^{(1)} Z_{H_s}^{\text{OS}} = -k (|\lambda|^2 + |\kappa|^2). \quad (7.31c)$$

If we renormalize all parameters in Tab. 7.1 in the $\overline{\text{DR}}$ scheme, we obtain at two-loop

$$\delta^{(2)} Z_{H_d}^{\overline{\text{DR}}} = -\frac{k^2}{2} |\lambda|^2 \left[2|\kappa|^2 + 3|\lambda|^2 + 3y_t^{\overline{\text{DR}^2}} \right] \left(\frac{1}{\epsilon^2} - \frac{1}{\epsilon} \right) \quad (7.32a)$$

$$\delta^{(2)} Z_{H_u}^{\overline{\text{DR}}} = -\frac{k^2}{2} |\lambda|^2 \left[2|\kappa|^2 + 3|\lambda|^2 + 9 \frac{y_t^{\overline{\text{DR}^2}}}{|\lambda|^2} \right] \left(\frac{1}{\epsilon^2} - \frac{1}{\epsilon} \right) \quad (7.32b)$$

$$\delta^{(2)} Z_{H_s}^{\overline{\text{DR}}} = -4k^2 \left[|\kappa|^4 + |\kappa|^2 |\lambda|^2 + \frac{|\lambda|^4}{2} + \frac{3}{4} |\lambda|^2 y_t^{\overline{\text{DR}^2}} \right] \left(\frac{1}{\epsilon^2} - \frac{1}{\epsilon} \right) \quad (7.32c)$$

In Eq. (7.31b) it was used that the $\overline{\text{DR}}$ and OS parameters are identical at tree-level. However, at the one-loop order this is no longer the case. From this, one can show that the scheme change from $y_t^{\overline{\text{DR}}}$ to y_t^{OS} will introduce additional higher-order contributions in the one-loop field constant $\delta^{(1)} Z_{H_u} (y_t^{\text{OS}} + \delta^{(1)} y_t^{\text{OS}})$ that are of two-loop order (i.e. contributing to $\delta^{(2)} Z_{H_u}$). Thus, the two-loop field constants with an OS-label are

$$\delta^{(2)} Z_{H_d}^{\text{OS}} = \delta^{(2)} Z_{H_d}^{\overline{\text{DR}}} \quad (7.33a)$$

$$\delta^{(2)} Z_{H_u}^{\text{OS}} = \delta^{(2)} Z_{H_u}^{\overline{\text{DR}}} (y_t^{\text{OS}}) + \left(\frac{\partial}{\partial y_t^{\text{OS}}} \delta^{(1)} Z_{H_u}^{\text{OS}} \right) \left(\delta^{(1)} y_t^{\text{OS}} \Big|_{\text{fin}} \right) \quad (7.33b)$$

$$\delta^{(2)} Z_{H_s}^{\text{OS}} = \delta^{(2)} Z_{H_s}^{\overline{\text{DR}}}, \quad (7.33c)$$

which are still $\overline{\text{DR}}$ -renormalized but only refer to the additional UV-divergent sub-loop contributions from the top sector. Using Eq. (7.15) and expanding to $\mathcal{O}(\epsilon^{-1})$ one finds:

$$\delta^{(2)} Z_{H_u}^{\text{OS}} - \delta^{(2)} Z_{H_u}^{\overline{\text{DR}}} = -\frac{1}{\epsilon} \frac{3m_t^{\text{OS}^2}}{4\pi^2 v^2 s_\beta^2} \left(\frac{\delta^{(1)} m_t^{\text{OS}} \Big|_{\text{fin}}}{m_t^{\text{OS}}} - \frac{\delta^{(1)} v^{\text{OS}} \Big|_{\text{fin}}}{v^{\text{OS}}} \right), \quad (7.34)$$

which is consistent with the result of the $\mathcal{O}(\alpha_t^2)$ calculation in Ref. [33]. The result can also be understood and validated with the diagrammatic calculation: the only way a finite part $\delta C|_{\text{fin}}$ of any OS counterterm δC can contribute to the UV-poles of the derivative of the selfenergy is via the counterterm-inserted diagram shown in Fig. 7.1. In all other diagrams there is no $\delta C|_{\text{fin}} \cdot \epsilon^{-1}$ -term left after taking the derivative w.r.t. p^2 . Therefore, only OS fermion masses and VEVs can generate a scheme shift in the two-loop Z -factors but no OS scalar masses. The analytic results for $\delta^{(1)} m_t^{\text{OS}}$ and $\delta^{(1)} v^{\text{OS}}$ are presented in Appendix A.

In general, the diagrammatic approach of calculating $\delta^{(2)} Z_{H_i}$ will give the same result for any value of p^2 in Eq. (7.29). Therefore, it is common to calculate the derivative in Eq. (7.29) at $p^2 = 0$ since it is less computational intensive. However, at $\mathcal{O}((\alpha_t + \alpha_\kappa + \alpha_\lambda)^2)$ in the limit $p^2 \rightarrow 0$ the coefficients of intermediate results of the derivatives of some Feynman diagrams feature logarithmic and quadratic IR divergences due to the massless Goldstone bosons. This issue is discussed in more detail in Chapter 8. By introducing a mass regulator for the vanishing Goldstone boson masses, we verified that there is no dependence on the mass regulator in

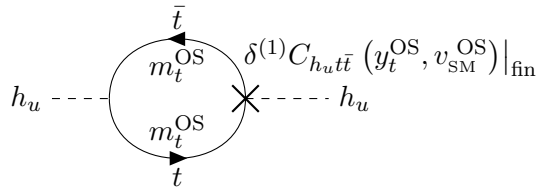


Figure 7.1.: The diagram that leads to a difference in the single pole of the two-loop wave function renormalization constant $\delta^{(2)} Z_{H_u}$ if the top quark and v are renormalized OS.

the sum of the derivatives of all Feynman diagrams. As a further cross-check, we have taken into account the full momentum dependence in the UV-divergent parts of all diagrams (which avoids all IR divergences) and verified that also the p^2 -dependence cancels in the sum of the derivatives of all diagrams. The two methods of calculating the Z -factors diagrammatically fully agree with the method of using the analytic results Eq. (7.30). This does not only serve as a good cross-check for the calculation of the Z -factors, but also for the selfenergies and the treatment of the IR divergences discussed later.

Finally, the field renormalization matrices which are used in the renormalized charged/neutral Higgs boson selfenergies, *cf.* Eqs. (7.3) and (7.4), are obtained with the rotation transformations defined in Eq. (5.26):

$$\delta^{(n)} \mathcal{Z}^G = \text{diag}(\Delta^{(n)} Z_{H_d}, \Delta^{(n)} Z_{H_u}, \Delta^{(n)} Z_S, \Delta^{(n)} Z_{H_d}, \Delta^{(n)} Z_{H_u}, \Delta^{(n)} Z_S), \quad (7.35a)$$

$$\delta^{(n)} \mathcal{Z} = R^G \left(\delta^{(n)} \mathcal{Z}_G \right) (R^G)^T, \quad (7.35b)$$

$$\delta^{(n)} \mathcal{Z}_{H^\pm} = R^{G^-} \left(\delta^{(n)} \mathcal{Z}_G \Big|_{\text{upper } 2 \times 2} \right) (R^{G^-})^T, \quad n = 1, 2, \quad (7.35c)$$

which separates the Goldstone modes. For the Z -factor matrix of the charged Higgs bosons, only the upper 2×2 sub-matrix of $\delta^{(n)} \mathcal{Z}^G$ is required.

Tadpole Parameters

The renormalization condition for the tadpole parameters is chosen such that the minimum at two-loop order is identical to the tree-level minimum, *cf.* Sec. 3.2. In the basis with $\phi = h_{d,u,s}, a_{d,s}$, where the Goldstone modes are separated, the counterterms read

$$\delta^{(1)} t_\phi = t_\phi^{(1)}, \quad (7.36a)$$

$$\delta^{(2)} t_\phi = t_\phi^{(2)} - \frac{\delta^{(1)} Z_\phi}{2} \delta^{(1)} t_\phi, \quad (7.36b)$$

where $t_\phi^{(n)}$ is the n -loop one-point function of the external field ϕ . In Tab. 7.1, we call this an OS condition even though the tadpoles are strictly speaking not associated with any on-shell field.

All one- and two-loop tadpole Feynman diagrams calculated in this thesis are discussed in Appendix D.1.

Ratio of the Up- and Down-Type VEVs ($\tan \beta$)

The ratio of the VEVs v_u and v_d of the doublets H_u and H_d defines the mixing angle $\tan \beta$ which diagonalizes the charged Higgs boson mass matrix at tree-level, *cf.* Sec. 5.3.1. Using the relation in Eq. (7.10), the counterterm of $\tan \beta(v_u, v_d)$ can be related to the field renormalization constants of H_u and H_d which are defined in the $\overline{\text{DR}}$ scheme. Therefore, $\tan \beta$ is also defined in the $\overline{\text{DR}}$ scheme. At one-loop order we find

$$\delta^{(1)} t_\beta = \frac{t_\beta}{2} \left(\Delta^{(1)} Z_{H_u} - \Delta^{(1)} Z_{H_d} \right) = k \frac{3 t_\beta}{2 \epsilon} y_t^{\overline{\text{DR}}^2}, \quad (7.37)$$

while the two-loop expansion yields

$$\delta^{(2)} t_\beta = \frac{t_\beta}{2} \left(\Delta^{(2)} Z_{H_u} - \Delta^{(2)} Z_{H_d} \right) + \frac{t_\beta}{4} \left[\left(\delta^{(1)} Z_{H_d} \right)^2 - \delta^{(1)} Z_{H_d} \delta^{(1)} Z_{H_u} \right]. \quad (7.38)$$

Since the two-loop t_β counterterm depends on $\delta^{(2)} Z_{H_u}$, it will also receive additional UV-divergent contributions if the top sector is renormalized in the OS rather than $\overline{\text{DR}}$ scheme. Therefore, we also define $\delta^{(2)} t_\beta^{\overline{\text{DR}}}$ and $\delta^{(2)} t_\beta^{\text{OS}}$ accordingly.

Charged Higgs Boson Mass Parameter

In Sec. 5.3.1 we showed that it is possible to trade the parameter $\text{Re}A_\lambda$ in terms of $M_{H^\pm}^2$. When doing so, the neutral Higgs boson mass matrix depends on $M_{H^\pm}^2$ rather than on $\text{Re}A_\lambda$ and thus is sensitive to a scheme change between OS and $\overline{\text{DR}}$ conditions in the charged Higgs boson mass at one as well as two-loop order. Likewise, the counterterm of $\text{Re}A_\lambda/M_{H^\pm}$ enters many Feynman rules (counterterm-inserted diagrams) which can affect the phenomenology. In this thesis, the charged Higgs boson selfenergy is always calculated in the limit of vanishing external momentum as discussed later in Chapter 8. Therefore, the mass counterterm receives additional field renormalization contributions (which would otherwise cancel if $p^2 = M_{H^\pm}^2$ is chosen). At one-loop order the counterterm reads:

$$\delta^{(1)} M_{H^\pm}^2 = \Sigma_{H^-H^-}^{(1)}(p^2 = 0) - M_{H^\pm}^2 \delta^{(1)} \mathcal{Z}_{H^\pm}^{(H^-, H^-)}, \quad (7.39)$$

while at two-loop order we have

$$\begin{aligned} \delta^{(2)} M_{H^\pm}^2 = & \Sigma_{H^-H^-}^{(2)}(p^2 = 0) - M_{H^\pm}^2 \left[\frac{1}{4} \left(\delta^{(1)} \mathcal{Z}_{H^\pm}^{(H^-, H^-)} \right)^2 + \delta^{(2)} \mathcal{Z}_{H^\pm}^{(H^-, H^-)} \right] \\ & - \delta^{(1)} \mathcal{Z}_{H^\pm}^{(H^-, H^-)} \delta^{(1)} M_{H^\pm}^2 - \delta^{(1)} \mathcal{Z}_{H^\pm}^{(H^-, G^-)} \delta^{(1)} m_{H-G^-}, \end{aligned} \quad (7.40)$$

with the (n, m) component of the charged Higgs boson Z -factor matrix $\mathcal{Z}_{H^\pm}^{(n, m)}$ given in Eq. (7.35) and the Goldstone-Higgs mixing counterterm

$$\delta^{(1)} m_{H-G^-} = \frac{-c_\beta^2 M_{H^\pm}^2 v \delta^{(1)} t_\beta + c_\beta \delta^{(1)} t_{h_u} - s_\beta \delta^{(1)} t_{h_d}}{v} + \frac{i \delta^{(1)} t_{ad}}{s_\beta v}. \quad (7.41)$$

In the $\overline{\text{DR}}$ scheme, we can set $\delta^{(n)} M_{H^\pm}^2, \overline{\text{DR}} = \delta^{(n)} M_{H^\pm}^2, \text{OS} \Big|_{\text{UV-div}}$. If $\text{Re}A_\lambda$ is chosen as input parameter, we can solve $M_{H^\pm}^2(\text{Re}A_\lambda)$ for $\text{Re}A_\lambda$ and can express $\delta^{(n)} \text{Re}A_\lambda$ in terms of $\delta^{(n)} M_{H^\pm}^2$ such that we effectively do not require the counterterm of $\text{Re}A_\lambda$. The definition of the soft-SUSY-breaking parameter counterterms is described in the next paragraph in more detail. Note that also some of the Feynman diagrams contributing to the charged Higgs boson selfenergy are IR-divergent. However, the sum of all diagrams and therefore the mass counterterm itself is IR-finite as described in Chapter 8.

Superpotential- and Soft-SUSY-Breaking Parameters

One benefit that comes with the enhanced symmetry of SUSY models is that the renormalization of all parameters in the superpotential is significantly simplified. The SUSY-nonrenormalization theorems, *cf.* Refs. [193–195], state that the superpotential is free of any UV divergences except for those originating from wave-function corrections. Consequently, the counterterms for the superpotential parameters are entirely fixed by the Z -factors.

The bare (unrenormalized) NMSSM-specific superpotential contributions,

$$\mathcal{W}_{\text{NMSSM}}^0 \supset \lambda^0 S^0 H_u^0 \cdot H_d^0 + \frac{\kappa^0}{3} (S^0)^3, \quad (7.42)$$

can be expressed in terms of the renormalized couplings and fields,

$$|\lambda^0| \rightarrow |\lambda| + \delta^{(1)} |\lambda| + \delta^{(2)} |\lambda|, \quad (7.43a)$$

$$|\kappa^0| \rightarrow |\kappa| + \delta^{(1)} |\kappa| + \delta^{(2)} |\kappa|, \quad (7.43b)$$

$$\Phi^0 \rightarrow \Phi \left(1 + \frac{1}{2} \Delta^{(1)} Z_\Phi + \frac{1}{2} \Delta^{(2)} Z_\Phi \right), \quad \Phi = H_{u,d}, S \quad (7.43c)$$

and expanded up to one- and two-loops. According to the SUSY-non-renormalization theorems, the resulting renormalized superpotential is UV-finite, such that we can solve for the counterterms of λ and κ . At the one-loop order, we find for the renormalized superpotential using Eqs. (7.42) and (7.43)

$$\begin{aligned} \mathcal{W}_{\text{NMSSM}} \supset & \underbrace{\left(|\lambda| + \delta^{(1)}|\lambda| + \frac{|\lambda|}{2} \sum_i^{H_d, H_u, S} \delta^{(1)} Z_i \right)}_{\stackrel{!}{=} 0} e^{i\varphi_\lambda} S H_u \cdot H_d \\ & + \left(\frac{|\kappa|}{3} + \underbrace{\frac{\delta^{(1)}|\kappa|}{3} + \frac{\delta^{(1)} Z_{H_s}}{2}}_{\stackrel{!}{=} 0} \right) e^{i\varphi_\kappa} S^3. \end{aligned} \quad (7.44)$$

Solving for the counterterms, we find full agreement with the results obtained from the beta functions for λ and κ :

$$\delta^{(1)}|\lambda| = \frac{k}{2\epsilon} \beta_{|\lambda|}^{(1)} = -\frac{|\lambda|}{2} \sum_i^{H_d, H_u, S} \delta^{(1)} Z_i = \frac{k|\lambda|}{2\epsilon} \left(2|\kappa|^2 + 4|\lambda|^2 + 3y_t^{\overline{\text{DR}}^2} \right), \quad (7.45a)$$

$$\delta^{(1)}|\kappa| = \frac{k}{2\epsilon} \beta_{|\kappa|}^{(1)} = -\frac{3|\kappa|}{2} \delta^{(1)} Z_{H_s} = \frac{3k}{\epsilon} |\kappa| (|\kappa|^2 + |\lambda|^2). \quad (7.45b)$$

The same procedure leads to the following two-loop counterterms in the $\overline{\text{DR}}$ scheme:

$$\delta^{(2)}|\lambda| = -\frac{|\lambda|}{2} \left[\sum_{i,j}^{H_d, H_u, S} \left(\Delta^{(2)} Z_i - \frac{1}{4} \delta^{(1)} Z_i \delta^{(1)} Z_j (1 + \delta_{ij}) \right) \right], \quad (7.46a)$$

$$\delta^{(2)}|\kappa| = -3 \frac{|\kappa|}{2} \left(\Delta^{(2)} Z_S - \left(\delta^{(1)} Z_S \right)^2 \right). \quad (7.46b)$$

Note that also $\delta^{(2)}|\lambda|$ depends on $\delta^{(2)} Z_{H_u}$ and therefore implicitly also depends on the renormalization scheme chosen in the top sector.

Analogous to the counterterm of the SM VEV in the $\overline{\text{DR}}$ scheme, we can also calculate the singlet VEV counterterm using the general identity from Eq. (7.10):

$$\delta^{(n)} v_S = \frac{v_S}{2} \Delta^{(n)} Z_{H_s}, \quad n = 1, 2. \quad (7.47)$$

We proceed with the counterterms of the soft-SUSY-breaking couplings. The counterterm $\delta^{(1)} \text{Re} A_\kappa$ is defined in the $\overline{\text{DR}}$ scheme and can be constructed using the one-loop beta function for κ and T_κ :

$$\begin{aligned} \delta^{(1)} \text{Re} A_\kappa &= \frac{k}{2\epsilon} \text{Re} \frac{\beta_{T_\kappa}^{(1)} - A_\kappa \beta_\kappa^{(1)}}{\kappa} \\ &= \frac{6k}{\epsilon} (|\kappa|^2 \text{Re} A_\kappa + |\lambda|^2 \text{Re} A_\lambda). \end{aligned} \quad (7.48)$$

Likewise, the counterterm of the soft-SUSY-breaking coupling $\text{Re} A_\lambda$, which is required if M_{H^\pm} is chosen in the $\overline{\text{DR}}$ scheme, reads:

$$\delta^{(1)} \text{Re} A_\lambda^{\overline{\text{DR}}} = \frac{k}{\epsilon} (2|\kappa|^2 \text{Re} A_\kappa + 4|\lambda|^2 \text{Re} A_\lambda + 3A_t y_t^2). \quad (7.49)$$

Inverting the relation between the charged Higgs boson mass and $\text{Re} A_\lambda$, *cf.* Eq. (5.30), one can choose to parametrize the counterterms of $\text{Re} A_\lambda$ and $\text{Re} A_\kappa$ in terms of the parameters

M_{H^\pm} , v , m_t and t_i :

$$\begin{aligned} \text{Re}A_\lambda = & m_{H^\pm}^2 + \frac{t_\beta v^2 |\lambda| c_{\varphi_w - \varphi_y}}{(1 + t_\beta^2) \sqrt{2} v_S} - \frac{v_S}{\sqrt{2}} |\kappa| c_{\varphi_w} \\ & + \frac{\sqrt{2}}{v v_S |\lambda|} (s_{\varphi_w - \varphi_y} t_{a_d} - c_{\varphi_w - \varphi_y} (s_\beta^3 t_{h_d} + c_\beta^3 t_{h_u})) . \end{aligned} \quad (7.50)$$

The implicit dependence of $\delta^{(1)} \text{Re}A_{\kappa, \lambda}$ on the potentially OS defined parameters is useful to study the generation of higher-order corrections when performing a scheme change by expanding $(\partial_{X^{\text{OS}}} \delta^{(1)} A_{\kappa, \lambda}) (\delta^{(1)} X^{\text{OS}}|_{\text{fin}})$, $X = \{v, M_{H^\pm}, m_t, t_i\}$.

Furthermore, we can perform a one- and two-loop counterterm expansion of Eq. (7.50) to obtain a relation between the counterterm of $\text{Re}A_\lambda$ and $M_{H^\pm}^2$. Thus, we can eliminate $\delta^{(n)} \text{Re}A_\lambda$, $n = 1, 2$ in both the $\overline{\text{DR}}$ and OS scheme using the numerical results for the UV-divergent and UV-finite parts of the charged Higgs selfenergy.

The last missing two-loop counterterm is $\delta^{(2)} \text{Re}A_\kappa$ which is defined in the $\overline{\text{DR}}$ scheme. Since multiple components of the renormalized neutral Higgs boson selfenergy matrix depend on $\delta^{(2)} \text{Re}A_\kappa$, we can determine it by demanding UV-finiteness in one of the components it contributes to. We choose to demand the (3,3)-component to be UV-finite,

$$\hat{\Sigma}_{h_3 h_3} \Big|_{\text{UV-div}} = 0, \quad (7.51)$$

and solve it for $\delta^{(2)} \text{Re}A_\kappa$. It was verified that the solution of Eq. (7.51) for $\delta^{(2)} \text{Re}A_\kappa$ also renders all other components of the selfenergy UV-finite. However, one can also obtain an analytic expression for $\delta^{(2)} \text{Re}A_\kappa$ (and analogously for $\delta^{(2)} \text{Re}A_\lambda$) using one- and two-loop beta functions, respectively counterterms [49]:

$$\delta^{(2)} \text{Re}A_\kappa = \frac{1}{2\epsilon} \text{Re} \frac{\beta_{T_\kappa}^{(2)} - A_\kappa \beta_\kappa^{(2)}}{\kappa} + \frac{1}{2} \sum_x \left(\frac{\partial}{\partial x} \delta^{(1)} \text{Re}A_\kappa \right) \delta^{(1)} x, \quad (7.52)$$

with $x = \{\text{Re}A_\kappa, \text{Re}A_\lambda, |\kappa|, |\lambda|, \text{Re}A_t, y_t\}$. Solving Eq. (7.51) for $\delta^{(2)} \text{Re}A_\kappa$ has been verified numerically with the analytic result of Eq. (7.52) using the two-loop beta functions for κ and T_κ obtained with SARAH and the counterterms derived above.

Neutral Higgs Boson Mass Matrix

The (one-loop) two-loop counterterm for the neutral Higgs boson mass matrix is given by the (one-loop) two-loop expansion of the tree-level mass matrix in the basis where the Goldstone bosons have been separated (*cf.* Eq. (5.27b)),

$$\mathcal{M}_{hh} + \delta^{(n)} \mathcal{M}_{hh} = \mathcal{M}_{hh}(x \rightarrow x + \sum_{m=1}^n \delta^{(m)} x), \quad n = 1, 2, \quad (7.53)$$

with all parameters x for which we have derived the one- and two-loop counterterms in the previous paragraphs. The resulting counterterm matrix was cross-validated with the previous calculation in Appendix G of Ref. [33].

7.2.4. Independence of $\mathcal{O}(\epsilon^1)$ Counterterms

A consistent expansion in ϵ using OS one-loop mass counterterms demands to expand all contributing loop functions and tensor structures up to $\mathcal{O}(\epsilon^1)$:

$$\delta^{(1)} X^{\text{OS}} = \delta^{(1)} X^{\text{OS}}|_{\text{fin}} + \frac{1}{\epsilon} \delta^{(1)} X^{\text{OS}}|_{\epsilon^{-1}} + \epsilon \delta^{(1)} X^{\text{OS}}|_{\epsilon^1}. \quad (7.54)$$

These contributions can be multiplied with the single-pole of other loop functions in counterterm-inserted diagrams, *cf.* Fig. 3.3(b-e), or with the single-pole of other one-loop counterterms $\delta^{(1)} X^{\text{OS}} \delta^{(1)} Y$ in the two-loop mass counterterm of the neutral Higgs bosons. Therefore, the $\mathcal{O}(\epsilon^1)$ contributions give a finite contribution after renormalization in the limit $\epsilon \rightarrow 0$.

At the order $\mathcal{O}(\alpha_t(\alpha_t + \alpha_s))$ it was shown that the finite contributions generated by the $\mathcal{O}(\epsilon^1)$ -terms of the top-quark mass counterterm can be compensated by a finite shift in the two-loop wave-function renormalization constant $\delta^{(2)} Z_{H_u}$ [29, 32, 33, 161].

In the calculation of this thesis, the OS counterterms of v , the charged Higgs boson mass and the tadpoles can generate finite parts in addition to the top quark mass counterterm. We find that these finite parts can also be canceled in the renormalized selfenergy if all two-loop $\overline{\text{DR}}$ counterterms which depend at one-loop order on the OS parameters, are *consistently* expanded in ϵ . *Consistent* means that the finite shifts generated at two-loop by the $\mathcal{O}(\epsilon^1)$ counterterms are also taken into account in the $\overline{\text{DR}}$ parameters. This is the same procedure as the consistent expansion in $\delta^{(2)} Z_{H_u}$, *cf.* Eq. (7.34), in order to cancel all the sub-loop divergences. The finite parts that are generated by the ϵ -expansion can be derived by expanding the one-loop counterterms in Eq. (7.31b) and Sec. 7.2.3:

$$\delta^{(2)} Z_{H_u}^{\text{OS}} \Big|_{\text{fin}} = \sum_{\alpha}^{v, m_t} \left(\frac{\partial}{\partial \alpha^{\text{OS}}} \delta^{(1)} Z_{H_u} \right) \left(\epsilon \delta^{(1)} \alpha^{\text{OS}} \Big|_{\epsilon^1} \right), \quad (7.55a)$$

$$\delta^{(2)} \tan^{\text{OS}} \beta \Big|_{\text{fin}} = \frac{\tan \beta}{2} \delta^{(2)} Z_{H_u}^{\text{OS}} \Big|_{\text{fin}}, \quad (7.55b)$$

$$\delta^{(2)} |\lambda^{\text{OS}}| \Big|_{\text{fin}} = -\frac{|\lambda|}{2} \delta^{(2)} Z_{H_u}^{\text{OS}} \Big|_{\text{fin}}, \quad (7.55c)$$

$$\delta^{(2)} \text{Re} A_{\kappa}^{\text{OS}} \Big|_{\text{fin}} = \sum_{\alpha} \left(\frac{\partial}{\partial \alpha} \delta^{(1)} \text{Re} A_{\kappa} \right) \left(\epsilon \delta^{(1)} \alpha^{\text{OS}} \Big|_{\epsilon^1} \right), \alpha = \{v, M_{H^{\pm}}^2, t_{h_d, h_u, a_d}\}. \quad (7.55d)$$

Furthermore, we require a finite shift of the OS VEV counterterm $\left(\partial_v \delta^{(1)} v \Big|_{\epsilon^{-1}} \right) \left(\delta^{(1)} v \Big|_{\epsilon^1} \right)$ which is generated at the two-loop order. The superscript "OS" on the left-hand side of Eq. (7.55) refers to the OS-nature of the implicit dependent parameters. We have explicitly verified that the renormalized selfenergies are identical if we calculate them (*i*) including the $\mathcal{O}(\epsilon^1)$ counterterm contributions *and* the finite shift from Eq. (7.55) or (*ii*) if we truncate the counterterms at $\mathcal{O}(\epsilon^0)$ and use the original $\overline{\text{DR}}$ counterterms derived in Secs. 7.2.1 to 7.2.3 which are compatible with the beta functions. Therefore, the parameters Z_{H_u} , $\tan \beta$, $|\lambda|$ and $\text{Re} A_{\kappa}$ using (*ii*) are $\overline{\text{DR}}$ quantities as the finite parts of their counterterms Eq. (7.55) do not contribute to the physical result. In summary, we have shown that the two renormalization procedures (*i*) and (*ii*) yield the same result and are therefore equivalent.

In order to save computational resources, the practical implementation in the computer code `NMSSMCALC` does not contain the $\mathcal{O}(\epsilon)$ contributions in the OS one-loop counterterms and does not include any finite terms in the two-loop $\overline{\text{DR}}$ counterterms.

Two-Loop Corrections in the Gaugeless limit

In Chapter 7, we already mentioned the appearance of IR divergences in intermediate results of the two-loop counterterms $\delta^{(2)}t_i$, $\delta^{(2)}v$, $\delta^{(2)}M_{H^\pm}$ and $\delta^{(2)}Z_{H_i}$ which cancel in the sum of all Feynman diagrams contributing to the counterterms. This kind of IR divergence is called *unphysical* in the following. However, in the calculation of the neutral Higgs boson selfenergies, in the limit of vanishing external momentum, also IR divergences appear which do not cancel in the final result. These divergences are called *genuine* IR divergences in the following. In this chapter, we discuss the different possible treatments of the unphysical as well as genuine IR divergences applied in this work in more detail.

In the following, we briefly review the appearance of IR divergences in the context of Higgs boson mass predictions. The term *Goldstone Boson Catastrophe* (GBC) goes back to unphysical results that appear in higher-order corrections to the SM effective potential [196]. In the general R_ξ gauge the Goldstone boson G , which gives the mass m_V to the vector boson V , has a squared mass of $m_G^2 = \xi_V m_V^2$. Therefore, the Goldstone boson mass vanishes in the Landau gauge where $\xi_V = 0$ is chosen. However, there are higher-order contributions to the n -loop effective potential which scale purely logarithmically with the Goldstone boson mass i.e. $V_{\text{eff}}^{(n)} \propto \overline{\log} m_G^2$ for n large enough. Therefore, the effective potential seems not to be IR-finite in the limit of vanishing Goldstone boson masses. Furthermore, derivatives of the effective potential will feature IR divergence at even lower orders in perturbation theory. This has strong implications for all Higgs boson mass calculations which use the approximation of vanishing external momentum⁶.

While this problem can in principle be avoided by choosing a different gauge, it cannot be fully circumvented. For instance, in the SM at three-loops in the Landau gauge, the effective potential was minimized iteratively using numerical methods in Ref. [196]. During the iterative procedure (where the Goldstone masses do not vanish since one is not at the minimum) the squared Goldstone masses can also become (close to) zero or even turn negative within intermediate iterations which causes numerical instabilities. See also Ref. [196] for a detailed study. Solutions to the problem of IR divergences in the effective potential have been worked

⁶The k th derivative of $V_{\text{eff}}^{(n)}$ w.r.t the scalar field S is identical to the sum of all 1PI Feynman diagrams of the k -point function with external fields S at vanishing external momentum i.e. the first derivative gives the n -loop tadpole and the second the n -loop $\overline{\text{MS}}/\overline{\text{DR}}$ mass in the limit of vanishing external momentum.

out in Refs. [24, 197] for the SM and extended to the MSSM in Ref. [26]. The principle of their solution is to resum the Goldstone contributions by integrating out all heavy degrees of freedom when calculating the $n - 1$ loop-corrected Goldstone boson mass and use this *effective* Goldstone boson mass in the minimization of the n -loop effective potential. The authors of Ref. [25] finally proved that this procedure resums the unphysical IR divergences to all orders in perturbation theory and leads to an IR-finite effective potential. Furthermore, Refs. [24, 25] introduced an alternative method which defines the Goldstone boson masses to vanish on-shell at the sub-loop level. The equivalence between the two approaches was shown recently in Ref. [27] at the two-loop order. Furthermore, Ref. [27] derived a closed analytic and IR-safe form of the effective potential and its first derivative at the two-loop order for arbitrary renormalizable QFTs.

However, the second derivative of the effective potential is not necessarily IR-finite even if the Goldstone boson contributions are resummed or the Goldstone boson mass is set on-shell. In the Feynman diagrammatic approach, these divergences are the *genuine* IR divergences which appear due to Feynman diagrams with external momentum flowing through a sub-loop diagram which is a Goldstone boson selfenergy graph. For a vanishing Goldstone boson mass, the only mass scale in the (sub) loop is the external momentum, such that the diagrams scale with $\overline{\log p^2}$. Therefore, $p^2 \rightarrow 0$ is not a good approximation for such diagrams since there is no other mass scale to which it could be comparably small.

A new solution to the GBC which also addresses the genuine divergences was derived in Ref. [27] which combines the resummation techniques with approximate solutions from diagrammatic calculations in the small-momentum region. In practice this means that Ref. [27] resums the IR divergences in the effective potential and its first derivative. Once the unphysical divergences have been removed, finite external momentum is introduced but only in the loop integrals which are genuinely IR divergent while all other contributions are still calculated in the zero-momentum approximation. In addition, the loop functions are expanded around small external momentum to only include the dangerous $\overline{\log p^2}$ terms. This is called the *generalized effective potential approximation* which is a big step towards automated calculations in the pure $\overline{\text{MS}}/\overline{\text{DR}}$ scheme. It was implemented in the computer code `SARAH` and used to investigate two-loop corrections to Higgs boson masses in the SM, 2HDM, NMSSM, Split SUSY and the Georgi-Machacek model, *cf.* Ref. [28].

The previous works were centered around the effective potential and its derivatives. This work uses the Feynman diagrammatic approach to calculate all scalar one- and two-point functions at the two-loop order in the CP-violating NMSSM. Starting from the approximation of vanishing external momenta, the two approaches should in general be equivalent. However, there is a minor but important difference: while the generalized effective potential developed in Ref. [27] was considered to be a UV-finite object renormalized in the $\overline{\text{MS}}/\overline{\text{DR}}$ scheme, our diagrammatic calculation involves intermediate UV- and possibly IR-divergent quantities defined in either $\overline{\text{DR}}$ or mixed $\text{OS}/\overline{\text{DR}}$ schemes. Furthermore, a diagrammatic calculation can be extended to also include the full-momentum dependence. In the following, we introduce the used framework to generate and calculate the required Feynman diagrams.

8.1. The Goldstone Boson Catastrophe from a Diagrammatic Approach

To obtain the Feynman rules for the CP-violating NMSSM we make use of the computer program `SARAH` 4.14.3 [52–54, 139, 140, 198] to generate a `FeynArts` model file which also includes the vertex counterterms. Using `FeynArts` 3.1 [199, 200] we generate all required one- and two-loop Feynman diagrams for the calculation of the mass corrections. The evaluation of

the fermion traces and the reduction of the one-loop integrals was performed using `FeynCalc` 9.2.0 [201, 202]. `FeynCalc` also provides an interface to `TARCER` 2.0 [57] which was used to reduce all two-loop integrals to the master integrals discussed in Sec. 3.2.1 while keeping the full external momentum dependence. We first perform the tensor reduction of all necessary diagrams using the most general tensor and coupling structure with arbitrary masses without any model assumptions. The result for each diagram is a product of generic couplings, masses and the master integrals of `TARCER` defined in Eqs. (3.14) and (3.37). The latter are potentially IR-divergent. The NMSSM-specific insertions for the masses and couplings are then summed over with the help of `FeynArts`. The numerical evaluation of the loop functions depends on the chosen method to treat the IR divergences. At the one-loop order, we do not encounter any IR divergences and therefore can evaluate all one-loop counterterms. At the two-loop order, all loop functions are known analytically in the limit of vanishing external momentum but are not necessarily IR-finite.

The IR divergences are treated in three different ways:

(i) Using only a mass regulator

When introducing an auxiliary non-zero mass M_R for the Goldstone bosons masses, we expect from the results of the effective potential that a subset of IR divergences cancels while another subset will have a residual dependence on M_R . This way, we can distinguish between a set of diagrams which requires momentum regularization and a set which contains only unphysical divergences i.e. is IR-finite. We can also use this rather simple approach to study the overall dependence of the Higgs boson mass prediction on the regulator M_R .

(ii) Using partial momentum dependence

Knowing the regulator-dependent subset of diagrams (i.e. with the physical divergences) from method (i), we use finite external momentum in this particular set of diagrams. Following the strategy of the generalized effective potential approximation [27, 28], we also expand around small external momentum.

(iii) Using full momentum dependence

Once the unphysical divergences have been canceled in (i), we can also calculate *all* Feynman diagrams of $\mathcal{O}((\alpha_t + \alpha_\kappa + \alpha_\lambda)^2)$ at arbitrary external momentum using the computer program `TSIL` [59].

In the following, we elaborate on them in detail.

8.2. Using only a Mass Regulator

The use of auxiliary masses is a common and convenient trick to regulate unphysical IR divergences. In the context of Higgs boson mass calculations, it was first done for the NMSSM in Refs. [28, 136] by replacing the vanishing Goldstone boson mass with a mass regulator M_R whenever an IR-divergent loop integral was encountered. However, this approach induces not only $\mathcal{O}(\overline{\log^n M_R^2})$ -terms which diverge in the limit $M_R \rightarrow 0$, but also $\mathcal{O}(M_R^2)$ -terms which vanish in the IR-limit. To circumvent the $\mathcal{O}(M_R^2)$ -terms, we proceed as follows. For an arbitrary loop integral $f(m_1^2, \dots, m_i^2, m_j^2, \dots, m_n^2)$ which diverges for any combination of at least two vanishing masses $m_i, m_j \rightarrow 0$, we expand $f(m_1^2, \dots, M_R^2, M_R^2, \dots, m_n^2)$ around $M_R^2 = 0$ up to first non-vanishing order in $\overline{\log^n M_R^2}$ and $M_R^{-2n \leq -2}$. The required set of loop functions expanded for small M_R^2 is given in Appendix B. The proper expansion in M_R^2 should reduce the dependence on the regulator mass to a minimum.

In order to investigate the IR-finite and IR-divergent subsets of Feynman diagrams, we divide them topologically into five different sets. Appendix C, Tabs. C.1 and C.2 contain the

complete list of IR-divergent two-loop tadpole and selfenergy topologies along with the responsible loop integrals and the set they belong to. In the last column of the lists, we give the information about whether the IR divergence is canceled against other diagrams (i.e. if it is unphysical) or if one needs to include external momentum (i.e. if it is a genuine divergence). We divide the sets according to:

- **Set A** contains all topologies which are tadpole-like i.e. have no external momentum flowing in the loop. Therefore, set A is expected to be IR-finite if all diagrams are summed over.
- **Set B** contains IR-divergent topologies which have two Goldstone propagators with the same loop momentum (i.e. a one-loop Goldstone boson selfenergy) and one additional massive propagator in the same loop.
- **Set C** has also one massive and two massless propagators but contains an off-diagonal Goldstone-Higgs one-loop selfenergy in the sub-loop.
- **Set D** contains a diagonal Goldstone selfenergy but, in contrast to set B, the external momentum is flowing only through one of the Goldstone propagators.
- **Set E** contains one completely massless (sub) loop.

We find that Set A, B and C are separately IR finite. However, the cancellation is only observed if the Goldstone boson mass counterterms take a particular form. From the Goldstone tree-level masses, *cf.* Eq. (5.28), one can show that the finite parts of the one-loop counterterms are given by the one-loop tadpole counterterms:

$$\delta^{(1)}m_{G^0}^2\Big|_{\text{fin}} = \delta^{(1)}m_{G^\pm}^2\Big|_{\text{fin}} = \frac{s_\beta \delta^{(1)}t_{h_u}\Big|_{\text{fin}} + c_\beta \delta^{(1)}t_{h_d}\Big|_{\text{fin}}}{v}. \quad (8.1)$$

We find that we need to include these finite contributions in order to cancel the associated IR divergences in all two-loop quantities. This is done by ensuring that the tree-level minimum is the *true* minimum of the potential, *cf.* Eq. (7.36). Due to this choice, the one-loop Goldstone boson masses are automatically on-shell. Thus, we are also in alignment with the solution to the GBC in the effective potential of Ref. [27] which showed that the use of vanishing OS Goldstone boson masses leads to an IR-finite subset.

While all five sets of Tab. C.2 contribute to the neutral Higgs boson selfenergies, the charged Higgs, Z and W boson selfenergies only receive contributions from the IR finite subsets A, B and C. Therefore, the derived two-loop counterterms are also IR-finite.

Since sets E and D have a left-over physical IR divergence, it looks surprising that the Z -factors, which are derived from the derivatives of the neutral selfenergies, are IR-finite and in agreement with the results from the anomalous dimension matrix (*cf.* Sec. 7.2.3). However, in Refs. [203–205] it was shown in a model-independent way that the beta functions do not depend on the mass regulator if appropriate counterterms for the mass regulator are introduced. In the calculation presented here, the Goldstone boson mass counterterms are sufficient to achieve IR-finite Z -factors.

Finally, the only two-loop quantity that suffers from a residual dependence on the mass regulator, scaling with $\mathcal{O}(\overline{\log}M_R^2)$ and $\mathcal{O}(\overline{\log}^2M_R^2)$, is the unrenormalized selfenergy for the massive neutral Higgs bosons. The responsible diagrams are depicted in Fig. D.3. In Sec. 9.2.4 we study of the phenomenological impact of M_R^2 on the prediction of the Higgs boson mass spectrum.

8.3. Using Partial Momentum Dependence

A solution to the GBC without introducing a dependence on the unphysical mass regulator but circumventing the time- and resource-consuming numerical evaluation of loop integrals at finite external momentum was worked out in the generalized effective potential approximation [27]. The idea of Ref. [27] is to use finite external momentum only in the IR-divergent subset and obtain analytic expressions for the loop integrals by expanding around small p^2 . In the notation of this thesis this means that only the diagrams within the set D and E in Tab. C.2, i.e. those in Fig. D.3, are computed at finite external momentum while all other diagrams are computed at $p^2 = 0$. Since the number of independent mass scales entering the diagrams in Fig. D.3 is at most three, it is possible to obtain analytical solutions for the involved loop integrals. In fact, all special cases for the loop integrals appearing in Fig. D.3 have already been worked out in general as well as in the low-momentum expansion in Refs. [27, 28, 46, 59, 206–208].

With these loop integrals at hand, some individual diagrams in set C and E still feature an unphysical IR divergence originating in the IR-divergent integrals $\mathbf{V}(x, 0, z, u)$ and $\mathbf{C}(x, 0, 0)$. The reason why the divergence of the \mathbf{V} -topology cancels against the \mathbf{C} -topologies becomes more clear when using the identity

$$\mathbf{V}(x, 0, z, u) = -\tilde{V}(x, z, u) - \mathbf{B}(z, u)|_{p^2=0} \mathbf{C}(x, 0, 0). \quad (8.2)$$

The integral $\tilde{V}(x, z, u)$ has been derived in Ref. [28]⁷. It scales with $\overline{\log} p^2$ and is IR-finite for non-zero p^2 . Therefore, the choice of regulating $\mathbf{C}(x, 0, 0)$ is not important as there is no dependence on this function in the final result. We validated that the resulting selfenergies are indeed independent of the mass regulator when using this set of loop integrals.

One disadvantage of the small-momentum expansion is that the description becomes unreliable at latest near thresholds, since they are not captured by the $\overline{\log} p^2$ terms, or for very large values of p^2 . Alternatively one can go one step further and include the full external momentum dependence.

8.4. Using Full Momentum Dependence

This method is similar to the partial momentum dependence, i.e. we cancel all unphysical divergences using a mass regulator and use finite external momentum to remove the genuine IR divergences. However, instead of taking only partial momentum dependence into account, we allow for $p^2 \neq 0$ in all two-loop diagrams of the $\mathcal{O}((\alpha_t + \alpha_\lambda + \alpha_\kappa)^2)$ calculation. While the momentum dependence for the leading two-loop $\mathcal{O}(\alpha_t \alpha_s)$ corrections is not yet available in NMSSMCALC, its size has already been studied in Refs. [29, 31] and [30] within the MSSM using differential equations and sector decomposition for the numerical evaluation of the loop integrals. We assume that the momentum dependence in the NMSSM at $\mathcal{O}(\alpha_t \alpha_s)$ is comparable to the MSSM $\mathcal{O}(\alpha_t \alpha_s)$ corrections which were found to be at most about one GeV in the loop-corrected Higgs boson mass compared to the zero momentum approximation.

The generalization of the calculation to non-zero external momentum is straightforward since we use the basis integrals of TARCER which are also used in the numerical tool TSIL.

The UV renormalization slightly changes in the full momentum calculation. Using $p^2 \neq 0$ in all two-loop diagrams introduces UV-divergences $\mathcal{O}(p^2 \epsilon^{-n})$ which require the inclusion of additional Z -factor contributions in the renormalized selfenergies, *cf.* Eq. (7.4). We verified that the inclusion of the Z -factor contributions indeed leads to a UV-finite result in the full

⁷Our notation slightly differs from appendix A.1.1 in Ref. [28]: their $\mathbf{B}(x, y')$ and $\mathbf{P}(z, u)$ corresponds to our $\mathbf{C}(x, y, y)$ and $-\mathbf{B}(z, u)|_{p^2=0}$.

momentum approach. Additional modifications to the two-loop counterterms are not necessary. It should be noted that we are neglecting p^2 contributions from the charged Higgs boson mass counterterm, which is calculated in the approximation of vanishing external momentum.

The iterative solution of the Higgs boson propagator pole, *cf.* Eq. (7.1), involves multiple evaluations of the renormalized selfenergy at different values of p^2 . This repeated evaluation is considerably fast at the one-loop order, which relies on analytic solutions of the loop integrals. However, the loop integration of *one* set of master integrals using differential equations in TSIL is about 20 times slower than using analytic result for the $p^2 = 0$ approximation. In addition, there are many different mass states entering the $\mathcal{O}((\alpha_t + \alpha_\kappa + \alpha_\lambda)^2)$ corrections which need to be summed over. In order to reduce the runtime of the program to a minimum, we chose a fixed value for p^2 in the calculation of the new selfenergy corrections $\hat{\Sigma}_{ij}^{(2),\mathcal{O}((\alpha_t+\alpha_\kappa+\alpha_\lambda)^2)}(p^2)$. Therefore, the selfenergies only need to be computed once for a given parameter point. We set $p^2 = (m_{h_i}^2 + m_{h_j}^2)/2$, where $m_{h_{i,j}}$ are the tree-level Higgs boson masses that enter $\hat{\Sigma}_{ij}^{(2),\mathcal{O}((\alpha_t+\alpha_\kappa+\alpha_\lambda)^2)}(p^2)$. This approximation was already studied in Ref. [28] within the SM. It was shown that the SM Higgs boson mass prediction is only altered by a few MeV if the external momentum is varied between several orders of magnitude.

As a closing remark we want to discuss the reliability of the full external momentum results. It is not known how the momentum-dependent corrections compare against e.g. the electroweak corrections which are neglected in this work. In the MSSM it can be argued that the momentum-dependent and the EW gauge contributions are of similar size [71]: The p^2 -dependent corrections to the SM-like Higgs boson mass are by construction $\mathcal{O}(\alpha_{m_h}^2)$ with $m_h \approx 125$ GeV. This is of similar size than the EW corrections in the MSSM which are of $\mathcal{O}(\alpha_{M_Z}^2)$, i.e. both contributions are expected to be of the size

$$\mathcal{O}(\alpha_p^2) \approx \mathcal{O}(\alpha_{m_h}^2) \approx \mathcal{O}(\alpha_{M_Z}^2) \approx \mathcal{O}\left(\frac{(100 \text{ GeV})^2}{(4\pi)^4}\right) \approx (0.5 \text{ GeV})^2. \quad (8.3)$$

However, the p^2 -dependent contributions in the NMSSM can also be proportional to λ and κ at $\mathcal{O}((\alpha_t + \alpha_\kappa + \alpha_\lambda)^2)$ which could yield an additional enhancement of the momentum dependent corrections if $\lambda, \kappa \gtrsim \mathcal{O}(1)$. In this case, there can also be a large mixing between the singlet scalar and SM-like Higgs boson. In this regime, the momentum corrections might be dominant over the EW gauge contributions. This behavior is studied in more detail in Chapter 9. However, MSSM-like scenarios might require the inclusion of gauge-dependent contributions which is reserved for future works.

Another interesting approach is to construct UV-finite selfenergies and tadpoles at a generic level by making use of the BPHZ [209] theorem as it is done in the computer program TLDR [146] for arbitrary renormalizable theories. Since TLDR includes also all contributions involving vector boson couplings, the GBC is not present in this approach and all unphysical IR divergences should cancel there as well. While TLDR itself does not yet provide a regularization method for such IR divergences, it is now also possible to extend it to make use of our IR-regulated loop integrals.

Phenomenological Impact of the $\mathcal{O}((\alpha_t + \alpha_\kappa + \alpha_\lambda)^2)$ Corrections

In this chapter we study the phenomenological impact of the $\mathcal{O}((\alpha_t + \alpha_\kappa + \alpha_\lambda)^2)$ corrections to the Higgs boson mass spectrum.

9.1. Setup of the Parameter Scan

The central tool for the numerical analysis is the computer program `NMSSMCALC` which incorporates the $\mathcal{O}((\alpha_t + \alpha_\kappa + \alpha_\lambda)^2)$ corrections discussed in the previous chapter since version 4.00. For a documentation of the technical implementation of the new corrections into the program code as well as a manual we refer to Ref. [210] and the `NMSSMCALC` webpage⁸.

In order to scrutinize the NMSSM parameter space, a random scan is performed over all input parameters that are important for the Higgs boson mass spectrum. In the following, we describe the setup used in this parameter scan.

The charged Higgs boson as well as the top and stop sector are renormalized in the OS scheme. The OS input for the top-quark mass as well as all other SM input values are chosen from Ref. [34]:

$$\begin{aligned}
\alpha(M_Z) &= 1/127.955, & \alpha_s^{\overline{\text{MS}}}(M_Z) &= 0.1181, \\
M_Z &= 91.1876 \text{ GeV}, & M_W &= 80.379 \text{ GeV}, \\
m_t &= 172.74 \text{ GeV}, & m_b^{\overline{\text{MS}}}(m_b^{\overline{\text{MS}}}) &= 4.18 \text{ GeV}, \\
m_c &= 1.274 \text{ GeV}, & m_s &= 95.0 \text{ MeV}, \\
m_u &= 2.2 \text{ MeV}, & m_d &= 4.7 \text{ MeV}, \\
m_\tau &= 1.77682 \text{ GeV}, & m_\mu &= 105.6584 \text{ MeV}, \\
m_e &= 510.9989 \text{ keV}, & G_F &= 1.16637 \cdot 10^{-5} \text{ GeV}^{-2}.
\end{aligned} \tag{9.1}$$

Table 9.1 summarizes the parameter ranges which are sampled using uniform distributions. The random scan assumes that all CP-violating phases vanish. The effects of the individual phases are studied in Sec. 9.2.5. The predictions for the Higgs boson mass spectrum and

⁸<https://www.itp.kit.edu/~maggie/NMSSMCALC/>

parameter	scan range [TeV]	parameter	scan range
M_{H^\pm}	[0.5, 1]	$\tan \beta$	[1, 10]
M_1, M_2	[0.4, 1]	λ	[0.01, 0.7]
M_3	2	κ	$\lambda \cdot \xi$
μ_{eff}	[0.1, 1]	ξ	[0.1, 1.5]
$m_{\tilde{Q}_3}, m_{\tilde{t}_R}$	[0.4, 3]	A_t	[-3, 3] TeV
$m_{\tilde{X} \neq \tilde{Q}_3, \tilde{t}_R}$	3	$A_{i \neq t}$	[-2, 2] TeV

Table 9.1.: Ranges for the randomized scan over the NMSSM parameter space. Values of $\kappa = \lambda \cdot \xi > 0.7$ are omitted. All soft breaking masses $m_{\tilde{X}}$ with $\tilde{X} = \tilde{b}_R, \tilde{L}, \tilde{\tau}$ and trilinear couplings A_i with $i = b, \tau, \kappa$, are set equal to 3 TeV.

decays are required to fulfil the most recent experimental constraints discussed in Chapter 6. For this purpose the programs `HiggsBounds` with version 5.9.0 [182–184] and `HiggsSignals` with version 2.6.1 [181, 185] were utilized. The theoretical uncertainty propagated to `HiggsSignals` is set to ± 3 GeV. This effectively requires at least one SM-like Higgs boson h within the mass range

$$122 \text{ GeV} \leq m_h \leq 128 \text{ GeV}, \quad (9.2)$$

which has mostly SM-like couplings. Since the gauge eigenstate h_u has the largest coupling to the top quark, similar to the SM-like Higgs boson, it is expected that h consists of a large h_u component with only small admixtures from the h_d and h_s eigenstates such that all Higgs signal strengths measured at the LHC are reproduced. Therefore, we use "h_u-like" and "SM-like" as equivalent terms in the following sections. The χ^2 values returned by `HiggsSignals` for the individual parameter points of the NMSSM are compared against the χ^2 value returned for the SM. Parameter points which do not agree with the SM⁹ χ^2 within 2σ (assuming 2 degrees of freedom) are not taken into account. For a detailed discussion about the statistical interpretation of the χ^2 -test, we refer to Ref. [185]. The numerical mass regulator introduced in Sec. 8.2 is chosen to be $M_R^2 = R\mu_0^2$ with the renormalization scale μ_0 and a default value of $R = 10^{-3}$ which is discussed later. The value of μ_0 is dynamically chosen from the input parameters of the stop sector, $\mu_0 = \sqrt{m_{\tilde{q}_3} m_{\tilde{t}_R}}$. The input scale at which all $\overline{\text{DR}}$ input parameters are defined is also given by μ_0 . Furthermore, we require that the resulting mass spectrum of the parameter points obeys the following conditions:

- (i) $m_{h_5}, m_{\chi_5^0}, m_{\chi_2^\pm} < 1 \text{ TeV}, m_{\tilde{t}_2} < 2 \text{ TeV},$
- (ii) $m_{h_i} - m_{h_j} > 0.1 \text{ GeV}, m_{\chi_i^{(\pm)}} - m_{\chi_j^{(\pm)}} > 0.1 \text{ GeV},$
- (iii) $m_{\chi_1^\pm} > 94 \text{ GeV}, m_{\tilde{t}_1} > 1 \text{ TeV}.$

Condition (i) restricts the largest Higgs boson and electroweakino masses to be smaller than 1 TeV as well as the largest stop mass to be smaller than 2 TeV. Thus, the resulting mass spectra contain only degrees of freedom which are not too heavy and well suited for precise fixed-order predictions. The constraint (ii) guarantees the absence of nearly-degenerate mass configurations for which not all ingredients of the of two-loop calculation are optimised. We also want to note, that the limit $\lambda, \kappa \rightarrow 0$ is numerically difficult and should be taken with care. Condition (iii) takes into account model-independent lower limits for the lightest chargino and stop masses [34].

The rather small scan range of the parameter λ in Tab. 9.1 is motivated by the renormalization

⁹In `HiggsSignals-2.6.1`, the SM χ^2 obtained with the latest data set is 84.44.

group running of the coupling λ , *cf.* Eqs. (7.45a) and (7.46a),

$$\beta_\lambda \approx \lambda \left(\frac{3}{(4\pi)^2} y_t^2 + \frac{9}{(4\pi)^4} y_t^4 \right). \quad (9.3)$$

The top-quark Yukawa coupling is large at the TeV scale, $y_t \approx 1$, and contributes with a positive sign to the running of λ . Therefore, large initial values of λ can spoil the validity of perturbation theory at relatively low scales. The authors of Ref. [211] found that $\lambda < 0.7$ ensures perturbativity up to the grand unification (GUT) scale. However, for illustrative purposes in the subsequent sections we will also consider the case of $\lambda, \kappa > 0.7$ for individual parameter points.

9.2. Results

The resulting parameter sample contains twenty thousand points which fulfil all constraints discussed in the previous section while the charged Higgs boson and the top/stop sector are renormalized on-shell and the new two-loop $\mathcal{O}(\alpha_{\text{new}}^2)$ corrected selfenergies are used. All individual parameter points of this sample are re-evaluated while calculating the Higgs boson mass spectrum only at $\mathcal{O}(\alpha_t(\alpha_t + \alpha_s))$ and $\mathcal{O}(\alpha_t\alpha_s)$ and only at the one-loop order, respectively. In addition, we change the renormalization in the top/stop sector from OS to $\overline{\text{DR}}$ for each order in perturbation theory. This allows us to perform a global comparison between the various loop corrections and renormalization schemes over a large part of the NMSSM parameter space. The results are visualized using scatter plots.

Furthermore, we pick two parameter points from the original scan sample and study their individual behavior under the change of the input parameters. The initial input parameters of the two points are shown in Tab. 9.2 which have been selected because of their specific admixtures between the SM-like and the singlet-like Higgs bosons. The parameter point P10S from Tab. 9.2 features a small h_u/h_s mixing while the parameter point P20S has the largest h_u/h_s mixing of the collected sample of around 12%. The stop-quark masses resulting from these input parameters are listed in Tab. 9.3. While the default renormalization scheme is the OS scheme, the obtained stop masses in the $\overline{\text{DR}}$ scheme are also given in Tab. 9.3 for both parameter points. Tables 9.4 and 9.5 list the values for the Higgs boson masses of P10S and P20S, respectively, at tree-level, one-loop, two-loop $\mathcal{O}(\alpha_t\alpha_s)$, $\mathcal{O}(\alpha_t(\alpha_t + \alpha_s))$ and $\mathcal{O}(\alpha_{\text{new}}^2)$ in the OS scheme of the top/stop sector. Numbers in parentheses are the mass values obtained if the top/stop sector is renormalized in the $\overline{\text{DR}}$ scheme.

In the following, we briefly describe the features of the two parameter points. For this purpose, we define the relative difference $\Delta_Y^X(M_h)$ of the mass M_h^X of the Higgs boson h calculated at order X with the mass M_h^Y calculated at the order Y in perturbation theory. Likewise, we define the relative difference $\Delta_{\text{ren.}}(M_h^X)$ for the result of $M_h^{X,\text{OS}}$ obtained if the top/stop sector is renormalized in the on-shell scheme and in the $\overline{\text{DR}}$ scheme, $M_h^{X,\overline{\text{DR}}}$, at a given order X in perturbation theory:

$$\Delta_Y^X(M_h) = \frac{|M_h^X - M_h^Y|}{M_h^Y}, \quad \Delta_{\text{ren.}}(M_h^X) = \frac{|M_h^{X,\text{OS}} - M_h^{X,\overline{\text{DR}}}|}{M_h^{X,\overline{\text{DR}}}}, \quad (9.4)$$

with $X, Y = \{\text{tree-level, one-loop, } \mathcal{O}(\alpha_t\alpha_s), \mathcal{O}(\alpha_t(\alpha_t + \alpha_s)), \mathcal{O}(\alpha_{\text{new}}^2)\}$.

The results for the parameter point P10S shown in Tab. 9.4 also list the dominant gauge eigenstate in the corresponding mass eigenstate in square brackets. The lightest Higgs boson h_1 is h_u -like at all considered orders and renormalization schemes. Furthermore, the point features a rather light singlet-like pseudoscalar with a mass of about $\mathcal{O}(100 \text{ GeV})$, a

$\mathcal{O}(350 \text{ GeV})$ -heavy singlet-like scalar and two down-type scalar/pseudoscalar Higgs bosons above 600 GeV. While the loop corrections of the non-SM-like Higgs bosons are relatively stable at the different loop-orders, the h_u -like Higgs boson h_1 receives sizeable corrections. From tree-level to one-loop it receives a rather large positive correction $\Delta_{\text{tree-level}}^{\text{one-loop}}(M_{h_1}) \approx 53\%$ in the OS scheme and around 31% in the $\overline{\text{DR}}$ scheme which yields a rather large scheme dependence of $\Delta_{\text{ren.}}(M_{h_1}^{\text{one-loop}}) = 16\%$. From one-loop to two-loop $\mathcal{O}(\alpha_t \alpha_s)$, the Higgs boson mass M_{h_1} is altered by -10% in the OS scheme while the scheme dependence $\Delta_{\text{ren.}}(M_{h_1}^{\mathcal{O}(\alpha_t \alpha_s)})$ becomes very small (0.7%) as the results obtained in the $\overline{\text{DR}}$ and OS scheme of the top/stop sector differ by less than 1 GeV. At $\mathcal{O}(\alpha_t(\alpha_t + \alpha_s))$ the scheme dependence is again increased to $\Delta_{\text{ren.}}(M_{h_1}^{\mathcal{O}(\alpha_t(\alpha_t + \alpha_s))}) = 4.5\%$ due to comparably large corrections in the OS scheme of about $\Delta_{\alpha_t(\alpha_t + \alpha_s)}^{\alpha_t \alpha_s}(M_{h_1}) = 5.2\%$. The new $\Delta\mathcal{O}((\alpha_t + \alpha_\kappa + \alpha_\lambda)^2)$ corrections¹⁰ decrease the Higgs boson mass in the OS scheme by about 500 MeV and at the same time increase the corrections in the $\overline{\text{DR}}$ scheme such that the scheme dependence is slightly reduced to the value $\Delta_{\text{ren.}}(M_{h_1}^{\mathcal{O}(\alpha_{\text{new}}^2)}) = 4.0\%$.

In Tab. 9.5 we see a very similar behavior for the h_u -like Higgs boson mass of the parameter point P20S. This parameter point features an SM-like Higgs boson and a light singlet-like scalar while all other Higgs bosons are heavier than 500 GeV. However, due to the large singlet admixture, the dominant h_u/h_s components in h_1/h_2 change upon inclusion of the higher-order corrections. In Tab. 9.5 we colorize the cells with a dominant h_s component in blue and those with a dominant h_u component in red. One can see that the behavior is almost as for P10S except for the one-loop corrected Higgs boson mass in the OS/ $\overline{\text{DR}}$ scheme. At this order, the h_u - and h_s -like Higgs bosons change their mass ordering due to the larger corrections in the OS scheme. The dominant gauge eigenstate determines the coupling strengths of the Higgs boson to all other sectors of the theory and therefore also the size of the loop corrections. Thus, we rather compare the mass values with the same dominant component (i.e. equal colors in Tab. 9.5) rather than the same mass eigenstates. This means that we compute $\Delta_{\text{one-loop}}^{\text{tree-level}}(M_{h_u}) = 28\%$ rather than $\Delta_{\text{one-loop}}^{\text{tree-level}}(M_{h_1}) = 25\%$. This strategy is also followed in the rest of this thesis.

We can summarize the behavior for M_{h_u} from Tabs. 9.4 and 9.5 when successively going from order X to Y as:

$$\begin{array}{c} X \\ \Delta_{\text{ren.}} \end{array} \xrightarrow[\Delta_{\text{ren.}}]{\Delta_Y^X} Y : \quad \begin{array}{c} \text{tree-level} \\ 0\% \end{array} \xrightarrow[16\%]{25-50\%} \begin{array}{c} \text{one-loop} \\ 16\% \end{array} \xrightarrow[0-1\%]{5-10\%} \begin{array}{c} \mathcal{O}(\alpha_t \alpha_s) \\ 0-1\% \end{array} \xrightarrow[3-4\%]{0-5\%} \begin{array}{c} \mathcal{O}(\alpha_t(\alpha_t + \alpha_s)) \\ 3-4\% \end{array} \xrightarrow[3-4\%]{0-1\%} \begin{array}{c} \mathcal{O}(\alpha_{\text{new}}^2) \\ 3-4\% \end{array}.$$

This pattern shows that the $\mathcal{O}(\alpha_t^2)$ corrections seem to introduce a larger scheme dependence which is only slightly reduced upon the inclusion of the $\Delta\mathcal{O}((\alpha_t + \alpha_\kappa + \alpha_\lambda)^2)$ corrections. We will study this behavior in more detail in the following sections.

	λ	κ	$\tan \beta$	$\text{Re}A_\kappa$	M_{H^\pm}	μ_{eff}	A_t	$m_{\tilde{q}_3}$	$m_{\tilde{t}_R}$	M_1	M_2	M_3
	[TeV]											
P10S	0.46	0.43	3.70	-0.004	0.64	0.200	2.0	1.00	1.80	0.80	0.40	2
P20S	0.59	0.23	2.05	-0.546	0.92	0.397	-0.9	1.20	1.37	0.66	0.67	2

Table 9.2.: Input parameters for the two sample parameter points. All trilinear soft-breaking couplings other than A_t and A_κ are set to zero, $A_{i \neq t, \kappa} = 0 \text{ GeV}$. The soft-breaking masses for all quarks and leptons except for \tilde{t}_R and \tilde{q}_3 are set to $m_{\tilde{X} \neq \tilde{q}_3, \tilde{t}_R} = 3 \text{ TeV}$.

¹⁰Note that $\Delta\mathcal{O}((\alpha_t + \alpha_\kappa + \alpha_\lambda)^2)$ only refers to the shift which is due to NMSSM-specific contributions while $\mathcal{O}(\alpha_{\text{new}}^2)$ refers to the sum of all two-loop corrections, cf. Eq. (5.18b).

	$m_{\tilde{t}_1}$ [GeV]		$m_{\tilde{t}_2}$ [GeV]	
	OS	$\overline{\text{DR}}$	OS	$\overline{\text{DR}}$
P10S	1022.64	991.64	1815.54	1815.40
P20S	1212.54	1190.44	1402.77	1392.33

Table 9.3.: The stop-quark masses $m_{\tilde{t}_1}$ and $m_{\tilde{t}_2}$ from the parameter points P10S and P20S defined in Tab. 9.2. The values are given for the OS scheme, which was used in the scan to obtain P10S and P20S, as well as when switching to the $\overline{\text{DR}}$ scheme in the top and stop sector. *The data for the table was taken from Ref. [210].*

	h_1 [h_u]	h_2 [h_s]	h_3 [h_d]	a_1 [a_s]	a_2 [a_d]
tree-level	87.64	365.32	646.65	103.09	639.83
one-loop	133.97 (115.21)	359.42 (359.35)	646.67 (646.4)	116.51 (116.8)	639.78 (639.8)
two-loop $\mathcal{O}(\alpha_t\alpha_s)$	119.09 (119.98)	359.36 (359.37)	646.5 (646.43)	116.76 (116.69)	639.81 (639.79)
two-loop $\mathcal{O}(\alpha_t(\alpha_t + \alpha_s))$	125.58 (120.15)	359.36 (359.37)	646.6 (646.43)	116.76 (116.69)	639.81 (639.79)
two-loop $\mathcal{O}(\alpha_{\text{new}}^2)$	125.03 (120.18)	359.68 (359.59)	646.62 (646.47)	116.58 (116.63)	639.77 (639.78)

Table 9.4.: Mass values in GeV for the parameter point P10S defined in Tab. 9.2 of the neutral Higgs bosons at tree-level, one-loop, two-loop $\mathcal{O}(\alpha_t\alpha_s)$, two-loop $\mathcal{O}(\alpha_t(\alpha_t + \alpha_s))$ and at two-loop $\mathcal{O}(\alpha_{\text{new}}^2)$ obtained by using OS renormalization in the top/stop sector. Numbers in parentheses are results obtained in the $\overline{\text{DR}}$ scheme. The main component (in square brackets) stays the same at all orders in both schemes. *The data for the table was taken from Ref. [210].*

	h_1 [h_u]	h_2 [h_s]	h_3 [h_d]	a_1 [a_s]	a_2 [a_d]
tree-level	96.86	112.10	926.25	511.34	925.86
one-loop	129.01 (116.3)	135.09 (130.1)	926.69 (926.33)	512.55 (512.66)	925.08 (925.18)
two-loop $\mathcal{O}(\alpha_t\alpha_s)$	121.36 (121.65)	129.7 (130.39)	926.37 (926.46)	512.62 (512.61)	925.11 (925.15)
two-loop $\mathcal{O}(\alpha_t(\alpha_t + \alpha_s))$	126.09 (121.54)	130.04 (130.38)	926.49 (926.45)	512.62 (512.61)	925.11 (925.15)
two-loop $\mathcal{O}(\alpha_{\text{new}}^2)$	125.28 (121.69)	129.92 (130.2)	926.63 (926.53)	511.92 (512.12)	925.08 (925.15)

Table 9.5.: Same as Tab. 9.4 but for the parameter point P20S. States with red numbers are h_u -like while states with blue numbers are h_s -like. *The data for the table was taken from Ref. [210].*

9.2.1. Impact of the $\mathcal{O}((\alpha_t + \alpha_\kappa + \alpha_\lambda)^2)$ Corrections

In this section we study the relative size of the $\mathcal{O}(\alpha_{\text{new}}^2)$ corrections compared to the previous predictions. We use the parameter points P10S and P20S as starting points and observe how the Higgs boson masses change if we change λ , κ or A_t . Furthermore, we investigate the whole scan sample obtained in Sec. 9.1.

Impact of λ and κ

We simultaneously vary $\kappa = \lambda \cdot \kappa_0 / \lambda_0$ where κ_0 and λ_0 are the starting values of the respective input parameters from Tab. 9.2. The reason for this choice is to be able to vary λ and κ over large ranges without the appearance of negative mass squares in the eigenvalues of the tree-level mass matrices.

In Fig. 9.1 (upper panels) we show the result for the Higgs boson mass prediction, M_{h_u} , as a function of λ for the parameter point P10S (left) and P20S (right). The results using the OS ($\overline{\text{DR}}$) scheme in the top/stop sector are shown with solid (dashed) lines. The red, black and blue lines are obtained at the $\mathcal{O}(\alpha_{\text{new}}^2)$, $\mathcal{O}(\alpha_t(\alpha_t + \alpha_s))$ and $\mathcal{O}(\alpha_t\alpha_s)$, respectively. We find that in all considered scenarios, the $\mathcal{O}(\alpha_t\alpha_s)$ and $\mathcal{O}(\alpha_t(\alpha_t + \alpha_s))$ results in the $\overline{\text{DR}}$ scheme are very close to each other for all considered values of λ and A_t (i.e. blue and black dashed are on top of each other) while a larger difference is found in the OS scheme. For small values of λ , the $\mathcal{O}(\alpha_{\text{new}}^2)$ results also agree with the previous calculations in the $\overline{\text{DR}}$ scheme but start to significantly deviate for large λ . This is a good cross-check since the $\mathcal{O}(\alpha_{\text{new}}^2)$ results should coincide with the $\mathcal{O}(\alpha_t(\alpha_t + \alpha_s))$ results in the MSSM-limit. In the middle panels, we show the relative difference $\Delta_{\alpha_{\text{new}}^2}^{\alpha_i^2}$ (cf. Eq. (9.4)) of the new corrections w.r.t $\alpha_i^2 = \mathcal{O}(\alpha_t(\alpha_t + \alpha_s))$ (black) and $\mathcal{O}(\alpha_t\alpha_s)$ (blue). We are mainly interested in the comparison with $\mathcal{O}(\alpha_t(\alpha_t + \alpha_s))$

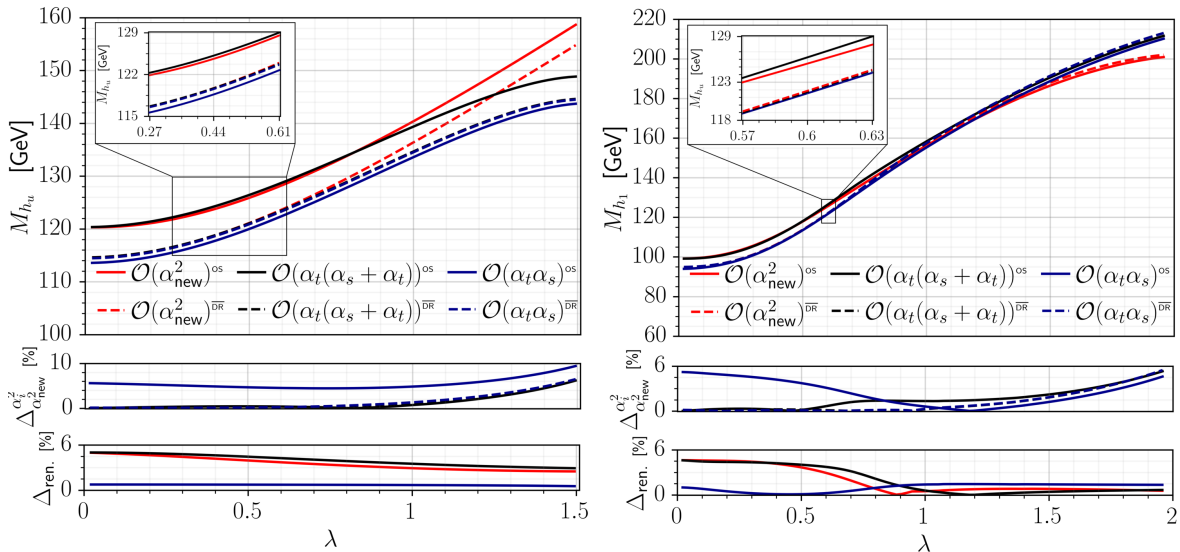


Figure 9.1.: Upper left (right) panel: Mass of the h_u -(h_1 -)like Higgs boson for the parameter point P10S (P20S) at two-loop $\mathcal{O}(\alpha_t\alpha_s)$ (blue), $\mathcal{O}(\alpha_t(\alpha_t + \alpha_s))$ (black) and $\mathcal{O}(\alpha_{\text{new}}^2)$ (red) in the OS (full) and $\overline{\text{DR}}$ (dashed) renormalization scheme as a function of λ . The black and blue dashed lines lie on top of each other. **Middle panels:** Relative difference $\Delta_{\alpha_{\text{new}}^2}^{\alpha_i^2}$ (cf. Eq. (9.4)) of the new corrections w.r.t $\alpha_i^2 = \mathcal{O}(\alpha_t(\alpha_t + \alpha_s))$ (black) and $\mathcal{O}(\alpha_t\alpha_s)$ (blue). **Lower panels:** Relative difference $\Delta_{\text{ren.}}$ due to the renormalization scheme change in the top/stop sector (i.e. between solid and dashed lines of the same color). The region of $|\lambda|$ which is compatible with the current LHC Higgs signals at $\mathcal{O}(\alpha_{\text{new}}^2)$ is shown in the zoomed regions. *The data for the figures was taken from Ref. [210].*

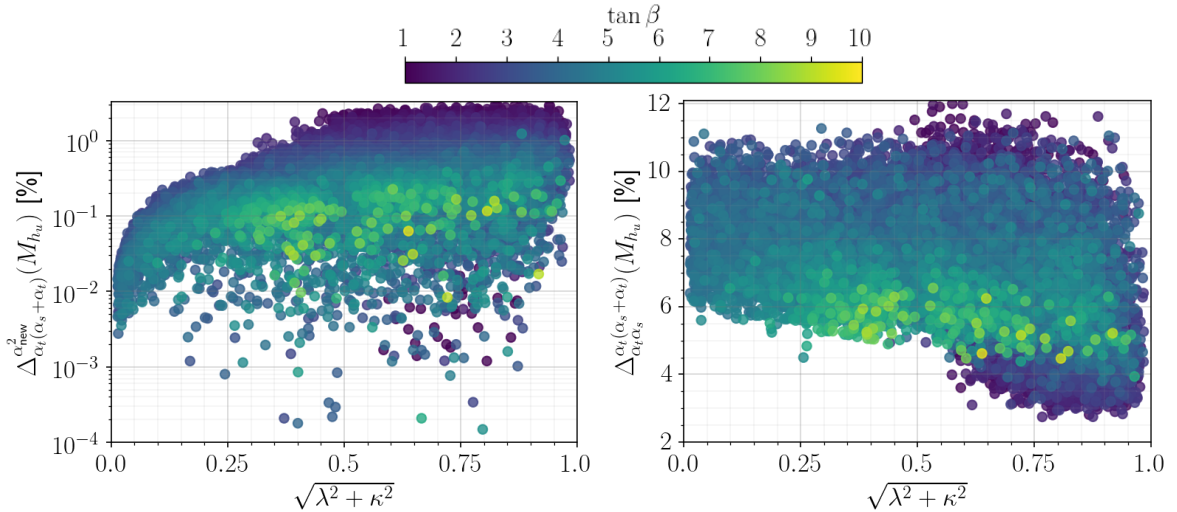


Figure 9.2.: **Left:** Relative size $\Delta_{\alpha_t(\alpha_t+\alpha_s)}^{\alpha_{\text{new}}^2}(M_{h_u})$ of the new two-loop $\mathcal{O}(\alpha_{\text{new}}^2)$ corrections to the h_u -like mass w.r.t. the $\mathcal{O}(\alpha_t(\alpha_t + \alpha_s))$ corrections as a function of $\sqrt{\lambda^2 + \kappa^2}$ for all points obtained in the scan described in Sec. 9.1. The color code indicates the value of $\tan \beta$. **Right:** The same but for $\Delta_{\alpha_t\alpha_s}^{\alpha_t(\alpha_t+\alpha_s)}(M_{h_u})$. The data for the figures was taken from Ref. [210].

since these are the precursors of the $\mathcal{O}(\alpha_{\text{new}}^2)$ corrections. In both scenarios we find that the new corrections remain small for moderate values of λ . In the case of small singlet mixing (P10S, left), $\lambda > 1$ is required to see a notable effect which is larger than 2%. The maximum deviation can be up to 7% for $\lambda = 2$. However, for a large singlet mixing (P20S, right), the new corrections start to deviate with more than 1.5% already at smaller values of λ for $\lambda > 0.5$.

To obtain a global picture of the impact of λ and κ on the size of the new corrections, we utilize the collected parameter points from the scan described in Sec. 9.1. In Fig. 9.2(left) we show the relative difference $\Delta_{\alpha_t(\alpha_t+\alpha_s)}^{\alpha_{\text{new}}^2}(M_{h_u})$ of all obtained parameter points as a function of $s_{\lambda\kappa} \equiv \sqrt{\lambda^2 + \kappa^2}$. The color code indicates the value of $\tan \beta$. One can see that in the MSSM limit, $s_{\lambda\kappa} \rightarrow 0$, the relative corrections are negligible as suggested by Eq. (5.34). For large values of $s_{\lambda\kappa} > 0.6$ and low values of $\tan \beta < 2$, the relative corrections can be as large as 3%. However, we note that in this scan λ and κ are separately not larger than 0.7 in order to ensure perturbativity below the GUT scale (*cf.* discussion of Eq. (9.3)).

In addition, we show the relative difference $\Delta_{\alpha_t\alpha_s}^{\alpha_t(\alpha_t+\alpha_s)}(M_{h_u})$ of the previous two calculations in Fig. 9.2(right). They are mostly unaffected by a change of $s_{\lambda\kappa}$ and are between about 4.5% and 12% for $s_{\lambda\kappa} < 0.6$ and therefore always larger than the largest $\mathcal{O}((\alpha_t + \alpha_\kappa + \alpha_\lambda)^2)$ corrections in this regime of the parameter space. This shows that applying the MSSM-limit in the two-loop calculation is a good approximation for a wider range of λ and κ . However, for large values of $s_{\lambda\kappa} > 0.6$ and small values of $\tan \beta$, the relative corrections can be as small as $\Delta_{\alpha_t\alpha_s}^{\alpha_t(\alpha_t+\alpha_s)}(M_{h_u}) \approx 2 - 4\%$. In this regime, the new relative corrections are maximized, $\Delta_{\alpha_t(\alpha_t+\alpha_s)}^{\alpha_{\text{new}}^2}(M_{h_u}) \approx 3\%$ (left plot in Fig. 9.2). Therefore, the NMSSM-specific corrections, which are proportional to λ and κ , can be of the same size as the $\mathcal{O}(\alpha_t^2)$ corrections if λ , κ are large and $\tan \beta$ is small.

Impact of A_t

In Fig. 9.3(left) we show the h_u -like Higgs boson mass of the parameter point P20S as a function of A_t . The notation in the figure is the same as in Fig. 9.1. The kinks which appear as A_t is varied are due to the fact that the dominant h_u component changes from the lightest

Higgs boson h_1 to the next-to-lightest Higgs boson h_2 . In the OS scheme of the top/stop sector, the $\mathcal{O}(\alpha_t(\alpha_t + \alpha_s))$ corrections are up to 10% larger than the $\mathcal{O}(\alpha_t\alpha_s)$ results (note that the blue solid line in the middle panel of Fig. 9.3(left) is re-scaled by a factor 0.1 for better readability) while the $\mathcal{O}(\alpha_{\text{new}}^2)$ result differs by at most 2 GeV from the $\mathcal{O}(\alpha_t(\alpha_t + \alpha_s))$ result. The overall dependence of $\Delta_{\alpha_{\text{new}}^2}^{\alpha_t^2}$ on A_t is rather flat for all corrections except for the regions $|A_t| \approx 1.2 - 2$ TeV where the dominant h_u component changes between the mass eigenstates. In the $\overline{\text{DR}}$ scheme, for $|A_t| < 2$ TeV, we observe that the three calculations are very close to each other. For larger $|A_t|$, the $\mathcal{O}(\alpha_t(\alpha_t + \alpha_s))$ and $\mathcal{O}(\alpha_{\text{new}}^2)$ results still agree in the $\overline{\text{DR}}$ scheme but disagree slightly more with the $\mathcal{O}(\alpha_t\alpha_s)$ result by up to 1-2%. Thus, the deviations in the OS scheme of the top/stop sector are again larger than in the $\overline{\text{DR}}$ scheme which is further discussed in Secs. 9.2.2 and 9.2.3.

Furthermore, we study in Fig. 9.3(right) the impact of the variation of A_t on the squared coupling $C_{VVh_u}^2$ of the h_u -like Higgs boson to the SM vector bosons, $V = W^\pm, Z$, normalized to the respective squared SM coupling. The figure is generated in the OS scheme of the top/stop sector. We plot the coupling when using the $\mathcal{O}(\alpha_{\text{new}}^2)$ (red), $\mathcal{O}(\alpha_t(\alpha_t + \alpha_s))$ (black) and $\mathcal{O}(\alpha_t\alpha_s)$ (blue) corrections in the Higgs boson mass calculation. The regions with transparent lines are either not compatible with the measured Higgs signal rates or do not fulfil the Higgs boson mass constraint. The solid (dashed) lines indicate regions where h_u is the dominant component in the lightest (second-lightest) mass eigenstate. We see that, throughout all calculations, the coupling $C_{VVh_u}^2$ needs to be at least as large as 75% of the SM coupling in order to fulfil the `HiggsSignals` constraints.

The Higgs boson mass obtained in the OS scheme of the $\mathcal{O}(\alpha_t(\alpha_t + \alpha_s))$ and $\mathcal{O}(\alpha_{\text{new}}^2)$ calculations is much larger than the $\mathcal{O}(\alpha_t\alpha_s)$ results (left plot). Therefore, the allowed regions with $M_{h_u} = (125 \pm 3)$ GeV in Fig. 9.3(right) (red/black compared to blue solid lines) are very distinct. The dips in the right plot are regions of large h_u/h_s mixing which are slightly moved horizontally when considering the different orders. This has a large influence on the allowed

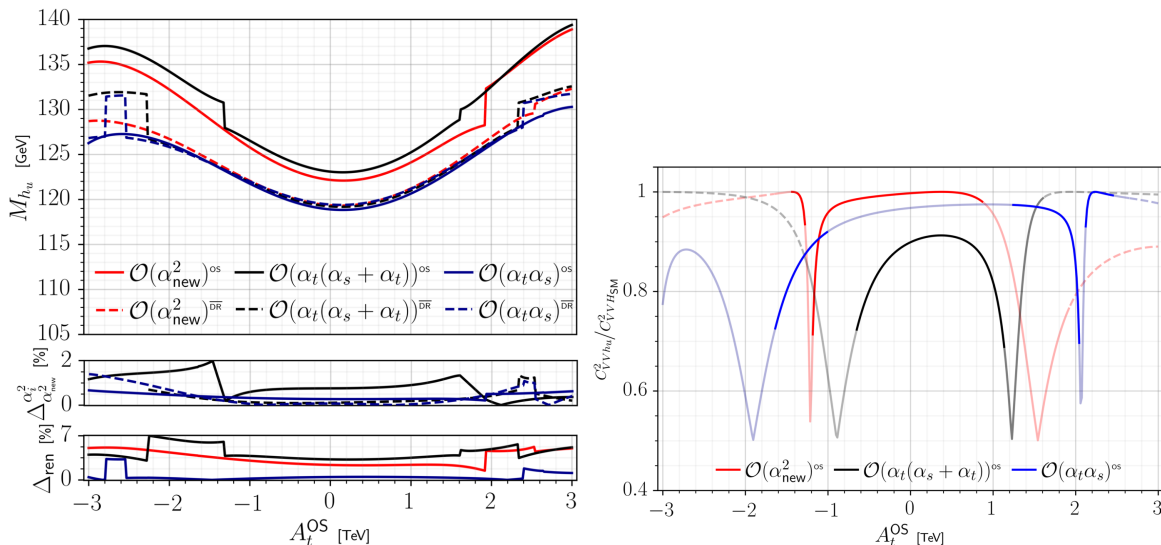


Figure 9.3.: The dependence of the parameter point P20S on A_t . **Left:** Same as Fig. 9.1(right) but as a function of the parameter A_t (the black and blue dashed lines lie on top of each other). The blue solid line in the middle panel has been rescaled by a factor of 0.1. **Right:** The squared couplings $C_{VVh_u}^2$ of the h_u -like Higgs boson to the massive vector bosons $V = W, Z$ normalized to the squared SM coupling. The result is given for the $\mathcal{O}(\alpha_{\text{new}}^2)$ (red), $\mathcal{O}(\alpha_t(\alpha_t + \alpha_s))$ (black), and $\mathcal{O}(\alpha_t\alpha_s)$ (blue) result. Transparent regions are either excluded by `HiggsSignals` or do not fulfill the Higgs boson mass constraint. For solid lines, h_u is the lightest Higgs, for dashed ones it is the next-to-lightest one. *The data for the figures was taken from Ref. [210].*

range of A_t . Even though the $\Delta\mathcal{O}((\alpha_t + \alpha_\kappa + \alpha_\lambda)^2)$ corrections add only about -1 GeV to the h_u -like Higgs boson mass, the shape of the A_t distribution is significantly modified due to a different mixing between h_u and h_s . This shows that aiming for a high precision in the Higgs boson mass calculations is mandatory in order to draw conclusions about the collider phenomenology of the considered model.

9.2.2. Renormalization Scheme Dependence

In the lower panels of Fig. 9.1 and Fig. 9.3(left) we also show the uncertainty $\Delta_{\text{ren.}}$ due to the change in the top/stop sector from the OS to the $\overline{\text{DR}}$ renormalization scheme at the considered orders. For large ranges of λ , κ and A_t we see a similar behavior to what was already observed in Tabs. 9.4 and 9.5: the renormalization scheme dependence is increased by the $\mathcal{O}(\alpha_t^2)$ corrections and only mildly reduced by the $\Delta\mathcal{O}((\alpha_t + \alpha_\kappa + \alpha_\lambda)^2)$ corrections. Therefore, the inclusion of 3-loop corrections of $\mathcal{O}(\alpha_t\alpha_s^2)$, which also depend on the scheme of the top/stop sector, or even beyond might be required. However, at $\mathcal{O}((\alpha_t + \alpha_\kappa + \alpha_\lambda)^2)$ also terms of $\mathcal{O}(\alpha_t(\alpha_\lambda + \alpha_\kappa))$ are contributing which could in principle reduce or increase the scheme dependence if they are of the same size as the $\mathcal{O}(\alpha_t^2)$ corrections. To investigate this case, we again make use of the collected scan sample and vary the renormalization scheme at $\mathcal{O}(\alpha_{\text{new}}^2)$ in the top/stop sector from OS to $\overline{\text{DR}}$. In Fig. 9.4(left) we show the scheme dependence $\Delta_{\text{ren.}}(M_{h_u})$ at $\mathcal{O}(\alpha_{\text{new}}^2)$ for the mass of the states with the largest h_u component as a function of $s_{\lambda\kappa} = \sqrt{\lambda^2 + \kappa^2}$. The color code indicates the value of $|A_t|$ in the OS scheme. For small values of $s_{\lambda\kappa} < 0.6$, the scheme dependence is always rather large compared to the overall size of the new corrections and between 4% to 8%. Furthermore, the scheme dependence is proportional to $|A_t|$ and becomes large for $|A_t| > 2$ TeV. In general, the higher-order corrections which depend on A_t can contain terms that are polynomials of $\mathcal{O}(A_t/m_{\tilde{t}_2})$. However, in our scan we required $m_{\tilde{t}_2} < 2$ TeV which means that, for all points with $|A_t| > 2$ TeV, the A_t power-corrections may become too large and lead to unreliable results. If we increase $s_{\lambda\kappa} > 0.6$ and stay below $|A_t| = 1 - 2$ TeV, the scheme dependence is significantly reduced to $\Delta_{\text{ren.}}(M_{h_u}^{\mathcal{O}(\alpha_{\text{new}}^2)}) = 1 - 3\%$. This is the same regime of $s_{\lambda\kappa}$ as in Fig. 9.2(left) where the $\mathcal{O}(\alpha_t^2)$

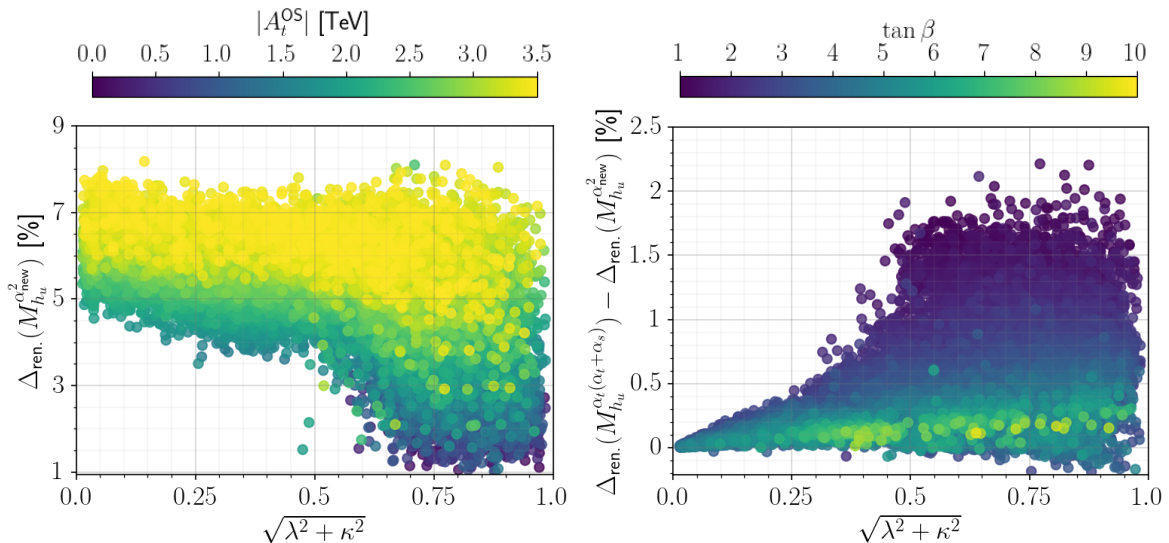


Figure 9.4.: The scheme dependence $\Delta_{\text{ren.}}$ (cf. Eq. (9.4)) for M_{h_u} as a function of $s_{\lambda\kappa} = \sqrt{\lambda^2 + \kappa^2}$. **Left:** $\Delta_{\text{ren.}}(M_{h_u})$ at $\mathcal{O}(\alpha_{\text{new}}^2)$. The color code indicates the value of $|A_t^{\text{OS}}|$. **Right:** The improvement $\Delta_{\text{ren.}}(M_{h_u}^{\mathcal{O}(\alpha_t(\alpha_t + \alpha_s))}) - \Delta_{\text{ren.}}(M_{h_u}^{\mathcal{O}(\alpha_{\text{new}}^2)})$ in the scheme dependence when going from $\mathcal{O}(\alpha_t(\alpha_t + \alpha_s))$ to $\mathcal{O}(\alpha_{\text{new}}^2)$. The color code indicates the value of $\tan\beta$. The data for the figures was taken from Ref. [210].

corrections can become smaller than the $\Delta\mathcal{O}((\alpha_t + \alpha_\kappa + \alpha_\lambda)^2)$ corrections and thus contribute with a smaller scheme dependence. To investigate this further, we plot the difference in the scheme uncertainties $\Delta_{\text{ren.}}(M_{h_u}^{\mathcal{O}(\alpha_t(\alpha_t + \alpha_s))}) - \Delta_{\text{ren.}}(M_{h_u}^{\mathcal{O}(\alpha_{\text{new}}^2)})$ between the $\mathcal{O}(\alpha_t(\alpha_t + \alpha_s))$ and $\mathcal{O}(\alpha_{\text{new}}^2)$ corrections as a function of $s_{\lambda\kappa}$ and $\tan\beta$ in Fig. 9.4(right). We observe that the region with $s_{\lambda\kappa} > 0.6$ and $\tan\beta < 2$ indeed leads to a reduction of the scheme dependence of up to 2.3% compared to the previous calculations. The scheme dependence for the singlet-like scalar/pseudoscalar (not plotted here) is found to be 5% (0%) for large (small) values of $s_{\lambda\kappa}$. We conclude that the two-loop $\mathcal{O}(\alpha_t(\alpha_\lambda + \alpha_\kappa))$ contributions, can reduce the scheme dependence for the h_u -like state for increasing λ and κ but increase the scheme dependence of the h_s - and a_s -like states on the top/stop sector at the same time.

9.2.3. Renormalization Scale Dependence

In this section we study the dependence of the two-loop-corrected Higgs boson mass M_{h_u} on the choice of the renormalization scale μ . For this purpose, we utilize the RGEs of the NMSSM which have been implemented in NMSSMCALC in Ref. [33]. Since the RGEs are only defined for $\overline{\text{MS}}$ input parameters, the top-quark mass is required in the $\overline{\text{MS}}$ scheme at the scale μ . In NMSSMCALC this is achieved by matching the measured OS top-quark mass onto the SM using one-loop and leading two-loop-QCD precision at the scale $\mu = m_Z$. Then, the SM RGEs are used to run $m_t^{\overline{\text{MS}},\text{SM}}(m_Z)$ to the scale μ where the one-loop and two-loop-QCD SUSY corrections are taken into account to obtain $m_t^{\overline{\text{MS}},\text{NMSSM}}(\mu)$. For more details we refer to Ref. [33]. This procedure partially avoids the appearance of large logarithmic corrections in the calculation of the top-quark mass.

In this thesis, the scale dependence Δ_{scale} of the mass M_{h_u} is defined as

$$\Delta_{\text{scale}} = \frac{|M_{h_u}(\mu) - M_{h_u}(\mu_0)|}{M_{h_u}(\mu_0)}, \quad (9.5)$$

where $\mu_0 = \sqrt{m_{\tilde{q}_3} m_{\tilde{t}_R}}$ is the default scale used in NMSSMCALC as described in Sec. 9.1. In Fig. 9.5(upper panels), we plot M_{h_u} as a function of μ/μ_0 calculated at $\mathcal{O}(\alpha_{\text{new}}^2)$ (red), $\mathcal{O}(\alpha_t(\alpha_t + \alpha_s))$ (black) and $\mathcal{O}(\alpha_t\alpha_s)$ (blue) for the parameter point P10S (left) and P20S (right). The lower panels show the result of $\Delta_{\text{scale}}(\mu/\mu_0)$ in percent.

We vary the renormalization scale from $\mu_0/2$ to $2\mu_0$ and observe the largest change in M_{h_u} of ± 1 GeV ($\pm \frac{1}{4}$ GeV) for the parameter point P10S (P20S) for the $\mathcal{O}(\alpha_t(\alpha_t + \alpha_s))$ result. At $\mathcal{O}(\alpha_{\text{new}}^2)$ the scheme dependence is slightly reduced compared to $\mathcal{O}(\alpha_t(\alpha_t + \alpha_s))$ while it is smallest at $\mathcal{O}(\alpha_t\alpha_s)$ for both parameter points. Thus, the relation between the individual corrections is very similar as in the renormalization scheme dependence. This leads to a similar conclusion as for the renormalization scheme dependence, *cf.* Sec. 9.2.2, that the inclusion of three-loop corrections from the top/stop sector is required in order to reduce the scale dependence.

However, comparing the scale dependence between the point P10S, which has a small h_u/h_s mixing, and P20S (large h_u/h_s mixing), we see that all three calculations perform almost equally bad in the case of a large h_u/h_s mixing while for small mixing the $\mathcal{O}(\alpha_t\alpha_s)$ has a very flat renormalization scale dependence. We argue that the origin of this behavior might be due to the extraction of the $\overline{\text{MS}}$ top-quark mass from the SM as described above. This approach assumes that all non-SM degrees of freedom are rather heavy and do not mix with the SM-like Higgs boson. This is a good approximation for P10S but not for P20S. In the latter case, we argue that a matching of the OS top quark mass to a singlet-extended SM rather than the SM might be more appropriate. A proper treatment of large-mixing contributions in the determination of the $\overline{\text{MS}}$ top-quark mass is reserved for future works.

Furthermore, we always use the full two-loop RGEs regardless of the considered two-loop

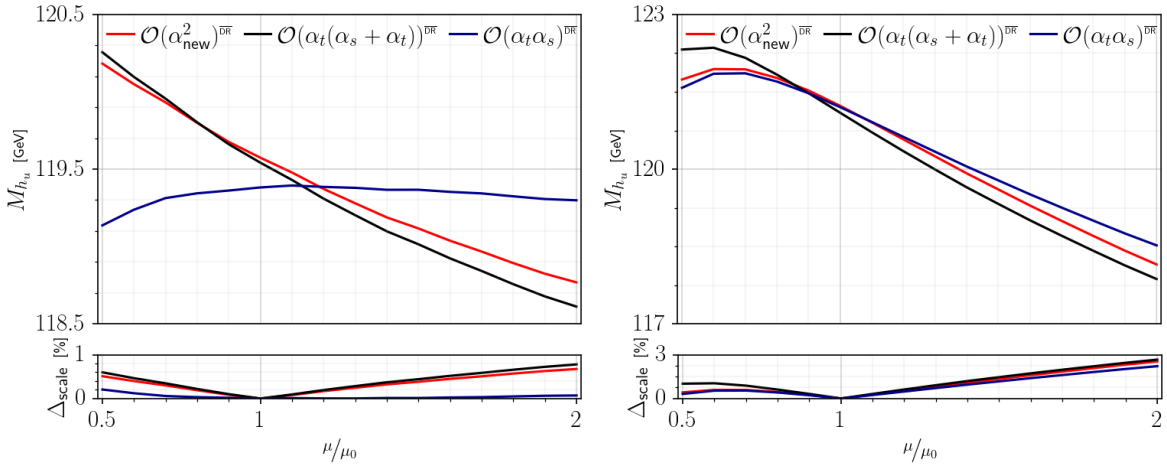


Figure 9.5.: Upper panels: The Higgs boson mass prediction for the h_u -like state as a function of the renormalization scale μ normalized to the default scale $\mu_0 = \sqrt{m_{\tilde{q}_3} m_{\tilde{t}_R}}$ for the parameter point P10S (left) and P20S (right). The prediction is shown at $\mathcal{O}(\alpha_{\text{new}}^2)$ (red), $\mathcal{O}(\alpha_t(\alpha_t + \alpha_s))$ (black) and $\mathcal{O}(\alpha_t\alpha_s)$ (blue). **Lower panels:** The scale dependence Δ_{scale} (Eq. (9.5)) in percent. *The data for the figures was taken from Ref. [210].*

corrections. In general, one needs to apply the same approximations in the RGEs as in the diagrammatic calculation, e.g. if calculating only $\hat{\Sigma}^{\mathcal{O}(\alpha_t(\alpha_t + \alpha_s))}$ one would only need to take into account terms of $\mathcal{O}(\alpha_t(\alpha_t + \alpha_s))$ in the RGEs. Thus, the comparison between the three different contributions has to be taken with caution.

9.2.4. Impact of the IR Regulator

In this section we study the numerical impact of the three different methods to regulate the physical IR divergences discussed in Chapter 8. We remind the reader that the previ-

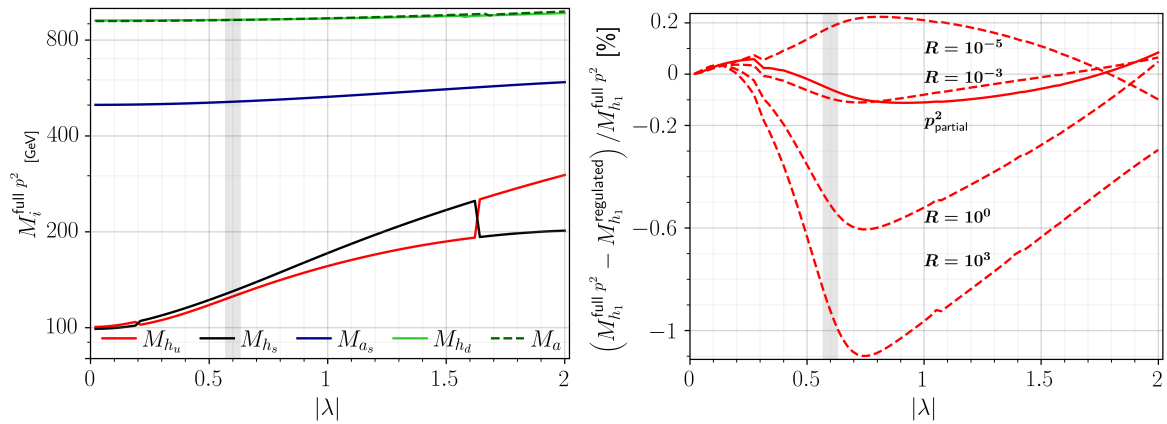


Figure 9.6.: Left: The five neutral Higgs boson masses $M_i^{\text{full } p^2}$ obtained for the point P20S when including the full external momentum dependence in all $\mathcal{O}((\alpha_t + \alpha_\kappa + \alpha_\lambda)^2)$ diagrams. The result is shown as a function of λ . **Right:** The relative difference between the lightest Higgs boson mass $M_{h_1}^{\text{full } p^2}$ obtained with full external momentum and the mass $M_{h_1}^{\text{mass regulated}}$ obtained using a mass regulator $M_R^2 = R\mu_0^2$ with $R = 10^{-5}, 10^{-3}, 1$ and 10^3 (dashed lines). The solid line shows the relative difference between $M_{h_1}^{\text{full } p^2}$ and the result obtained using a small external momentum expansion in the IR divergent diagrams. The grey shaded region fulfils the HiggsSignals constraints. *The data for the figures was taken from Ref. [210].*

ously studied parameter samples have been obtained using the method of a mass regulator $M_R^2 = R\mu_0^2$ with the specific value $R = 10^{-3}$. In this section we will justify this choice by comparing the results for the Higgs boson mass M_{h_u} obtained at $\mathcal{O}(\alpha_{\text{new}}^2)$ for different values of R with the results obtained when taking the full and partial momentum dependence into account.

In Fig. 9.6(left) we show all neutral Higgs boson masses $M_i^{\text{full } p^2}$, with $i = \{h_{u,d,s}, a_s, a\}$ (where the label marks the dominant gauge eigenstate contributing to the respective mass eigenstate), as a function of λ within the range $\lambda = [0, 2]$. The Higgs boson masses have been obtained at $\mathcal{O}(\alpha_{\text{new}}^2)$ by using the full external momentum dependence in all $\mathcal{O}((\alpha_t + \alpha_\kappa + \alpha_\lambda)^2)$ diagrams as described in Sec. 8.4. The h_u -, h_s - and a_s -like Higgs boson masses (black, red, and blue lines) depend strongly on λ while the heavy and nearly-degenerate h_d and a (green solid and dashed lines) only change for very large values of λ (note that a log scale is used). Due to the large mixing, the h_u - and h_s -like Higgs bosons change in the role of the lightest Higgs boson near $\lambda = 0.2$ and again near $\lambda = 1.6$. The grey shaded region is compatible with the `HiggsSignals` constraint.

In the right plot of Fig. 9.6 we compare the relative difference of $M_{h_1}^{\text{full } p^2}$ with the result obtained using a mass regulator, *cf.* Sec. 8.2, for different values of $R = \{10^{-5}, 10^{-3}, 10^0, 10^3\}$ (dashed lines from top to bottom) in percent. In addition, we also plot the relative difference of $M_{h_1}^{\text{full } p^2}$ with the result obtained using a small external momentum expansion in the IR-divergent diagrams (solid line), *cf.* Sec. 8.3. An important cross-check is that all dashed and the solid lines converge for $\lambda \rightarrow 0$ since they only differ in the treatment of the IR-divergent diagrams which are all proportional to λ and κ . However, they do not necessarily need to converge at $M_{h_1}^{\text{full } p^2} - M_{h_1}^{\text{regulated}} = 0$ since the full-momentum result also takes into account the momentum dependence in the $\mathcal{O}(\alpha_t^2)$ contributions which are IR-finite.

The partial-momentum result can be considered as physically well-motivated (compared to the mass regulated result) and should be closest to the full-momentum result. We find that the relative difference is not larger than 0.1% in the considered range of λ . In the range compatible with `HiggsSignals`, we find an absolute difference of less than 100 MeV. The results obtained with different values for the mass regulator differ between -1.1% ($R = 10^3$) and +0.2% ($R = 10^{-5}$) from the full external momentum result. For $R = 10^{-3}$ we find excellent agreement with the partial momentum result with a relative difference in the sub per mille level. In Sec. 8.3 we argued that the logarithmic dependence of the selfenergies on the mass regulator compared to the $\overline{\log} p^2$ dependence in the small-momentum expansion is very similar. However, the chosen value for the mass regulator is artificial while the external momentum can be identified with the tree-level mass. Thus, it is expected that the mass regulator should also be of the same order as the tree-level masses. For typical values of the renormalization scale $\mu_0 \approx 1 - 2 \text{ TeV}$ and tree-level masses $m_h \approx m_Z$ one indeed finds that $R = 10^{-3}$ is a good choice.

To further investigate the behavior of the different regulators, we utilize the scan sample collected in Sec. 9.1 which was obtained with $R = 10^{-3}$. In Fig. 9.7(left) we re-evaluate the scan sample using the small momentum expansion and show the relative difference $\Delta_{R=10^{-3}}^{\text{partial } p^2}(M_{h_u})$ of the h_u -like Higgs boson mass to the mass-regulated result in percent (which is analogously defined to the Δ_Y^X in Eq. (9.4)). The effect is shown as a function of $s_{\lambda\kappa} = \sqrt{\lambda^2 + \kappa^2}$ and $\tan\beta$. The distribution of the points is very similar to the relative difference of the $\mathcal{O}(\alpha_{\text{new}}^2)$ to $\mathcal{O}(\alpha_t(\alpha_t + \alpha_s))$ corrections in Fig. 9.2. However, overall the scale is one order of magnitude smaller. Therefore, the error introduced by a mass regulator with $R = 10^{-3}$ w.r.t. the small-momentum expansion is negligible compared to the overall size of the new two-loop corrections.

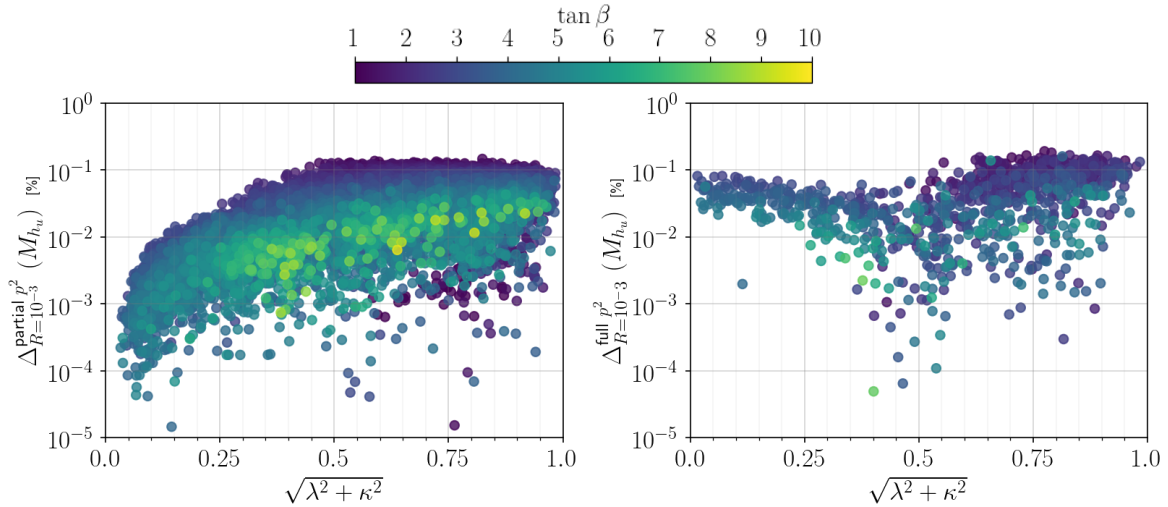


Figure 9.7.: **Left:** Comparison of the result for M_{h_u} obtained when using partial external momentum or a mass regulator ($R = 10^{-3}$) to cure the IR-divergences. **Right:** The same comparison but using full instead of partial external momentum dependence for a randomly selected subset of 1000 points. *The data for the figures was taken from Ref. [210].*

We also investigate how the mass-regulated result compares with the full-momentum result in the considered parameter space. For this purpose, we choose a random subset¹¹ of one thousand parameter points and re-evaluate them using the full external momentum approach. The calculation was restricted to a smaller number of points in order to save computational resources¹². In Fig. 9.7(right) we show the relative difference of $M_{h_u}^{\text{full } p^2}$ and $M_{h_u}^{\text{mass-regulated}}$ with $R = 10^{-3}$ in percent. Also in this comparison the relative difference is always smaller than 0.3%. However, in contrast to the comparison between the two IR-regulators, the difference to the full-momentum result does not tend to zero for $s_{\lambda\kappa} \rightarrow 0$. In this limit, the full external momentum is still taken into account in the $\mathcal{O}((\alpha_t + \alpha_\kappa + \alpha_\lambda)^2) \stackrel{\lambda, \kappa=0}{=} \mathcal{O}(\alpha_t^2)$ corrections. These corrections can also be as large as 0.1% compared to the mass-regulated result. Therefore, the full external momentum dependent corrections at $\mathcal{O}(\alpha_t^2)$ can be as important as those at $\Delta\mathcal{O}((\alpha_t + \alpha_\kappa + \alpha_\lambda)^2)$ for large λ and κ .

9.2.5. Impact of the CP-Violating Phases

In this section we study the impact of the CP-violating phases on the size of the two-loop $\mathcal{O}(\alpha_{\text{new}}^2)$ corrections. For this purpose we utilize the parameter point P20S from Tab. 9.2, which was evaluated assuming CP-conservation, and study its dependence on the CP-violating phases.

However, the CP-violating phases already enter the tree-level mass matrices which makes it difficult to identify loop-induced effects if the phases are varied individually. In Sec. 5.3 we discussed that there are two common linear combinations called φ_w and φ_y of the phases φ_λ , φ_κ , φ_u and φ_s which enter all tree-level relations, *cf.* Eq. (5.29). In particular, the neutral Higgs boson mass matrix only depends on $\sin \varphi_y$ at tree-level. We choose one possible solution for $\varphi_y = 0$,

$$\varphi_\lambda = 2\varphi_s \quad \text{and} \quad \varphi_\kappa = \varphi_u = 0, \quad (9.6)$$

in order to prevent the appearance of any CP-violating phase in the tree-level mass matrix of the neutral Higgs bosons. The phase φ_{A_t} of the parameter A_t only contributes at higher orders. Using the condition in Eq. (9.6), there are only two independent CP-violating phases,

¹¹We validated that this subset still has all important features of the original sample.

¹²The evaluation of all points still took about 2 months of CPU time.

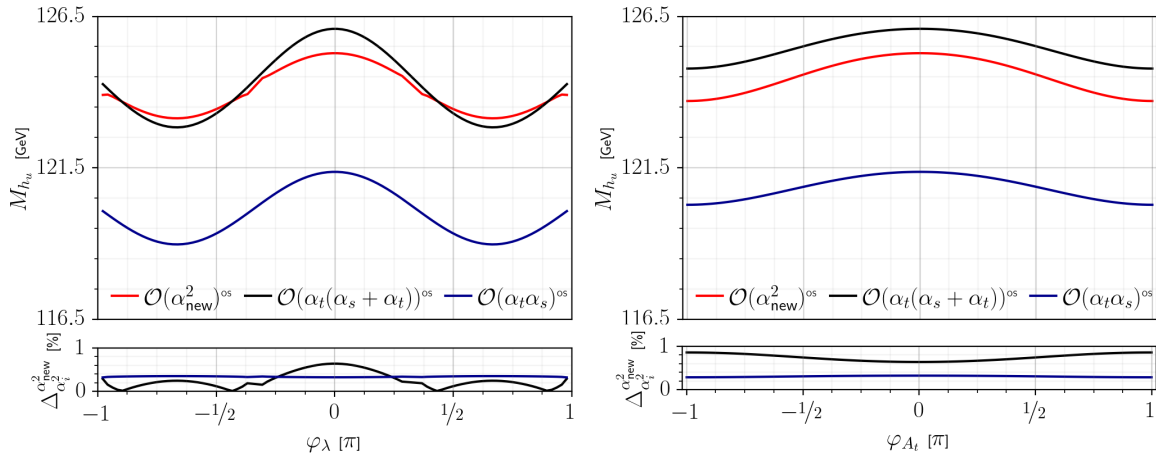


Figure 9.8.: Upper panels: Mass of the h_u -like Higgs boson for the parameter point P20S as a function of φ_λ (left) and φ_{A_t} (right) at two-loop $\mathcal{O}(\alpha_{\text{new}}^2)$ (red), $\mathcal{O}(\alpha_t(\alpha_t + \alpha_s))$ (black), and $\mathcal{O}(\alpha_t\alpha_s)$ (blue) in the OS renormalization scheme of the top/stop sector. **Lower panels:** Relative difference $\Delta_{\alpha_i^2}^{\alpha_{\text{new}}^2}$ between the new two-loop $\mathcal{O}(\alpha_{\text{new}}^2)$ corrections and the $\mathcal{O}(\alpha_i^2)$ result with $\alpha_i^2 = \mathcal{O}(\alpha_t(\alpha_t + \alpha_s))$ (black) and $\mathcal{O}(\alpha_t\alpha_s)$ (blue). The blue line in the lower panels is rescaled by a factor 0.1. The data for the figure was taken from Ref. [210].

φ_λ and φ_{A_t} , which enter the higher-order corrections.

In Fig. 9.8 (upper panels) we show the Higgs boson mass prediction for the h_u -like state as a function of φ_λ (left) and φ_{A_t} (right) at $\mathcal{O}(\alpha_{\text{new}}^2)$ (red), $\mathcal{O}(\alpha_t(\alpha_t + \alpha_s))$ (black), and $\mathcal{O}(\alpha_t\alpha_s)$ (blue) in the OS renormalization scheme of the top/stop sector. The lower panels show the relative difference $\Delta_{\alpha_i^2}^{\alpha_{\text{new}}^2}$ between the result obtained at $\mathcal{O}(\alpha_{\text{new}}^2)$ and $\mathcal{O}(\alpha_i^2) = \mathcal{O}(\alpha_t(\alpha_t + \alpha_s))$ (black) and $\mathcal{O}(\alpha_t\alpha_s)$ (blue, rescaled by a factor 0.1 for readability). The phases are varied between $-\pi$ and π . Using the EDMs calculated by NMSSMCALC and the experimental upper bounds discussed in Sec. 6.3 we find that non-zero values of φ_λ for this parameter point are excluded while φ_{A_t} is allowed for all considered values. Furthermore, the `HiggsSignals` constraint is also fulfilled in the whole considered range of φ_{A_t} .

The variation of φ_λ at $\mathcal{O}(\alpha_{\text{new}}^2)$ changes whether the mass eigenstate with the dominant h_u component is h_1 or h_2 . This explains the kinks observed at $|\varphi_\lambda| \approx 0.3\pi$ in Fig. 9.8(left). At $\mathcal{O}(\alpha_t(\alpha_t + \alpha_s))$ and $\mathcal{O}(\alpha_t\alpha_s)$ the mixing is such that h_1 is always the h_u -like Higgs boson. The overall dependence on the phases in Fig. 9.8 is governed by the one-loop contributions which are not shown here for the sake of readability. Successively introducing the two-loop contributions does change the relative difference to the $\mathcal{O}(\alpha_{\text{new}}^2)$ result by at most 0.6% for φ_λ and at most 0.3% for φ_{A_t} as the phases are varied (note that the blue lines in the lower panels are scaled by a factor of 0.1).

We conclude that the overall dependence of the two-loop corrections on the CP-violating phases is rather small. The new corrections proportional to φ_λ are larger than those proportional to φ_{A_t} . However, in the region allowed by the current EDM and collider constraints the corrections of φ_{A_t} play the dominant role. This is also in agreement with the findings of Ref. [187] which identified only a small window of allowed values for the NMSSM-specific phases using a random scan (with $\tan\beta < 5$) rather than a fixed input parameter (the experimental EDM constraints have been improved by one order of magnitude in the meantime, such that this window is much smaller today).

Final Conclusion and Outlook

This thesis studied the higher-order corrections to Higgs boson masses in the CP-violating Next-to-Minimal Supersymmetric Standard Model (NMSSM). We calculated the two-loop corrections that are proportional to the NMSSM-specific superpotential parameters λ and κ at the order $(\alpha_t + \alpha_\kappa + \alpha_\lambda)^2$, to the charged and neutral Higgs boson masses in the limit of vanishing gauge couplings in the Feynman diagrammatic approach. This is a major step towards precision predictions for Higgs boson masses in the NMSSM. The renormalization prescription involved mixed $\overline{\text{DR}}$ and on-shell (OS) conditions in the Higgs boson sector and OS as well as $\overline{\text{DR}}$ conditions in the top/stop sector. The possibility to choose between OS and $\overline{\text{DR}}$ conditions in the top/stop sector was used to estimate the size of missing higher-order corrections.

In Part I of this thesis, we introduced the Standard Model (SM) and studied the leading one-loop corrections to the Higgs boson, top-quark and Z -boson mass within the SM which we used to discuss the hierarchy problem. We introduced the concepts of regularization and renormalization as well as the notation used in this thesis to describe higher-order corrections to mass parameters.

In Part II, we introduced SUSY as one possible solution to the hierarchy problem and motivated the NMSSM as one possible candidate to solve the little hierarchy and the μ -problem of the Minimal Supersymmetric Standard Model (MSSM). We introduced the notation used to describe SUSY models and discussed the tree-level relations of the NMSSM which are important for the two-loop $\mathcal{O}((\alpha_t + \alpha_\kappa + \alpha_\lambda)^2)$ corrections. Furthermore, we gave a short of the state-of-the-art of higher-order corrections to Higgs boson masses in the MSSM and NMSSM.

Part III presented the two-loop $\mathcal{O}((\alpha_t + \alpha_\kappa + \alpha_\lambda)^2)$ calculation which has been performed in this thesis in detail. We prepared the diagrammatic two-loop calculation of the neutral and charged Higgs boson selfenergies by computing all necessary one- and two-loop counterterms. These include an OS two-loop counterterm for the SM vacuum expectation value (VEV) as well as the charged Higgs boson mass and the tadpole parameters, two-loop $\overline{\text{DR}}$ wave function renormalization constants and superpotential parameter counterterms, one-loop OS as well as $\overline{\text{DR}}$ counterterms for the top/stop sector and one-loop $\overline{\text{DR}}$ counterterms for all remaining

parameters. We found that additional finite parts are generated in intermediate results of the renormalized selfenergies due to $\mathcal{O}(\epsilon^1)$ -terms in OS counterterms. We confirmed that these finite parts cancel in the total renormalized selfenergies if the ϵ -expansion in $D = 4 - 2\epsilon$ dimensions is consistently applied to all counterterms including the generation of additional finite shifts in $\overline{\text{DR}}$ counterterms. These findings are in agreement with works that studied the same behavior at two-loop $\mathcal{O}(\alpha_t\alpha_s)$ and $\mathcal{O}(\alpha_t^2)$. Furthermore, we encountered unphysical infra-red (IR) divergences in the derivation of some two-loop OS counterterms, due to the appearance of massless Goldstone bosons, which cancel in the sum of all Feynman diagrams. To show this cancellation, we introduced a mass regulator in order to regularize the IR divergences and verified that the final results for the counterterms are independent of the mass regulator. The analytic expressions for the Feynman diagrams calculated in this thesis have been obtained using the `Mathematica` packages `SARAH`, `FeynArts`, `FeynCalc` and `TARCER`. If the Feynman diagrams have been evaluated at vanishing external momentum, we relied on analytic expressions from the literature for the two-loop integrals. In the case of IR-divergent loop integrals, we complemented these results with a set of IR-regulated loop functions which have been expanded around the mass regulator. In the calculation of the neutral Higgs selfenergies we encountered also a different type of IR divergence which does not cancel in the final sum but leads to a residual dependence on the mass regulator. The subset of Feynman diagrams leading to this residual dependence was identified and optionally evaluated at finite external momentum using a small momentum expansion. This is similar to the *generalized effective potential approximation* which has recently been developed in the literature. Furthermore, we optionally evaluated all Feynman diagrams of the $\mathcal{O}((\alpha_t + \alpha_\kappa + \alpha_\lambda)^2)$ corrections with arbitrary external momentum while solving the loop-integrals numerically using the computer package `TSIL`.

In the numerical analysis of the $\mathcal{O}((\alpha_t + \alpha_\kappa + \alpha_\lambda)^2)$ corrections, we found that the SM-like Higgs boson mass is altered by 0 – 3% for $\sqrt{\lambda^2 + \kappa^2} = 0 - 1$ using a random parameter scan. The choice of λ and κ was motivated by ensuring perturbativity below the grand unification scale. In this scan, the previously calculated $\mathcal{O}(\alpha_t^2)$ corrections were found to be as large as 12% but can also become as small as 2-4% for large values of λ and κ . Therefore, the $\mathcal{O}((\alpha_t + \alpha_\kappa + \alpha_\lambda)^2)$ corrections calculated in this work are of particular importance in the regime of large λ and κ since they can become large relative to the previously calculated $\mathcal{O}(\alpha_t^2)$ corrections. For even larger values of λ and κ , we found corrections which can amount up to 6% by studying the dependence of individual parameter points on λ and κ . We further studied the impact of the two-loop corrections on the phenomenologically important couplings of the SM-like Higgs boson to the SM vector bosons which were significantly modified upon inclusion of the higher-order corrections. We also investigated the dependence of the SM-like neutral Higgs boson mass on the chosen renormalization scheme in the top/stop sector as well as on the chosen renormalization scale. We found that the renormalization scheme dependence is slightly reduced by 0-2% compared to the previous calculation to an overall size of 1-8% in the considered parameter space. The renormalization scale dependence was found to be between 1-3% and largest if the singlet-like state mixes with the SM-like Higgs boson. Furthermore, we investigated the three different methods of treating the residual IR divergences with a mass regulator, partial- or full-external momentum and their impact on the prediction of the SM-like Higgs boson mass. We found that a mass regulator of $M_R^2 = R\mu_0^2$ with $R = 10^{-3}$, where μ_0 is the renormalization scale, introduces a deviation compared to the partial- and full-external momentum results which is one order of magnitude smaller than the overall size of the $\mathcal{O}((\alpha_t + \alpha_\kappa + \alpha_\lambda)^2)$ two-loop corrections. The impact of the CP-violating phases on the Higgs boson mass prediction was found to be only mildly modified by the $\mathcal{O}((\alpha_t + \alpha_\kappa + \alpha_\lambda)^2)$ corrections. Overall the effect of was found to be smaller than 1% compared to the two-loop $\mathcal{O}(\alpha_t(\alpha_t + \alpha_s))$ corrections.

In conclusion, we have calculated the two-loop $\mathcal{O}((\alpha_t + \alpha_\kappa + \alpha_\lambda)^2)$ corrections to the Higgs boson masses in the CP-violating NMSSM while providing an efficient way of regularizing intermediate and residual IR divergences which has been implemented in the computer code `NMSSMCALC 4.00`. This is a major step towards precision predictions for the NMSSM Higgs boson masses.

In the following we briefly give an outlook on future directions that can be taken to further improve on the precision predictions for the NMSSM Higgs boson masses. We found that dependence of the Higgs boson mass prediction on the renormalization scheme in the top/stop sector is not significantly reduced compared to the previous calculations. This demands for the inclusion of higher-order corrections which are specific to the top/stop sector such as the three-loop $\mathcal{O}(\alpha_s^2 \alpha_t)$ corrections. To increase the precision of the calculation at the two-loop level, the momentum-dependent corrections in the $\mathcal{O}(\alpha_t \alpha_s)$ calculation as well as the corrections proportional to the electroweak gauge couplings are required. Completing the two-loop calculation is a difficult but technically feasible calculation that could be studied in the future. Furthermore, the extraction of the $\overline{\text{MS}}$ top-quark mass from the measured OS value using an effective SM could be extended by a matching to an effective singlet-extended SM in the future in order to reduce the renormalization scale dependence in the case of a large mixing between the SM-like and singlet-like Higgs boson. Another aspect of the $\mathcal{O}((\alpha_t + \alpha_\kappa + \alpha_\lambda)^2)$ corrections which was not studied in this thesis is the renormalization scheme dependence of the neutral Higgs boson masses on the choice of OS/ $\overline{\text{DR}}$ renormalization conditions for the charged Higgs boson mass. It would be interesting to perform a detailed study of the scheme uncertainty when including the new two-loop corrections compared to the one-loop result. Furthermore, the two-loop calculation presented in this work can be used as an independent cross-check of the calculation implemented in the computer tool `SARAH`. However, `SARAH` uses a pure $\overline{\text{DR}}$ scheme to obtain the loop-corrected Higgs boson masses. Therefore, a comparison of the selfenergies (or even the loop-corrected masses) computed by both programs requires to control all input parameters accordingly. Another direction, which was not the focus of this thesis, is to calculate the Higgs boson masses in the NMSSM using an Effective Field Theory (EFT) approach by integrating out all heavy fields. This has already been studied in detail for the MSSM. However, the NMSSM has more degrees of freedom which entails a large number of possible EFT scenarios such as e.g. a singlet-extended SM, a Two-Higgs-Doublet Model (2HDM) or a singlet-extended 2HDM, to name but a few. Performing one- and two-loop matchings in all possible scenarios is a tedious but feasible task.

Finite One-Loop Counterterm Contributions

In the following, we present the results for the finite parts of the one-loop OS counterterms for m_t and v which were already presented in Ref. [210]. The finite part of the one-loop top-quark mass counterterm reads

$$\begin{aligned}
\delta^{(1)}m_t^{\text{OS}}|_{\text{fin}} = & m_t^3 \left(-c_\beta^2 B_1(m_t^2, 0, M_{H^\pm}^2) + \frac{s_\beta^2}{2} + B_0(m_t^2, m_{\tilde{Q}_3}^2, m_{\tilde{\chi}_2^+}^2) + B_1(m_t^2, m_{\tilde{Q}_3}^2, m_{\tilde{\chi}_2^+}^2) \right) \\
& + m_t^3 \sum_{i=1}^5 \left((\mathcal{R}_{i2}^2 - \mathcal{R}_{i5}^2) B_0(m_t^2, m_t^2, m_{h_i}^2) - (\mathcal{R}_{i2}^2 + \mathcal{R}_{i5}^2) B_1(m_t^2, m_t^2, m_{h_i}^2) \right) \\
& + \sum_{i=1}^3 \sum_{j=1}^2 \left[m_t^3 B_1(m_t^2, m_{\tilde{t}_j}^2, m_{\tilde{\chi}_i^0}^2) |N_{i2}|^2 + m_t^2 B_0(m_t^2, m_{\tilde{t}_j}^2, m_{\tilde{\chi}_i^0}^2) (m_t |N_{i2}|^2 \right. \\
& \left. + e^{-i\varphi_u} m_{\tilde{\chi}_i^0} (N_{i2}^*)^2 \mathcal{U}_{i2}^{\tilde{t}} \mathcal{U}_{i1}^{*\tilde{t}} + e^{i\varphi_u} m_{\tilde{\chi}_i^0} N_{i2}^2 \mathcal{U}_{i1}^{\tilde{t}} \mathcal{U}_{i2}^{*\tilde{t}}) \right]. \tag{A.1}
\end{aligned}$$

The functions A_0 , B_0 (B_1) are the UV-finite parts of the one-loop scalar one-point, and scalar (tensor) two-point functions [33]. The finite part of the one-loop VEV counterterm reads

$$\begin{aligned}
\delta^{(1)}v^{\text{OS}}|_{\text{fin}} = & \frac{3}{32\pi^2 s_{\theta_W}^2 v} \left(c_{2\theta_W} |\mathcal{U}_{11}^{\tilde{t}}|^2 F_0(m_{\tilde{t}_1}^2, m_{\tilde{Q}_3}^2) + c_{2\theta_W} |\mathcal{U}_{t_{21}}|^2 F_0(m_{\tilde{t}_2}^2, m_{\tilde{Q}_3}^2) \right. \\
& \left. - c_{\theta_W}^2 |\mathcal{U}_{11}^{\tilde{t}}|^2 |\mathcal{U}_{12}^{\tilde{t}}|^2 F_0(m_{\tilde{t}_1}^2, m_{\tilde{t}_2}^2) \right) + \frac{1}{16\pi^2 v s_{\theta_W}^2} \Delta v, \tag{A.2}
\end{aligned}$$

with

$$\begin{aligned}
\Delta v = & -c_{2\theta_W} A_0(M_{H^\pm}^2) + c_{2\theta_W} \sum_{i=1}^3 \left[(|N_{i1}|^2 + |N_{i2}|^2) F_1(m_{\tilde{\chi}^\pm}^2, m_{\tilde{\chi}_i^0}^2) \right. \\
& \left. + 8m_{\tilde{\chi}^\pm} m_{\tilde{\chi}_i^0} \operatorname{Re}(e^{i\varphi_s} N_{i1}^* N_{i2}) B_0(0, m_{\tilde{\chi}^\pm}^2, m_{\tilde{\chi}_i^0}^2) \right] \\
& - \frac{1}{4} c_{2\theta_W} \sum_{i,j=1}^3 \left[|(N_{i1}^* N_{j1} - N_{i2}^* N_{j2})|^2 F_1(m_{\tilde{\chi}_j^0}^2, m_{\tilde{\chi}_i^0}^2) \right. \\
& \left. + 4m_{\tilde{\chi}_i^0} m_{\tilde{\chi}_j^0} B_0(0, m_{\tilde{\chi}^\pm}^2, m_{\tilde{\chi}_i^0}^2) (N_{i1}^* N_{j1} - N_{i2}^* N_{j2})^2 \right] \\
& + \frac{1}{4} \sum_{i=1}^5 \left[2s_{\theta_W}^2 (\mathcal{R}_{i1}^2 + \mathcal{R}_{i2}^2 + \mathcal{R}_{i4}^2) A_0(m_{h_i}^2) + c_{2\theta_W} F_2(m_{h_i}^2, M_{H^\pm}^2) \right. \\
& \left. \times ((s_\beta \mathcal{R}_{i1} - c_\beta \mathcal{R}_{i2})^2 + \mathcal{R}_{i4}^2) + F_2(m_{h_i}^2, 0) (-s_{\theta_W}^2 (c_\beta \mathcal{R}_{i1} + s_\beta \mathcal{R}_{i2})^2) \right] \\
& - \frac{1}{8} c_{2\theta_W} \sum_{i,j=1}^5 F_2(m_{h_i}^2, m_{h_j}^2) ((s_\beta \mathcal{R}_{j1} - c_\beta \mathcal{R}_{j2}) \mathcal{R}_{i4} + (s_\beta \mathcal{R}_{i1} - c_\beta \mathcal{R}_{i2}) \mathcal{R}_{j4}) \quad (\text{A.3})
\end{aligned}$$

and

$$F_0(x, y) = x + y - \frac{2xy}{x-y} \log \frac{x}{y}, \quad (\text{A.4a})$$

$$F_1(x, y) = x + y - 2 \frac{x^2 \overline{\log}(x) - y^2 \overline{\log}(y)}{x-y}, \quad (\text{A.4b})$$

$$F_2(x, y) = 3x + 3y - 2 \frac{x^2 \overline{\log}(x) - y^2 \overline{\log}(y)}{x-y}. \quad (\text{A.4c})$$

Expressions for finite parts of the two-loop one-shell counterterms are quite lengthy and not shown here.

Mass Regulated One- and Two-Loop Functions

In this appendix, we extend the analytically known one- and two-loop selfenergy integrals at vanishing external momentum, $p^2 = 0$, by a set of IR-regularized integrals. For $p^2 = 0$, all scalar two- and one-loop integrals can be written in terms of the two- and one-loop tadpole integral $I(x, y, z)$ and $A(x)$, respectively. The integral I and its analytical solutions for all possible combinations of mass parameters have been studied in Refs. [58, 142]. The tadpole integrals $I(x, y, z)$ and $A(x)$ are IR-finite. However, the derivatives w.r.t. their squared mass parameters are IR divergent, i.e. diverge if the derivatives are evaluated at zero mass squared. If this is the case, we replace the vanishing scalar masses with a mass regulator $0 \rightarrow M_R^2$ and expand the loop integrals around the small regulator mass. We keep all terms of order $\mathcal{O}(\overline{\log}^{n \leq 2} M_R^2)$ and $\mathcal{O}(M_R^{-n \leq 0})$ in the expansion.

All necessary one- and two-loop scalar integrals have already been introduced in Chapter 2, Eqs. (3.14a), (3.14b), (3.37) and (3.39). The notation used for describing the integrals is the same as in the computer program TSIL, *cf.* Ref. [46, 59]. In addition, we introduce the scalar three-point integral \mathbf{C} , *cf.* Eq. (3.39). This integral allows us to keep track of the IR divergences caused by the function $\mathbf{C}(x, 0, 0)$ which are cancelled between counterterm-inserted diagrams and genuine two-loop diagrams involving the \mathbf{V} -integral, as discussed in Sec. 8.3.

At one-loop order, we need the following IR-safe integrals

$$\mathbf{C}(x, 0, 0) = \partial \mathbf{B}(0, x) \tag{B.1}$$

$$\mathbf{C}(0, y, 0) = \frac{\mathbf{B}(y, 0) - \mathbf{B}(0, 0)}{x} \tag{B.2}$$

$$\mathbf{B}(0, 0) = -\overline{\log} M_R^2 + \epsilon \frac{(\zeta_2 + \overline{\log}^2 M_R^2)}{2} + \frac{1}{\epsilon} \tag{B.3}$$

$$\partial \mathbf{B}(0, 0) = -\frac{1}{2M_R^2} + \epsilon \frac{\overline{\log} M_R^2}{2M_R^2} \tag{B.4}$$

$$\partial \mathbf{B}(0, y) = \frac{B(0, y)}{y} + \frac{\overline{\log} M_R^2}{y} + \frac{\epsilon}{y} \left(1 - \overline{\log} y + \overline{\log}^2 y - \frac{\overline{\log}^2 M_R^2}{2} \right). \tag{B.5}$$

There are also two-loop diagrams which can be written as products of two one-loop functions. If a one- and three-point function are multiplied, a strict expansion in the mass regulator yields

$$\mathbf{A}(M_R^2)\mathbf{C}(M_R^2, M_R^2, M_R^2) = \frac{1}{2} + \overline{\log}M_R^2 + \frac{1}{2\epsilon} + \mathcal{O}(M_R^2). \quad (\text{B.6})$$

However, the one-point function vanishes for a vanishing argument, $\mathbf{A}(0) = 0$. Thus, this kind of diagram would vanish if we were to calculate it at finite external momentum. Therefore, we neglect the contributions from such diagrams in the expansion.

At two-loop order, we can write all scalar selfenergies in terms of I and its first and second derivative using the following notation

$$\partial I(x, y, z) \equiv \frac{\partial}{\partial x'} I(x', y, z)|_{x'=x} \quad (\text{B.7})$$

$$\partial^2 I(x, y, z) \equiv \frac{\partial^2}{\partial x' \partial y'} I(x', y', z)|_{x'=x, y'=y}. \quad (\text{B.8})$$

For the NMSSM, we need the following special cases of IR-regularized two-loop functions

$$\partial I(0, x, y) = \overline{\log}M_R^2 B(x, y) - \overline{T}(0, x, y) \quad (\text{B.9})$$

$$\partial^2 I(0, 0, z) = \frac{z(2\overline{\log}z - 5) - 2I(0, 0, z)}{z^2} + \frac{\overline{\log}M_R^2(-2\overline{\log}z + \overline{\log}M_R^2 + 2)}{z} \quad (\text{B.10})$$

$$\partial^2 I(0, y, 0) = \frac{\overline{\log}y}{y} - \frac{\overline{\log}M_R^2}{y} \quad (\text{B.11})$$

$$\partial^2 I(0, y, y) = \frac{\overline{\log}y - \overline{\log}M_R^2 + 1}{2y} \quad (\text{B.12})$$

$$\partial^2 I(0, y, z) = z \frac{2I(0, y, z) - \overline{\log}y(4y + z) + (\overline{\log}y - 2)\overline{\log}z(y + z)}{(y - z)^3} \quad (\text{B.13})$$

$$+ \frac{y^2\overline{\log}y + 5z(y + z)}{(y - z)^3} + \frac{\overline{\log}M_R^2(z\overline{\log}y - z\overline{\log}z - y + z)}{(y - z)^2}. \quad (\text{B.14})$$

The function \overline{T} is IR-finite and has been introduced in Ref. [46]. It is identical to the function $R_{SS}(x, y)$ used in Refs. [26, 27]. For completeness, we repeat here the solutions required for the NMSSM $\mathcal{O}((\alpha_t + \alpha_\kappa + \alpha_\lambda)^2)$ calculation:

$$\overline{T}(0, x, y) = \frac{(x + y)I(0, x, y) + 2(A(x) - y)(A(y) - x) + x^2 + y^2}{(x - y)^2} \quad (\text{B.15})$$

$$\overline{T}(0, x, x) = -\frac{1}{2}\overline{\log}x^2 - \overline{\log}x - \frac{3}{2}. \quad (\text{B.16})$$

Using this set of IR-safe functions, we can write the remaining two-loop functions, which are IR-divergent at vanishing external momentum, in an IR-regulated manner. We begin with the UV-divergent \mathbf{U} -integral,

$$\mathbf{U}(x, y, z, u) = U(x, y, z, u) + \frac{\mathbf{B}(x, y)}{\epsilon} + \frac{1}{2} \left(\frac{1}{\epsilon} - \frac{1}{\epsilon^2} \right) \quad (\text{B.17})$$

$$U(x, y, z, u) \stackrel{p^2=0}{=} \frac{I(z, u, y) - I(z, u, x)}{x - y} \quad (\text{B.18})$$

$$U(x, x, y, z) = -\partial I(x, y, z). \quad (\text{B.19})$$

Thus, we are required to regulate

$$\mathbf{U}(0, 0, x, y) = -\partial I(0, x, y) + \frac{\zeta_2 + \overline{\log}^2 M_R^2}{2} + \frac{1 - 2\overline{\log}M_R^2}{2\epsilon} + \frac{1}{2\epsilon^2}. \quad (\text{B.20})$$

There are also unphysical UV-IR mixing terms $\mathcal{O}(\overline{\log}M_R^2/\epsilon)$. We verified that these terms cancel with contributions from counterterm-inserted diagrams that involve a vertex counterterm and an IR-divergent $\mathbf{B}(0,0)$ integral.

The \mathbf{V} -integral

$$\mathbf{V}(x, y, z, u) = -\frac{\partial}{\partial y}\mathbf{U}(x, y, z, u) \quad (\text{B.21})$$

also contributes with UV-IR mixing terms since its single pole can be written as

$$\mathbf{V}(x, 0, z, u)|_{\epsilon^{-1}} = -\frac{\partial}{\partial y}\mathbf{U}(x, y, z, u)|_{y=0}|_{\epsilon^{-1}} = -\frac{\mathbf{C}(x, 0, 0)}{\epsilon}. \quad (\text{B.22})$$

It was checked to cancel against counterterm-inserted diagrams involving a Higgs boson mass counterterm and a three-point function. Furthermore, we need the following special cases of vanishing arguments,

$$\mathbf{V}(0, 0, 0, u) = -\frac{\overline{\log} u}{2M_R^2} - \frac{\overline{\log} u}{2u} - \frac{\overline{\log}M_R^2}{2M_R^2} + \frac{\overline{\log}M_R^2}{2u} + \frac{1}{2M_R^2}\left(1 + \frac{1}{\epsilon}\right) \quad (\text{B.23})$$

$$\mathbf{V}(0, 0, z, z) = -\frac{\overline{\log}(z)}{2M_R^2} - \frac{\overline{\log}M_R^2}{2M_R^2} + \frac{1}{2M_R^2\epsilon} \quad (\text{B.24})$$

$$\begin{aligned} \mathbf{V}(0, 0, z, u) = & \frac{1}{2(z-u)^4} \left\{ -u\overline{\log} u [2z\overline{\log} z(u+z) + 2(\overline{\log}M_R^2 - 3)uz - (2\overline{\log}M_R^2 + 3)z^2 + u^2] \right. \\ & + z\overline{\log} z ((2\overline{\log}M_R^2 + 3)u^2 - 2(\overline{\log}M_R^2 - 3)uz - z^2) \\ & \left. - 4uzI(z, 0, u) + (u+z)(\overline{\log}M_R^2(z-u)^2 - 10uz) \right\} \\ & + \frac{u\overline{\log} u - z\overline{\log} z - u + z}{2M_R^2(z-u)} - \frac{\overline{\log}M_R^2}{2M_R^2} + \frac{1}{2M_R^2\epsilon} \end{aligned} \quad (\text{B.25})$$

$$\mathbf{V}(x, 0, z, u) = \frac{I(x, z, u) - I(0, z, u) - x\partial I(0, z, u)}{x^2} \quad (\text{B.26})$$

$$+ \frac{2\overline{\log} x - \overline{\log}^2 x + \overline{\log}^2 M_R^2 - 2}{2x} + \frac{\overline{\log} x - \overline{\log}M_R^2 - 1}{x\epsilon}. \quad (\text{B.27})$$

The two-loop master integral \mathbf{M} at vanishing external momentum is UV-finite and requires to be IR-regularized in the following two special cases,

$$\mathbf{M}(x, 0, z, 0, v) = \frac{\partial I(0, x, v) - \partial I(0, z, v)}{x-z} \quad (\text{B.28})$$

$$\mathbf{M}(x, 0, x, 0, v) = \partial^2 I(0, x, v). \quad (\text{B.29})$$

For the calculation of the wave function renormalization constant, we further need the derivatives of the one-loop integrals and the derivatives of the UV-divergent parts of the two-loop integrals w.r.t. the external momentum. For the regularized expansion, we get

$$\partial_{p^2}\mathbf{U}(0, 0, x, y)|_{\text{UV-div}} = \frac{\partial_{p^2}\mathbf{B}(0, 0)}{\epsilon} \quad (\text{B.30})$$

$$\partial_{p^2}\mathbf{C}(x, 0, 0) = \frac{5 + 2\overline{\log}M_R^2 - \overline{\log} x}{2x^2} \quad (\text{B.31})$$

$$\partial_{p^2}\mathbf{C}(0, 0, 0) = -\frac{1}{12M_R^4} \quad (\text{B.32})$$

$$\partial_{p^2}\mathbf{B}(0, 0) = \frac{1}{6M_R^2}. \quad (\text{B.33})$$

The finite part of the derivative of the \mathbf{U} -integral is not necessary since all all wave functions are renormalized in the $\overline{\text{DR}}$ scheme.

We only simplify all expressions for Feynman diagrams up to the level of the **M**, **U**, **V** and **S** two-loop integrals, even in the zero-momentum approximation (i.e. we do not write them in terms of the I -integral). During the numerical evaluation at zero external momentum, we express them in terms of the I integrals given above. If we compute the Feynman diagrams using partial external momentum dependence, we only replace those loop-functions with the IR-regularized ones which cannot be regularized by momentum according to Tab. C.2 and use the partial momentum results from the literature [27, 28] for the remaining integrals. If we include the full external momentum dependence in all Feynman diagrams, we proceed as in the partial-momentum case but rely on the numerical results obtained with the computer program TSIL.

When using only a mass regulator, we find that the final result of the neutral Higgs boson self-energies only depends on $\mathcal{O}(\overline{\log} M_R^2)$ and $\mathcal{O}(\overline{\log}^2 M_R^2)$ divergences while all $\mathcal{O}(M_R^{-n \leq -2})$ -terms cancel. The logarithmic divergences correspond to $\mathcal{O}(\epsilon_{\text{IR}}^{-1})$ and $\mathcal{O}(\epsilon_{\text{IR}}^{-2})$ poles in dimensional regularization while the quadratic divergences are of kinematic nature. Thus, only the physical divergences (which can be regularized by finite external momentum) remain while all other divergences are cancelled.

IR-Divergent Topologies

We list all IR-divergent two-loop tadpole and selfenergy topologies in Tab. C.1 and Tab. C.2. The first column contains a counting index. The second column shows a graph of the topology with labels on each generic propagator. The third column lists all special cases which lead to IR-divergent loop functions. The notation is such that e.g. $m_{3,4,5} = 0$ means that all masses need to vanish (logical *and*) while $m_3 = m_{4/5} = 0$ means that only one of the two masses labeled with 5 and 4 vanishes (logical *or*). The fourth column collects the various sets discussed in Chapter 8. The fifth column lists the IR-divergent loop functions that appear in all possible field-insertions after applying TARCER's reduction algorithm. The last column indicates whether the IR divergence cancels in the final result or if it requires the inclusion of external momentum. Note that the IR divergences can only be caused by massless scalars which can be shown from first principles using dimensional arguments.

The tadpole diagrams shown in Tab. C.1 cannot be treated with external momentum and are therefore manifestly IR-finite if the sum of all contributions is consistently taken into account

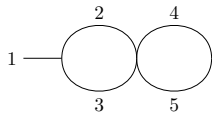
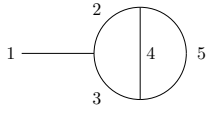
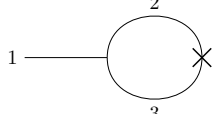
#	topology	conditions for IR divergence	set	IR-divergent functions	momentum regularizable?
1		$m_2 = m_3 = 0$	A	$\mathbf{B}(0, 0)$	no
2		$m_2 = m_3 = 0$	A	$\mathbf{U}(0, 0, m_4^2, m_5^2), \mathbf{B}(0, 0)$	no
3		$m_2 = m_3 = 0$	A	$\mathbf{B}(0, 0)$	no

Table C.1.: All IR-divergent two-loop tadpole topologies. The IR divergences can only be caused by vanishing scalar masses while all remaining lines can be scalars or fermions if the couplings allow for it. *Table taken from Ref. [210].*

as described in Sec. 8.2. However, the selfenergy diagrams require external momentum for a few special cases. In addition, there are cases (such as for instance $m_3 = m_4 = 0$ in topology 4) which cannot be made IR-finite by including external momentum. In these cases, we found a cancellation between other diagrams which are connected by the BPHZ theorem [209] (such as set C which forms an IR-finite subset). Similarly to the tadpole diagrams, the tadpole-like topologies 8, 10 and 13 (set A) form an IR-finite subset since there is no external momentum running into the loops.

Applying these rules to the NMSSM, we find that only the diagrams in Fig. D.3 are regularized by momentum. To cross-check this result, we validated that the residual dependence of the mass regulator (when not using finite external momentum) reduces to the same subset of diagrams.

#	topology	conditions for IR divergence	set	IR-divergent functions	momentum regularizable?
4		$m_{3,4,5} = 0$	E	$\mathbf{C}(0, 0, 0)$	yes
		$m_4 = m_5 = 0$	B	$\mathbf{C}(0, m_{4/3}^2, 0)$	no
		$m_3 = m_{4/5} = 0$	C	$\mathbf{C}(m_5^2, 0, 0)$	no
5		$m_5 = m_6 = 0$	D	$\mathbf{U}(0, 0, m_3^2, m_4^2)$	yes
6		$m_4 = m_7 = 0$	D	$\mathbf{M}(m_3^2, m_4^2, m_6^2, m_7^2, m_5^2),$	yes
		$m_3 = m_6 = 0$	D	$\mathbf{B}(0, 0)$	
7		$m_{3,4,7} = 0$	E	$\mathbf{V}(0, 0, m_5^2, m_6^2), \mathbf{C}(0, 0, 0)$	yes
		$m_4 = m_7 = 0$	B	$\mathbf{V}(m_3^2, 0, m_5^2, m_6^2), \mathbf{C}(m_3^2, 0, 0)$	no
		$m_3 = m_{4/7} = 0$	C	$\mathbf{U}(0, 0, m_5^2, m_6^2), \mathbf{C}(0, m_{7/4}^2, 0)$	no
8		$m_3 = m_4 = 0$	A	$\mathbf{B}(0, 0)$	no
9		$m_3 = m_4 = 0$ $m_5 = m_6 = 0$	D D	$\mathbf{B}(0, 0)$	yes
10		$m_5 = m_6 = 0$	A	$\mathbf{U}(0, 0, m_4^2, m_3^2), \mathbf{B}(0, 0)$	no
11		$m_{3,4,5} = 0$	E	$\mathbf{C}(0, 0, 0)$	yes
		$m_3 = m_4 = 0$	B	$\mathbf{C}(0, m_{4/3}^2, 0)$	no
		$m_{3/4} = m_5 = 0$	C	$\mathbf{C}(m_5^2, 0, 0)$	no
12		$m_3 = m_4 = 0$	D	$\mathbf{B}(0, 0)$	yes
13		$m_3 = m_4 = 0$	A	$\mathbf{B}(0, 0)$	no

Table C.2.: All two-loop selfenergy topologies. For topologies 5 and 12 mirror diagrams exist which can be derived by renaming the indices accordingly. *Table taken from Ref. [210].*

Two-Loop Feynman Diagrams

In this appendix we show the Feynman diagrams calculated in this thesis. All Feynman diagrams shown in this thesis have been created with the help of `TikZ-Feynman` [212].

D.1. Tadpoles

Figure D.1 shows all generic two-loop tadpole diagrams with internal scalars and fermions. The summation over internal fields considers all possible NMSSM permutations which obey the constraint

$$n_{h_i} + n_{h_j^\pm} + n_{\chi_k} + n_{\chi_l^\pm} \geq 2, \tag{D.1}$$

where n_Φ is the number of internal propagators of the field type Φ . Furthermore, we calculate the two-loop diagrams of $\mathcal{O}(\alpha_t^2)$, *cf.* Ref. [33] Fig. 3, while this time taking into account terms of the order $\mathcal{O}(\alpha_t \alpha_\lambda)$ which were neglected in the applied MSSM-limit in Ref. [33]. At the one-loop order, all tadpole diagrams (*cf.* Fig. 3.2) with at least one Higgs boson, electroweakino, stop or top-quark field in the loop are taken into account.

In Fig. D.1 we colorize all propagators in red which lead to IR divergences for $S = G^0, G^\pm$ i.e. if the propagators become massless. However, if we use the mass regularized loop functions given in Appendix B, we confirm that the sum of all tadpole diagrams is IR-finite and does not depend on the regulator mass.

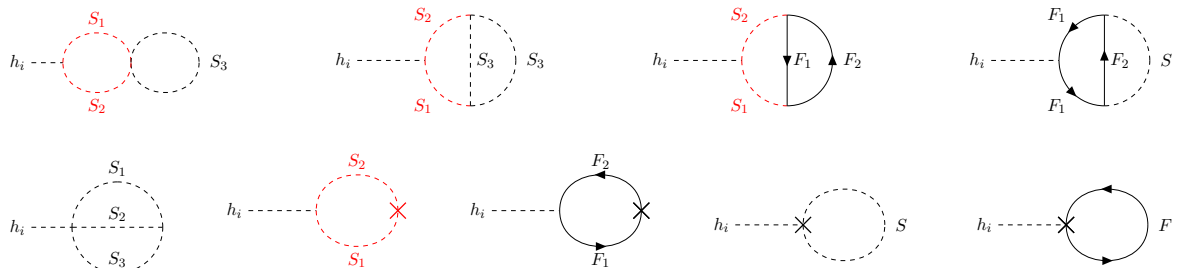


Figure D.1.: All generic two-loop tadpole diagrams considered in this work. S denotes scalars and F denotes fermions. Diagrams with red propagators become IR divergent for massless Goldstone bosons. *Figure taken from Ref. [210].*

D.2. Selfenergies

Figure D.2 lists all generic selfenergy diagrams appearing in the calculation of the two-loop $\mathcal{O}((\alpha_t + \alpha_\kappa + \alpha_\lambda)^2)$ Higgs boson and vector boson selfenergies. The external fields s_i can be the neutral (h_i) or charged (h^\pm) Higgs bosons as well as massive SM vector bosons (Z or W^\pm). Similar to the two-loop tadpole diagrams, we re-calculate all selfenergy diagrams from the $\mathcal{O}(\alpha_t^2)$ calculation, *cf.* Ref. [33] Figs. 14 and 15, while also taking into account contributions of $\mathcal{O}(\alpha_t \alpha_\lambda)$.

The summation over the internal degrees of freedom is carried out in the same way as for the tadpole diagrams, i.e. using Eq. (D.1). For asymmetric diagrams such as (b), (d), (p) or (q), an additional factor of two need to be taken into account in order to include the contributions from the mirrored diagrams.

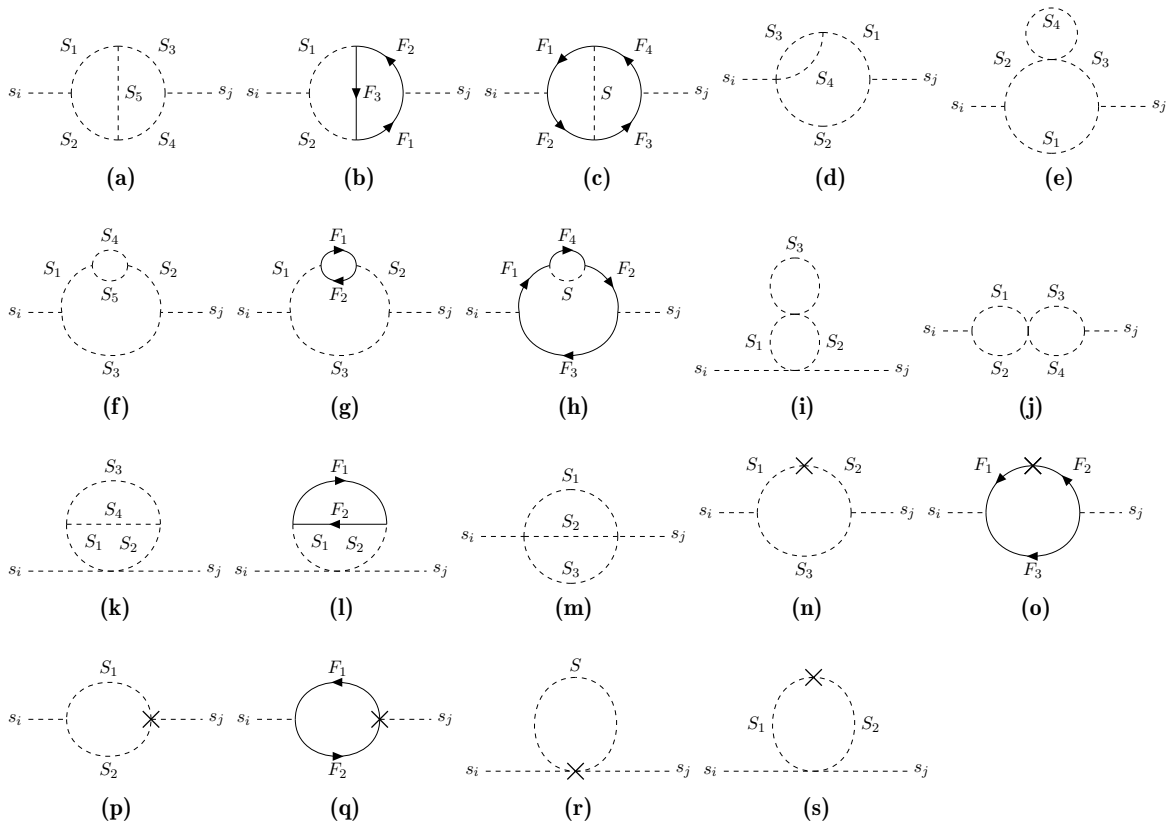


Figure D.2.: All generic two-loop selfenergy diagrams. The external fields can be neutral or charged scalars as well as vector bosons (in the case of vector bosons, some diagrams such as (j) and (m) are not present due to gauge invariance or the approximation of vanishing external momentum). The summation of the internal degrees of freedom follows Eq. (D.1). *Figure taken from Ref. [210].*

D.2.1. Momentum Regulated Diagrams

We list the full set of Feynman diagrams which feature a residual dependence on the IR regulator in Fig. D.3. The sum of all other diagrams not shown here is IR-finite if the IR-safe loop functions from Appendix B are used. The list of diagrams shown in Fig. D.3 can also be derived from the information given in Tab. C.2. However, for the sake of completeness we give here the full list of diagrams including the insertions of internal fields (generation and color indices have been suppressed).

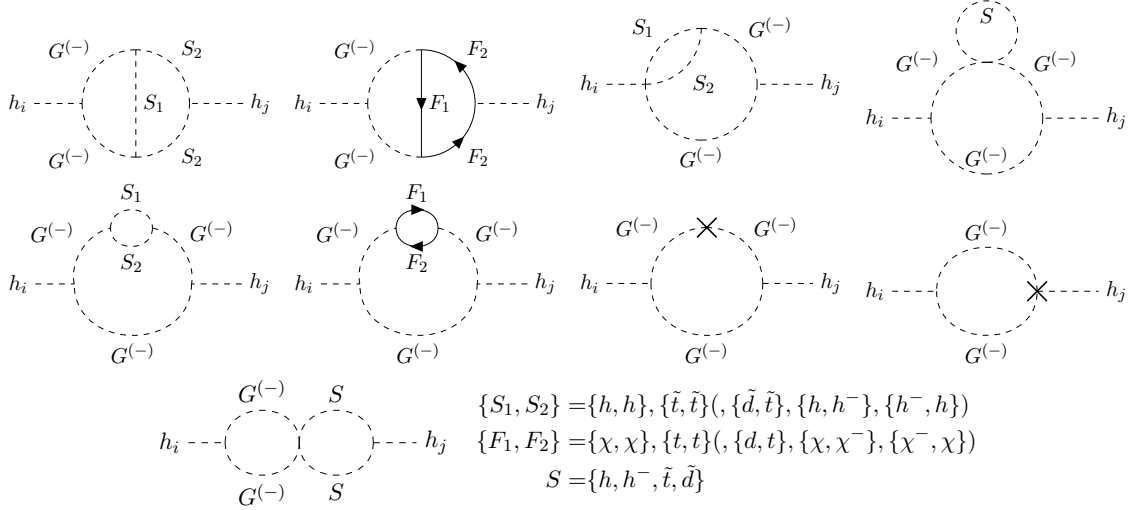


Figure D.3.: All two-loop selfenergy diagrams which feature a residual dependence on the IR mass regulator. *Figure taken from Ref. [210].*

References

- [1] Y. Golfand and E. Likhtman, “Extension of the Algebra of Poincare Group Generators and Violation of p Invariance,” *JETP Lett.* **13** (1971) 323–326.
- [2] J. Wess and B. Zumino, “A Lagrangian Model Invariant Under Supergauge Transformations,” *Phys. Lett. B* **49** (1974) 52.
- [3] J. Wess and B. Zumino, “Supergauge Transformations in Four-Dimensions,” *Nucl. Phys. B* **70** (1974) 39–50.
- [4] P. Fayet, “Supergauge Invariant Extension of the Higgs Mechanism and a Model for the electron and Its Neutrino,” *Nucl. Phys. B* **90** (1975) 104–124.
- [5] P. Fayet, “Spontaneously Broken Supersymmetric Theories of Weak, Electromagnetic and Strong Interactions,” *Phys. Lett. B* **69** (1977) 489.
- [6] P. Fayet and S. Ferrara, “Supersymmetry,” *Phys. Rept.* **32** (1977) 249–334.
- [7] H. P. Nilles, “Supersymmetry, Supergravity and Particle Physics,” *Phys. Rept.* **110** (1984) 1–162.
- [8] J. F. Gunion, H. E. Haber, G. L. Kane, and S. Dawson, *The Higgs Hunter’s Guide*, vol. 80. 2000.
- [9] S. P. Martin, *A Supersymmetry primer*, vol. 21, pp. 1–153. 2010. [arXiv:hep-ph/9709356](#).
- [10] S. Chatrchyan *et al.*, “Observation of a new boson at a mass of 125 GeV with the CMS experiment at the LHC,” *Phys.Lett.* **B716** (2012) 30–61.
- [11] G. Aad *et al.*, “Observation of a new particle in the search for the Standard Model Higgs boson with the ATLAS detector at the LHC,” *Phys. Lett.* **B716** (2012) 1–29.
- [12] G. Aad *et al.*, “Combined Measurement of the Higgs Boson Mass in pp Collisions at $\sqrt{s} = 7$ and 8 TeV with the ATLAS and CMS Experiments,” *Phys. Rev. Lett.* **114** (2015) 191803.
- [13] J. R. Ellis, J. Gunion, H. E. Haber, L. Roszkowski, and F. Zwirner, “Higgs Bosons in a Nonminimal Supersymmetric Model,” *Phys. Rev. D* **39** (1989) 844.
- [14] M. Drees, “Supersymmetric Models with Extended Higgs Sector,” *Int. J. Mod. Phys. A* **4** (1989) 3635.
- [15] U. Ellwanger, M. Rausch de Traubenberg, and C. A. Savoy, “Particle spectrum in supersymmetric models with a gauge singlet,” *Phys. Lett. B* **315** (1993) 331–337, [arXiv:hep-ph/9307322](#).
- [16] U. Ellwanger, M. Rausch de Traubenberg, and C. A. Savoy, “Higgs phenomenology of the supersymmetric model with a gauge singlet,” *Z. Phys. C* **67** (1995) 665–670, [arXiv:hep-ph/9502206](#).

- [17] M. Maniatis, “The Next-to-Minimal Supersymmetric extension of the Standard Model reviewed,” *Int. J. Mod. Phys. A* **25** (2010) 3505–3602, [arXiv:0906.0777 \[hep-ph\]](#).
- [18] U. Ellwanger, C. Hugonie, and A. M. Teixeira, “The Next-to-Minimal Supersymmetric Standard Model,” *Phys. Rept.* **496** (2010) 1–77, [arXiv:0910.1785 \[hep-ph\]](#).
- [19] U. Ellwanger, G. Espitalier-Noel, and C. Hugonie, “Naturalness and Fine Tuning in the NMSSM: Implications of Early LHC Results,” *JHEP* **09** (2011) 105, [arXiv:1107.2472 \[hep-ph\]](#).
- [20] **CMS** Collaboration, A. M. Sirunyan *et al.*, “A measurement of the Higgs boson mass in the diphoton decay channel,” *Phys. Lett. B* **805** (2020) 135425, [arXiv:2002.06398 \[hep-ex\]](#).
- [21] **ATLAS** Collaboration, C. Arcangeletti, “Measurement of the Higgs boson properties using the ATLAS detector,” *J. Phys. Conf. Ser.* **1690** no. 1, (2020) 012154.
- [22] S. P. Martin, “Two Loop Effective Potential for the Minimal Supersymmetric Standard Model,” *Phys. Rev. D* **66** (2002) 096001, [arXiv:hep-ph/0206136](#).
- [23] S. P. Martin, “Complete Two Loop Effective Potential Approximation to the Lightest Higgs Scalar Boson Mass in Supersymmetry,” *Phys. Rev. D* **67** (2003) 095012, [arXiv:hep-ph/0211366](#).
- [24] J. Espinosa, M. Garny, and T. Konstandin, “Interplay of Infrared Divergences and Gauge-Dependence of the Effective Potential,” *Phys. Rev. D* **94** no. 5, (2016) 055026.
- [25] J. R. Espinosa and T. Konstandin, “Resummation of Goldstone Infrared Divergences: A Proof to All Orders,” *Phys. Rev. D* **97** no. 5, (2018) 056020.
- [26] N. Kumar and S. P. Martin, “Resummation of Goldstone boson contributions to the MSSM effective potential,” *Phys. Rev. D* **94** no. 1, (2016) 014013.
- [27] J. Braathen and M. D. Goodsell, “Avoiding the Goldstone Boson Catastrophe in general renormalisable field theories at two loops,” *JHEP* **12** (2016) 056.
- [28] J. Braathen, M. D. Goodsell, and F. Staub, “Supersymmetric and non-supersymmetric models without catastrophic Goldstone bosons,” *Eur. Phys. J. C* **77** no. 11, (2017) 757.
- [29] G. Degrandi, S. Di Vita, and P. Slavich, “Two-loop QCD corrections to the MSSM Higgs masses beyond the effective-potential approximation,” *Eur. Phys. J. C* **75** no. 2, (2015) 61, [arXiv:1410.3432 \[hep-ph\]](#).
- [30] S. Borowka, T. Hahn, S. Heinemeyer, G. Heinrich, and W. Hollik, “Momentum-dependent two-loop QCD corrections to the neutral Higgs-boson masses in the MSSM,” *Eur. Phys. J. C* **74** no. 8, (2014) 2994.
- [31] F. Domingo and S. Paßehr, “Towards Higgs masses and decay widths satisfying the symmetries in the (N)MSSM,” [arXiv:2007.11010 \[hep-ph\]](#).
- [32] M. Mühlleitner, D. T. Nhung, and H. Ziesche, “The order $\mathcal{O}(\alpha_t\alpha_s)$ corrections to the trilinear Higgs self-couplings in the complex NMSSM,” *JHEP* **12** (2015) 034.
- [33] T. Dao, R. Gröber, M. Krause, M. Mühlleitner, and H. Rzehak, “Two-loop $\mathcal{O}(\alpha_t^2)$ corrections to the neutral Higgs boson masses in the CP-violating NMSSM,” *JHEP* **08** (2019) 114.
- [34] **Particle Data Group** Collaboration, P. Zyla *et al.*, “Review of Particle Physics,” *PTEP* **2020** no. 8, (2020) 083C01.

- [35] M. Kobayashi and T. Maskawa, “CP Violation in the Renormalizable Theory of Weak Interaction,” *Prog. Theor. Phys.* **49** (1973) 652–657.
- [36] F. Englert and R. Brout, “Broken symmetry and the mass of gauge vector mesons,” *Phys. Rev. Lett.* **13** (Aug, 1964) 321–323.
<https://link.aps.org/doi/10.1103/PhysRevLett.13.321>.
- [37] P. W. Higgs, “Broken symmetries and the masses of gauge bosons,” *Phys. Rev. Lett.* **13** (Oct, 1964) 508–509. <https://link.aps.org/doi/10.1103/PhysRevLett.13.508>.
- [38] G. S. Guralnik, C. R. Hagen, and T. W. B. Kibble, “Global conservation laws and massless particles,” *Phys. Rev. Lett.* **13** (Nov, 1964) 585–587.
<https://link.aps.org/doi/10.1103/PhysRevLett.13.585>.
- [39] J. Goldstone, A. Salam, and S. Weinberg, “Broken symmetries,” *Phys. Rev.* **127** (Aug, 1962) 965–970. <https://link.aps.org/doi/10.1103/PhysRev.127.965>.
- [40] M. E. Peskin and D. V. Schroeder, *An Introduction to quantum field theory*. Addison-Wesley, Reading, USA, 1995.
- [41] D. Stockinger, “Regularization by dimensional reduction: consistency, quantum action principle, and supersymmetry,” *JHEP* **03** (2005) 076, [arXiv:hep-ph/0503129](https://arxiv.org/abs/hep-ph/0503129).
- [42] D. Stöckinger and J. Unger, “Three-loop MSSM Higgs-boson mass predictions and regularization by dimensional reduction,” *Nucl. Phys. B* **935** (2018) 1–16, [arXiv:1804.05619](https://arxiv.org/abs/1804.05619) [hep-ph].
- [43] L. M. Brown and R. P. Feynman, “Radiative corrections to Compton scattering,” *Phys. Rev.* **85** (1952) 231–244.
- [44] G. Passarino and M. J. G. Veltman, “One Loop Corrections for $e^+ e^-$ Annihilation Into $\mu^+ \mu^-$ in the Weinberg Model,” *Nucl. Phys. B* **160** (1979) 151–207.
- [45] G. ’t Hooft and M. J. G. Veltman, “Scalar One Loop Integrals,” *Nucl. Phys. B* **153** (1979) 365–401.
- [46] S. P. Martin, “Evaluation of two loop selfenergy basis integrals using differential equations,” *Phys. Rev. D* **68** (2003) 075002.
- [47] H. Lehmann, K. Symanzik, and W. Zimmermann, “On the formulation of quantized field theories,” *Nuovo Cim.* **1** (1955) 205–225.
- [48] M. Srednicki, *Quantum field theory*. Cambridge University Press, 1, 2007.
- [49] M. E. Machacek and M. T. Vaughn, “Two Loop Renormalization Group Equations in a General Quantum Field Theory. 1. Wave Function Renormalization,” *Nucl. Phys. B* **222** (1983) 83–103.
- [50] M. E. Machacek and M. T. Vaughn, “Two Loop Renormalization Group Equations in a General Quantum Field Theory. 2. Yukawa Couplings,” *Nucl. Phys. B* **236** (1984) 221–232.
- [51] M. E. Machacek and M. T. Vaughn, “Two Loop Renormalization Group Equations in a General Quantum Field Theory. 3. Scalar Quartic Couplings,” *Nucl. Phys. B* **249** (1985) 70–92.
- [52] F. Staub, “SARAH,” [arXiv:0806.0538](https://arxiv.org/abs/0806.0538) [hep-ph].
- [53] F. Staub, “SARAH 4 : A tool for (not only SUSY) model builders,” *Comput. Phys. Commun.* **185** (2014) 1773–1790, [arXiv:1309.7223](https://arxiv.org/abs/1309.7223) [hep-ph].

- [54] F. Staub, “Automatic Calculation of supersymmetric Renormalization Group Equations and Self Energies,” *Comput. Phys. Commun.* **182** (2011) 808–833, [arXiv:1002.0840 \[hep-ph\]](#).
- [55] I. Schienbein, F. Staub, T. Steudtner, and K. Svirina, “Revisiting RGEs for general gauge theories,” *Nucl. Phys. B* **939** (2019) 1–48, [arXiv:1809.06797 \[hep-ph\]](#). [Erratum: *Nucl.Phys.B* 966, 115339 (2021)].
- [56] O. V. Tarasov, “Generalized recurrence relations for two loop propagator integrals with arbitrary masses,” *Nucl. Phys. B* **502** (1997) 455–482, [arXiv:hep-ph/9703319](#).
- [57] R. Mertig and R. Scharf, “TARCER: A Mathematica program for the reduction of two loop propagator integrals,” *Comput. Phys. Commun.* **111** (1998) 265–273, [arXiv:hep-ph/9801383](#).
- [58] C. Ford, I. Jack, and D. Jones, “The Standard model effective potential at two loops,” *Nucl. Phys. B* **387** (1992) 373–390. [Erratum: *Nucl.Phys.B* 504, 551–552 (1997)].
- [59] S. P. Martin and D. G. Robertson, “TSIL: A Program for the calculation of two-loop self-energy integrals,” *Comput. Phys. Commun.* **174** (2006) 133–151.
- [60] A. Djouadi and P. Gambino, “Electroweak gauge bosons selfenergies: Complete QCD corrections,” *Phys. Rev. D* **49** (1994) 3499–3511, [arXiv:hep-ph/9309298](#). [Erratum: *Phys.Rev.D* 53, 4111 (1996)].
- [61] A. Denner, “Techniques for calculation of electroweak radiative corrections at the one loop level and results for W physics at LEP-200,” *Fortsch. Phys.* **41** (1993) 307–420, [arXiv:0709.1075 \[hep-ph\]](#).
- [62] M. J. G. Veltman, “The Infrared - Ultraviolet Connection,” *Acta Phys. Polon. B* **12** (1981) 437.
- [63] I. Masina and M. Quiros, “On the Veltman Condition, the Hierarchy Problem and High-Scale Supersymmetry,” *Phys. Rev. D* **88** (2013) 093003, [arXiv:1308.1242 \[hep-ph\]](#).
- [64] B. Zumino, “Supersymmetry and the Vacuum,” *Nucl. Phys. B* **89** (1975) 535.
- [65] M. B. Einhorn and D. R. T. Jones, “The Effective potential and quadratic divergences,” *Phys. Rev. D* **46** (1992) 5206–5208.
- [66] M. Drees, R. Godbole, and P. Roy, *Theory and phenomenology of Sparticles: an account of four-dimensional N=1 supersymmetry in high-energy physics*. World Scientific, Singapore, 2004. <https://cds.cern.ch/record/873465>.
- [67] S. Dawson, “The MSSM and why it works,” in *Theoretical Advanced Study Institute in Elementary Particle Physics (TASI 97): Supersymmetry, Supergravity and Supercolliders*. 6, 1997. [arXiv:hep-ph/9712464](#).
- [68] J. E. Kim and H. P. Nilles, “The mu Problem and the Strong CP Problem,” *Phys. Lett. B* **138** (1984) 150–154.
- [69] P. Z. Skands *et al.*, “SUSY Les Houches accord: Interfacing SUSY spectrum calculators, decay packages, and event generators,” *JHEP* **07** (2004) 036.
- [70] B. Allanach, C. Balazs, G. Belanger, M. Bernhardt, F. Boudjema, *et al.*, “SUSY Les Houches Accord 2,” *Comput.Phys.Commun.* **180** (2009) 8–25.
- [71] P. Slavich *et al.*, “Higgs-mass predictions in the MSSM and beyond,” *Eur. Phys. J. C* **81** no. 5, (2021) 450, [arXiv:2012.15629 \[hep-ph\]](#).

- [72] J. R. Ellis, G. Ridolfi, and F. Zwirner, “Radiative corrections to the masses of supersymmetric Higgs bosons,” *Phys. Lett. B* **257** (1991) 83–91.
- [73] Y. Okada, M. Yamaguchi, and T. Yanagida, “Upper bound of the lightest Higgs boson mass in the minimal supersymmetric standard model,” *Prog. Theor. Phys.* **85** (1991) 1–6.
- [74] Y. Okada, M. Yamaguchi, and T. Yanagida, “Renormalization group analysis on the Higgs mass in the softly broken supersymmetric standard model,” *Phys. Lett. B* **262** (1991) 54–58.
- [75] K. Sasaki, M. Carena, and C. Wagner, “Renormalization group analysis of the Higgs sector in the minimal supersymmetric standard model,” *Nucl. Phys. B* **381** (1992) 66–86.
- [76] P. H. Chankowski, S. Pokorski, and J. Rosiek, “Charged and neutral supersymmetric Higgs boson masses: Complete one loop analysis,” *Phys. Lett. B* **274** (1992) 191–198.
- [77] A. Brignole, “Radiative corrections to the supersymmetric neutral Higgs boson masses,” *Phys. Lett. B* **281** (1992) 284–294.
- [78] R. Hempfling and A. H. Hoang, “Two loop radiative corrections to the upper limit of the lightest Higgs boson mass in the minimal supersymmetric model,” *Phys. Lett. B* **331** (1994) 99–106, [arXiv:hep-ph/9401219](#).
- [79] A. Dabelstein, “The One loop renormalization of the MSSM Higgs sector and its application to the neutral scalar Higgs masses,” *Z. Phys. C* **67** (1995) 495–512, [arXiv:hep-ph/9409375](#).
- [80] J. Casas, J. Espinosa, M. Quiros, and A. Riotto, “The Lightest Higgs boson mass in the minimal supersymmetric standard model,” *Nucl. Phys. B* **436** (1995) 3–29, [arXiv:hep-ph/9407389](#). [Erratum: *Nucl.Phys.B* 439, 466–468 (1995)].
- [81] M. Carena, M. Quiros, and C. Wagner, “Effective potential methods and the Higgs mass spectrum in the MSSM,” *Nucl. Phys. B* **461** (1996) 407–436, [arXiv:hep-ph/9508343](#).
- [82] M. Carena, J. Espinosa, M. Quiros, and C. Wagner, “Analytical expressions for radiatively corrected Higgs masses and couplings in the MSSM,” *Phys. Lett. B* **355** (1995) 209–221, [arXiv:hep-ph/9504316](#).
- [83] H. E. Haber, R. Hempfling, and A. H. Hoang, “Approximating the radiatively corrected Higgs mass in the minimal supersymmetric model,” *Z. Phys. C* **75** (1997) 539–554, [arXiv:hep-ph/9609331](#).
- [84] D. M. Pierce, J. A. Bagger, K. T. Matchev, and R.-j. Zhang, “Precision corrections in the minimal supersymmetric standard model,” *Nucl. Phys. B* **491** (1997) 3–67, [arXiv:hep-ph/9606211](#).
- [85] S. Heinemeyer, W. Hollik, and G. Weiglein, “QCD corrections to the masses of the neutral CP - even Higgs bosons in the MSSM,” *Phys. Rev. D* **58** (1998) 091701, [arXiv:hep-ph/9803277](#).
- [86] R.-J. Zhang, “Two loop effective potential calculation of the lightest CP even Higgs boson mass in the MSSM,” *Phys. Lett. B* **447** (1999) 89–97, [arXiv:hep-ph/9808299](#).
- [87] S. Heinemeyer, W. Hollik, and G. Weiglein, “The Masses of the neutral CP - even Higgs bosons in the MSSM: Accurate analysis at the two loop level,” *Eur. Phys. J. C* **9** (1999) 343–366, [arXiv:hep-ph/9812472](#).

- [88] S. Heinemeyer, W. Hollik, and G. Weiglein, “The Mass of the lightest MSSM Higgs boson: A Compact analytical expression at the two loop level,” *Phys. Lett. B* **455** (1999) 179–191, [arXiv:hep-ph/9903404](#).
- [89] J. R. Espinosa and R.-J. Zhang, “MSSM lightest CP even Higgs boson mass to $O(\alpha(s)\alpha(t))$: The Effective potential approach,” *JHEP* **03** (2000) 026, [arXiv:hep-ph/9912236](#).
- [90] J. R. Espinosa and R.-J. Zhang, “Complete two loop dominant corrections to the mass of the lightest CP even Higgs boson in the minimal supersymmetric standard model,” *Nucl. Phys. B* **586** (2000) 3–38, [arXiv:hep-ph/0003246](#).
- [91] J. Espinosa and I. Navarro, “Radiative corrections to the Higgs boson mass for a hierarchical stop spectrum,” *Nucl. Phys. B* **615** (2001) 82–116, [arXiv:hep-ph/0104047](#).
- [92] A. Brignole, G. Degrassi, P. Slavich, and F. Zwirner, “On the $O(\alpha(t)^2)$ two loop corrections to the neutral Higgs boson masses in the MSSM,” *Nucl. Phys. B* **631** (2002) 195–218, [arXiv:hep-ph/0112177](#).
- [93] G. Degrassi, P. Slavich, and F. Zwirner, “On the neutral Higgs boson masses in the MSSM for arbitrary stop mixing,” *Nucl. Phys. B* **611** (2001) 403–422, [arXiv:hep-ph/0105096](#).
- [94] B. Allanach, “SOFTSUSY: a program for calculating supersymmetric spectra,” *Comput. Phys. Commun.* **143** (2002) 305–331, [arXiv:hep-ph/0104145](#).
- [95] G. Degrassi, S. Heinemeyer, W. Hollik, P. Slavich, and G. Weiglein, “Towards high precision predictions for the MSSM Higgs sector,” *Eur. Phys. J. C* **28** (2003) 133–143, [arXiv:hep-ph/0212020](#).
- [96] A. Brignole, G. Degrassi, P. Slavich, and F. Zwirner, “On the two loop sbottom corrections to the neutral Higgs boson masses in the MSSM,” *Nucl. Phys. B* **643** (2002) 79–92, [arXiv:hep-ph/0206101](#).
- [97] A. Dedes, G. Degrassi, and P. Slavich, “On the two loop Yukawa corrections to the MSSM Higgs boson masses at large $\tan\beta$,” *Nucl. Phys. B* **672** (2003) 144–162, [arXiv:hep-ph/0305127](#).
- [98] S. Heinemeyer, W. Hollik, H. Rzehak, and G. Weiglein, “High-precision predictions for the MSSM Higgs sector at $O(\alpha(b)\alpha(s))$,” *Eur. Phys. J. C* **39** (2005) 465–481, [arXiv:hep-ph/0411114](#).
- [99] B. Allanach, A. Djouadi, J. Kneur, W. Porod, and P. Slavich, “Precise determination of the neutral Higgs boson masses in the MSSM,” *JHEP* **09** (2004) 044.
- [100] M. Frank, T. Hahn, S. Heinemeyer, W. Hollik, H. Rzehak, and G. Weiglein, “The Higgs Boson Masses and Mixings of the Complex MSSM in the Feynman-Diagrammatic Approach,” *JHEP* **02** (2007) 047, [arXiv:hep-ph/0611326](#).
- [101] S. P. Martin, “Three-loop corrections to the lightest Higgs scalar boson mass in supersymmetry,” *Phys. Rev. D* **75** (2007) 055005, [arXiv:hep-ph/0701051](#).
- [102] R. Harlander, P. Kant, L. Mihaila, and M. Steinhauser, “Higgs boson mass in supersymmetry to three loops,” *Phys. Rev. Lett.* **100** (2008) 191602, [arXiv:0803.0672 \[hep-ph\]](#).
- [103] G. Degrassi and P. Slavich, “On the radiative corrections to the neutral Higgs boson masses in the NMSSM,” *Nucl. Phys. B* **825** (2010) 119–150, [arXiv:0907.4682 \[hep-ph\]](#).

- [104] P. Kant, R. Harlander, L. Mihaila, and M. Steinhauser, “Light MSSM Higgs boson mass to three-loop accuracy,” *JHEP* **08** (2010) 104, [arXiv:1005.5709 \[hep-ph\]](#).
- [105] W. Hollik and S. Paßehr, “Higgs boson masses and mixings in the complex MSSM with two-loop top-Yukawa-coupling corrections,” *JHEP* **10** (2014) 171, [arXiv:1409.1687 \[hep-ph\]](#).
- [106] S. Borowka, T. Hahn, S. Heinemeyer, G. Heinrich, and W. Hollik, “Renormalization scheme dependence of the two-loop QCD corrections to the neutral Higgs-boson masses in the MSSM,” *Eur. Phys. J. C* **75** no. 9, (2015) 424, [arXiv:1505.03133 \[hep-ph\]](#).
- [107] R. V. Harlander, J. Klappert, and A. Voigt, “Higgs mass prediction in the MSSM at three-loop level in a pure $\overline{\text{DR}}$ context,” *Eur. Phys. J. C* **77** no. 12, (2017) 814, [arXiv:1708.05720 \[hep-ph\]](#).
- [108] S. Paßehr and G. Weiglein, “Two-loop top and bottom Yukawa corrections to the Higgs-boson masses in the complex MSSM,” *Eur. Phys. J. C* **78** no. 3, (2018) 222, [arXiv:1705.07909 \[hep-ph\]](#).
- [109] S. Borowka, S. Paßehr, and G. Weiglein, “Complete two-loop QCD contributions to the lightest Higgs-boson mass in the MSSM with complex parameters,” *Eur. Phys. J. C* **78** no. 7, (2018) 576, [arXiv:1802.09886 \[hep-ph\]](#).
- [110] A. Fazio and E. Reyes R., “The Lightest Higgs Boson Mass of the MSSM at Three-Loop Accuracy,” *Nucl. Phys. B* **942** (2019) 164–183, [arXiv:1901.03651 \[hep-ph\]](#).
- [111] N. Bernal, A. Djouadi, and P. Slavich, “The MSSM with heavy scalars,” *JHEP* **07** (2007) 016.
- [112] P. Draper, G. Lee, and C. E. M. Wagner, “Precise estimates of the Higgs mass in heavy supersymmetry,” *Phys. Rev. D* **89** no. 5, (2014) 055023, [arXiv:1312.5743 \[hep-ph\]](#).
- [113] T. Hahn, S. Heinemeyer, W. Hollik, H. Rzehak, and G. Weiglein, “High-Precision Predictions for the Light CP -Even Higgs Boson Mass of the Minimal Supersymmetric Standard Model,” *Phys. Rev. Lett.* **112** no. 14, (2014) 141801, [arXiv:1312.4937 \[hep-ph\]](#).
- [114] E. Bagnaschi, G. F. Giudice, P. Slavich, and A. Strumia, “Higgs Mass and Unnatural Supersymmetry,” *JHEP* **09** (2014) 092.
- [115] J. Pardo Vega and G. Villadoro, “SusyHD: Higgs mass Determination in Supersymmetry,” *JHEP* **07** (2015) 159, [arXiv:1504.05200 \[hep-ph\]](#).
- [116] G. Lee and C. E. Wagner, “Higgs bosons in heavy supersymmetry with an intermediate m_A ,” *Phys. Rev. D* **92** no. 7, (2015) 075032, [arXiv:1508.00576 \[hep-ph\]](#).
- [117] H. Bahl and W. Hollik, “Precise prediction for the light MSSM Higgs boson mass combining effective field theory and fixed-order calculations,” *Eur. Phys. J. C* **76** no. 9, (2016) 499, [arXiv:1608.01880 \[hep-ph\]](#).
- [118] P. Athron, J.-h. Park, T. Steudtner, D. Stöckinger, and A. Voigt, “Precise Higgs mass calculations in (non-)minimal supersymmetry at both high and low scales,” *JHEP* **01** (2017) 079.

- [119] P. Athron, M. Bach, D. Harries, T. Kwasnitza, J.-h. Park, D. Stöckinger, A. Voigt, and J. Ziebell, “FlexibleSUSY 2.0: Extensions to investigate the phenomenology of SUSY and non-SUSY models,” *Comput. Phys. Commun.* **230** (2018) 145–217, [arXiv:1710.03760 \[hep-ph\]](#).
- [120] H. Bahl, S. Heinemeyer, W. Hollik, and G. Weiglein, “Reconciling EFT and hybrid calculations of the light MSSM Higgs-boson mass,” *Eur. Phys. J. C* **78** no. 1, (2018) 57, [arXiv:1706.00346 \[hep-ph\]](#).
- [121] E. Bagnaschi, J. Pardo Vega, and P. Slavich, “Improved determination of the Higgs mass in the MSSM with heavy superpartners,” *Eur. Phys. J.* **C77** no. 5, (2017) 334.
- [122] B. Allanach and A. Voigt, “Uncertainties in the Lightest CP Even Higgs Boson Mass Prediction in the Minimal Supersymmetric Standard Model: Fixed Order Versus Effective Field Theory Prediction,” *Eur. Phys. J. C* **78** no. 7, (2018) 573, [arXiv:1804.09410 \[hep-ph\]](#).
- [123] R. Harlander, J. Klappert, A. Ochoa ranco, and A. Voigt, “The light CP -even MSSM Higgs mass resummed to fourth logarithmic order,” *Eur. Phys. J. C* **78** no. 10, (2018) 874.
- [124] H. Bahl and W. Hollik, “Precise prediction of the MSSM Higgs boson masses for low MA ,”.
- [125] H. Bahl, T. Hahn, S. Heinemeyer, W. Hollik, S. PaSSehr, H. Rzehak, and G. Weiglein, “Precision calculations in the MSSM Higgs-boson sector with FeynHiggs 2.14,” *Comput. Phys. Commun.* **249** (2020) 107099.
- [126] E. Bagnaschi *et al.*, “Supersymmetric Models in Light of Improved Higgs Mass Calculations,” *Eur. Phys. J. C* **79** no. 2, (2019) 149.
- [127] E. Bagnaschi, G. Degrassi, S. PaSSehr, and P. Slavich, “Full two-loop QCD corrections to the Higgs mass in the MSSM with heavy superpartners,” *Eur. Phys. J. C* **79** no. 11, (2019) 910.
- [128] H. Bahl, I. Sobolev, and G. Weiglein, “Precise prediction for the mass of the light MSSM Higgs boson for the case of a heavy gluino,” *Phys. Lett. B* **808** (2020) 135644.
- [129] H. Bahl, S. Heinemeyer, W. Hollik, and G. Weiglein, “Theoretical uncertainties in the MSSM Higgs boson mass calculation,” *Eur. Phys. J. C* **80** no. 6, (2020) 497, [arXiv:1912.04199 \[hep-ph\]](#).
- [130] R. Harlander, J. Klappert, and A. Voigt, “The light CP -even MSSM Higgs mass including N^3LO+N^3LL QCD corrections,” *Eur. Phys. J. C* **80** no. 3, (2020) 186.
- [131] E. Reyes R. and A. Fazio, “Comparison of the EFT Hybrid and Three-Loop Fixed-Order Calculations of the Lightest MSSM Higgs Boson Mass,” *Phys. Rev. D* **100** no. 11, (2019) 115017, [arXiv:1908.00693 \[hep-ph\]](#).
- [132] T. Kwasnitza, D. Stöckinger, and A. Voigt, “Improved MSSM Higgs mass calculation using the 3-loop FlexibleEFTHiggs approach including x_t -resummation,” *JHEP* **07** no. 07, (2020) 197.
- [133] S. Heinemeyer, W. Hollik, and G. Weiglein, “FeynHiggs: A Program for the calculation of the masses of the neutral CP even Higgs bosons in the MSSM,” *Comput. Phys. Commun.* **124** (2000) 76–89, [arXiv:hep-ph/9812320](#).
- [134] W. Porod, “SPHeno, a program for calculating supersymmetric spectra, SUSY particle decays and SUSY particle production at e^+e^- colliders,” *Comput. Phys. Commun.* **153** (2003) 275–315, [arXiv:hep-ph/0301101](#).

- [135] W. Porod and F. Staub, “SPheno 3.1: Extensions including flavour, CP-phases and models beyond the MSSM,” *Comput. Phys. Commun.* **183** (2012) 2458–2469, [arXiv:1104.1573 \[hep-ph\]](#).
- [136] F. Staub and W. Porod, “Improved predictions for intermediate and heavy Supersymmetry in the MSSM and beyond,” *Eur. Phys. J.* **C77** no. 5, (2017) 338.
- [137] P. Athron, J.-h. Park, D. Stöckinger, and A. Voigt, “FlexibleSUSYA spectrum generator generator for supersymmetric models,” *Comput. Phys. Commun.* **190** (2015) 139–172.
- [138] P. Athron, M. Bach, D. Harries, W. Kotlarski, T. Kwasnitza, J.-H. Park, T. Steudtner, D. Stöckinger, A. Voigt, and J. Ziebell, “FlexibleSUSY: Precise automated calculations in any BSM theory,” *PoS ICHEP2018* (2019) 456, [arXiv:1810.05371 \[hep-ph\]](#).
- [139] M. D. Goodsell, K. Nickel, and F. Staub, “Two-Loop Higgs mass calculations in supersymmetric models beyond the MSSM with SARAH and SPheno,” *Eur. Phys. J.* **C75** no. 1, (2015) 32.
- [140] M. D. Goodsell, K. Nickel, and F. Staub, “Two-loop corrections to the Higgs masses in the NMSSM,” *Phys. Rev.* **D91** (2015) 035021.
- [141] F. Staub, W. Porod, and B. Herrmann, “The Electroweak sector of the NMSSM at the one-loop level,” *JHEP* **1010** (2010) 040.
- [142] S. P. Martin, “Two Loop Effective Potential for a General Renormalizable Theory and Softly Broken Supersymmetry,” *Phys. Rev. D* **65** (2002) 116003.
- [143] S. P. Martin, “Two loop scalar self energies in a general renormalizable theory at leading order in gauge couplings,” *Phys. Rev. D* **70** (2004) 016005.
- [144] S. P. Martin, “Two-loop scalar self-energies and pole masses in a general renormalizable theory with massless gauge bosons,” *Phys. Rev. D* **71** (2005) 116004.
- [145] M. Goodsell, K. Nickel, and F. Staub, “Generic two-loop Higgs mass calculation from a diagrammatic approach,” *Eur. Phys. J.* **C75** no. 6, (2015) 290.
- [146] M. D. Goodsell and S. Paßehr, “All two-loop scalar self-energies and tadpoles in general renormalisable field theories,” *Eur. Phys. J. C* **80** no. 5, (2020) 417.
- [147] U. Ellwanger, “Radiative corrections to the neutral Higgs spectrum in supersymmetry with a gauge singlet,” *Phys. Lett. B* **303** (1993) 271–276, [arXiv:hep-ph/9302224](#).
- [148] P. Pandita, “Radiative corrections to the scalar Higgs masses in a nonminimal supersymmetric Standard Model,” *Z. Phys. C* **59** (1993) 575–584.
- [149] U. Ellwanger and C. Hugonie, “Yukawa induced radiative corrections to the lightest Higgs boson mass in the NMSSM,” *Phys. Lett. B* **623** (2005) 93–103, [arXiv:hep-ph/0504269](#).
- [150] K. Ender, T. Graf, M. Muhlleitner, and H. Rzehak, “Analysis of the NMSSM Higgs Boson Masses at One-Loop Level,” *Phys. Rev. D* **85** (2012) 075024.
- [151] G. Bélanger, V. Bizouard, F. Boudjema, and G. Chalons, “One-loop renormalization of the NMSSM in SloopS. II. The Higgs sector,” *Phys. Rev. D* **96** no. 1, (2017) 015040.
- [152] G. Belanger, V. Bizouard, F. Boudjema, and G. Chalons, “One-loop renormalization of the NMSSM in SloopS: The neutralino-chargino and sfermion sectors,” *Phys. Rev. D* **93** no. 11, (2016) 115031.

- [153] P. Drechsel, L. Galeta, S. Heinemeyer, and G. Weiglein, “Precise Predictions for the Higgs-Boson Masses in the NMSSM,” *Eur. Phys. J. C* **77** no. 1, (2017) 42.
- [154] S. W. Ham, J. Kim, S. K. Oh, and D. Son, “The Charged Higgs boson in the next-to-minimal supersymmetric standard model with explicit CP violation,” *Phys. Rev. D* **64** (2001) 035007, [arXiv:hep-ph/0104144](#).
- [155] S. Ham, S. Oh, and D. Son, “Neutral Higgs sector of the next-to-minimal supersymmetric standard model with explicit CP violation,” *Phys. Rev. D* **65** (2002) 075004, [arXiv:hep-ph/0110052](#).
- [156] S. W. Ham, Y. S. Jeong, and S. K. Oh, “Radiative CP violation in the Higgs sector of the next-to-minimal supersymmetric model,” [arXiv:hep-ph/0308264](#).
- [157] K. Cheung, T.-J. Hou, J. S. Lee, and E. Senaha, “The Higgs Boson Sector of the Next-to-MSSM with CP Violation,” *Phys. Rev. D* **82** (2010) 075007, [arXiv:1006.1458 \[hep-ph\]](#).
- [158] F. Domingo, “A New Tool for the study of the CP-violating NMSSM,” *JHEP* **06** (2015) 052.
- [159] T. Graf, R. Grober, M. Muhlleitner, H. Rzehak, and K. Walz, “Higgs Boson Masses in the Complex NMSSM at One-Loop Level,” *JHEP* **10** (2012) 122.
- [160] M. D. Goodsell and F. Staub, “The Higgs mass in the CP violating MSSM, NMSSM, and beyond,” *Eur. Phys. J. C* **77** no. 1, (2017) 46.
- [161] M. Mühlleitner, D. T. Nhung, H. Rzehak, and K. Walz, “Two-loop contributions of the order $\mathcal{O}(\alpha_t\alpha_s)$ to the masses of the Higgs bosons in the CP-violating NMSSM,” *JHEP* **05** (2015) 128, [arXiv:1412.0918 \[hep-ph\]](#).
- [162] U. Ellwanger, J. F. Gunion, and C. Hugonie, “NMHDECAY: A Fortran code for the Higgs masses, couplings and decay widths in the NMSSM,” *JHEP* **02** (2005) 066.
- [163] U. Ellwanger and C. Hugonie, “NMHDECAY 2.0: An Updated program for sparticle masses, Higgs masses, couplings and decay widths in the NMSSM,” *Comput. Phys. Commun.* **175** (2006) 290–303.
- [164] D. Das, U. Ellwanger, and A. M. Teixeira, “NMSDECAY: A Fortran Code for Supersymmetric Particle Decays in the Next-to-Minimal Supersymmetric Standard Model,” *Comput. Phys. Commun.* **183** (2012) 774–779, [arXiv:1106.5633 \[hep-ph\]](#).
- [165] U. Ellwanger and C. Hugonie, “NMSPEC: A Fortran code for the sparticle and Higgs masses in the NMSSM with GUT scale boundary conditions,” *Comput. Phys. Commun.* **177** (2007) 399–407.
- [166] U. Ellwanger, C. C. Jean-Louis, and A. M. Teixeira, “Phenomenology of the General NMSSM with Gauge Mediated Supersymmetry Breaking,” *JHEP* **05** (2008) 044, [arXiv:0803.2962 \[hep-ph\]](#).
- [167] G. Bélanger, F. Boudjema, A. Goudelis, A. Pukhov, and B. Zaldivar, “micrOMEGAs5.0 : Freeze-in,” *Comput. Phys. Commun.* **231** (2018) 173–186, [arXiv:1801.03509 \[hep-ph\]](#).
- [168] U. Ellwanger, “NMSSMTOOLS,”
<https://www.lupm.univ-montp2.fr/users/nmssm/index.html>.
- [169] B. Allanach, P. Athron, L. C. Tunstall, A. Voigt, and A. Williams, “Next-to-Minimal SOFTSUSY,” *Comput. Phys. Commun.* **185** (2014) 2322–2339. [Erratum: *Comput.Phys.Commun.* 250, 107044 (2020)].

- [170] T. N. Dao, L. Fritz, M. Krause, M. Mühlleitner, and S. Patel, “Gauge dependences of higher-order corrections to NMSSM Higgs boson masses and the charged Higgs Decay $H^\pm \rightarrow W^\pm h_i$,” *Eur. Phys. J. C* **80** no. 3, (2020) 292, [arXiv:1911.07197 \[hep-ph\]](#).
- [171] J. Baglio, T. N. Dao, and M. Mühlleitner, “One-Loop Corrections to the Two-Body Decays of the Neutral Higgs Bosons in the Complex NMSSM,”.
- [172] J. Baglio, R. Gröber, M. Mühlleitner, D. Nhung, H. Rzehak, M. Spira, J. Streicher, and K. Walz, “NMSSMCALC: A Program Package for the Calculation of Loop-Corrected Higgs Boson Masses and Decay Widths in the (Complex) NMSSM,” *Comput. Phys. Commun.* **185** no. 12, (2014) 3372–3391.
- [173] T. N. Dao, M. Mühlleitner, S. Patel, and K. Sakurai, “One-loop Corrections to the Two-Body Decays of the Charged Higgs Bosons in the Real and Complex NMSSM,” *Eur. Phys. J. C* **81** no. 4, (2021) 340, [arXiv:2012.14889 \[hep-ph\]](#).
- [174] P. Drechsel, R. Gröber, S. Heinemeyer, M. M. Mühlleitner, H. Rzehak, and G. Weiglein, “Higgs-Boson Masses and Mixing Matrices in the NMSSM: Analysis of On-Shell Calculations,” *Eur. Phys. J. C* **77** no. 6, (2017) 366, [arXiv:1612.07681 \[hep-ph\]](#).
- [175] F. Staub, P. Athron, U. Ellwanger, R. Gröber, M. Mühlleitner, P. Slavich, and A. Voigt, “Higgs mass predictions of public NMSSM spectrum generators,” *Comput. Phys. Commun.* **202** (2016) 113–130.
- [176] L. Zarate, “The Higgs mass and the scale of SUSY breaking in the NMSSM,” *JHEP* **07** (2016) 102, [arXiv:1601.05946 \[hep-ph\]](#).
- [177] M. Gabelmann, M. Mühlleitner, and F. Staub, “Automatised matching between two scalar sectors at the one-loop level,” *Eur. Phys. J. C* **79** no. 2, (2019) 163.
- [178] M. Krämer, B. Summ, and A. Voigt, “Completing the scalar and fermionic Universal One-Loop Effective Action,” *JHEP* **01** (2020) 079.
- [179] B. Summ and A. Voigt, “Extending the Universal One-Loop Effective Action by Regularization Scheme Translating Operators,” *JHEP* **08** (2018) 026.
- [180] M. Gabelmann, M. M. Mühlleitner, and F. Staub, “The Singlet Extended Standard Model in the Context of Split Supersymmetry,” *Phys. Rev. D* **100** (2019) 075026.
- [181] P. Bechtle, S. Heinemeyer, O. Stål, T. Stefaniak, and G. Weiglein, “*HiggsSignals*: Confronting arbitrary Higgs sectors with measurements at the Tevatron and the LHC,” *Eur. Phys. J. C* **74** no. 2, (2014) 2711, [arXiv:1305.1933 \[hep-ph\]](#).
- [182] P. Bechtle, O. Brein, S. Heinemeyer, G. Weiglein, and K. E. Williams, “HiggsBounds: Confronting Arbitrary Higgs Sectors with Exclusion Bounds from LEP and the Tevatron,” *Comput. Phys. Commun.* **181** (2010) 138–167, [arXiv:0811.4169 \[hep-ph\]](#).
- [183] P. Bechtle, O. Brein, S. Heinemeyer, G. Weiglein, and K. E. Williams, “HiggsBounds 2.0.0: Confronting Neutral and Charged Higgs Sector Predictions with Exclusion Bounds from LEP and the Tevatron,” *Comput. Phys. Commun.* **182** (2011) 2605–2631, [arXiv:1102.1898 \[hep-ph\]](#).
- [184] P. Bechtle, O. Brein, S. Heinemeyer, O. Stål, T. Stefaniak, G. Weiglein, and K. E. Williams, “HiggsBounds – 4: Improved Tests of Extended Higgs Sectors against Exclusion Bounds from LEP, the Tevatron and the LHC,” *Eur. Phys. J. C* **74** no. 3, (2014) 2693, [arXiv:1311.0055 \[hep-ph\]](#).

- [185] P. Bechtle, S. Heinemeyer, T. Klingl, T. Stefaniak, G. Weiglein, and J. Wittbrodt, “HiggsSignals-2: Probing new physics with precision Higgs measurements in the LHC 13 TeV era,” *Eur. Phys. J. C* **81** no. 2, (2021) 145, [arXiv:2012.09197 \[hep-ph\]](#).
- [186] **ACME** Collaboration, V. Andreev *et al.*, “Improved limit on the electric dipole moment of the electron,” *Nature* **562** no. 7727, (2018) 355–360.
- [187] S. F. King, M. Muhlleitner, R. Nevzorov, and K. Walz, “Exploring the CP-violating NMSSM: EDM Constraints and Phenomenology,” *Nucl. Phys. B* **901** (2015) 526–555, [arXiv:1508.03255 \[hep-ph\]](#).
- [188] F. Domingo, P. Drechsel, and S. PaSSehr, “On-Shell neutral Higgs bosons in the NMSSM with complex parameters,” *Eur. Phys. J. C* **77** no. 8, (2017) 562.
- [189] M. Sperling, D. Stöckinger, and A. Voigt, “Renormalization of vacuum expectation values in spontaneously broken gauge theories: Two-loop results,” *JHEP* **01** (2014) 068.
- [190] M. Sperling, D. Stöckinger, and A. Voigt, “Renormalization of vacuum expectation values in spontaneously broken gauge theories,” *JHEP* **07** (2013) 132.
- [191] M. E. Peskin and T. Takeuchi, “A New constraint on a strongly interacting Higgs sector,” *Phys. Rev. Lett.* **65** (1990) 964–967.
- [192] S. Heinemeyer, W. Hollik, H. Rzehak, and G. Weiglein, “The Higgs sector of the complex MSSM at two-loop order: QCD contributions,” *Phys. Lett. B* **652** (2007) 300–309, [arXiv:0705.0746 \[hep-ph\]](#).
- [193] A. Salam and J. Strathdee, “On Superfields and Fermi-Bose Symmetry,” *Phys. Rev. D* **11** (1975) 1521–1535.
- [194] M. T. Grisaru, W. Siegel, and M. Rocek, “Improved Methods for Supergraphs,” *Nucl. Phys. B* **159** (1979) 429.
- [195] P. C. West, “A Comment on the nonrenormalization theorem in supersymmetric theories,” *Phys. Lett. B* **258** (1991) 375–381.
- [196] S. P. Martin, “Three-Loop Standard Model Effective Potential at Leading Order in Strong and Top Yukawa Couplings,” *Phys. Rev. D* **89** no. 1, (2014) 013003.
- [197] S. P. Martin, “Taming the Goldstone contributions to the effective potential,” *Phys. Rev. D* **90** no. 1, (2014) 016013.
- [198] F. Staub, “SARAH 3.2: Dirac Gauginos, UFO output, and more,” *Comput. Phys. Commun.* **184** (2013) 1792–1809, [arXiv:1207.0906 \[hep-ph\]](#).
- [199] J. Kublbeck, M. Bohm, and A. Denner, “Feyn Arts: Computer Algebraic Generation of Feynman Graphs and Amplitudes,” *Comput. Phys. Commun.* **60** (1990) 165–180.
- [200] T. Hahn, “Generating Feynman diagrams and amplitudes with FeynArts 3,” *Comput. Phys. Commun.* **140** (2001) 418–431, [arXiv:hep-ph/0012260](#).
- [201] R. Mertig, M. Bohm, and A. Denner, “FEYN CALC: Computer algebraic calculation of Feynman amplitudes,” *Comput. Phys. Commun.* **64** (1991) 345–359.
- [202] V. Shtabovenko, R. Mertig, and F. Orellana, “New Developments in FeynCalc 9.0,” *Comput. Phys. Commun.* **207** (2016) 432–444, [arXiv:1601.01167 \[hep-ph\]](#).
- [203] K. G. Chetyrkin, M. Misiak, and M. Munz, “Beta functions and anomalous dimensions up to three loops,” *Nucl. Phys. B* **518** (1998) 473–494.

-
- [204] A. Vladimirov, “Method of calculating renormalization-group functions in the scheme of dimensional regularization,” *Teor. Mat. Fiz.* **43** no. 210, (1980) 417–422.
- [205] J. Brod and Z. Polonsky, “Two-loop Beta Function for Complex Scalar Electroweak Multiplets,”.
- [206] D. J. Broadhurst, “The Master Two Loop Diagram With Masses,” *Z. Phys. C* **47** (1990) 115–124.
- [207] A. I. Davydychev and J. Tausk, “Two loop selfenergy diagrams with different masses and the momentum expansion,” *Nucl. Phys. B* **397** (1993) 123–142.
- [208] R. Scharf and J. Tausk, “Scalar two loop integrals for gauge boson selfenergy diagrams with a massless fermion loop,” *Nucl. Phys. B* **412** (1994) 523–552.
- [209] W. Zimmermann, “Convergence of Bogolyubov’s method of renormalization in momentum space,” *Commun. Math. Phys.* **15** (1969) 208–234.
- [210] T. N. Dao, M. Gabelmann, M. Mühlleitner, and H. Rzehak, “Two-Loop $\mathcal{O}((\alpha_t + \alpha_\lambda + \alpha_\kappa)^2)$ Corrections to the Higgs Boson Masses in the CP-Violating NMSSM,” *J. High Energ. Phys.* (6, 2021) 54, [arXiv:2106.06990](https://arxiv.org/abs/2106.06990) [hep-ph].
- [211] M. Masip, R. Munoz-Tapia, and A. Pomarol, “Limits on the mass of the lightest Higgs in supersymmetric models,” *Phys. Rev. D* **57** (1998) R5340, [arXiv:hep-ph/9801437](https://arxiv.org/abs/hep-ph/9801437).
- [212] J. Ellis, “TikZ-Feynman: Feynman diagrams with TikZ,” *Comput. Phys. Commun.* **210** (2017) 103–123, [arXiv:1601.05437](https://arxiv.org/abs/1601.05437) [hep-ph].

Acknowledgements

I would like to express my deep gratitude to Prof. Dr. Margarete Mühlleitner, my research supervisor, for her patient guidance, enthusiastic encouragement and useful critiques of this research work. It has been a great pleasure to participate in her research group for the last four years, including my Master's thesis. I also thank Prof. Dr. Dieter Zepfenfeld for agreeing to be the second supervisor of this thesis.

I would also like to extend my thanks to the NMSSMCALC collaboration, Dr. Thi Nhung Dao, Dr. Margarete Mühlleitner, Dr. Heidi Rzehak for the fruitful discussions about the various obstacles that we encountered during the calculations. I also want to thank Dr. Marcel Krause for various discussions and cross-checks regarding the $\mathcal{O}(\alpha_t^2)$ corrections.

I also want to thank all former colleagues, Philipp Basler and Jonas Müller, with whom I had the pleasure to share an office during my PhD. I will never stop bothering you about the coolness of VIM! Congratulations to the new landlady Lisa Biermann as well as to Thanh Tien Dat Nguyen who will faithfully reign the realm of 12-17.

I wish to thank various people for proof-reading this thesis; Lisa Biermann, Felix Egle, Dr. Jonas Müller, Dr. Heidi Rzehak and Dr. Sophie Williamson. Your feedback, corrections, questions and discussions were always welcome.

I would like to thank all members of ITP and TTP for the nice time at the institute and for the countless discussions about the SM, BSM and beyond. I also want to thank the KSETA and GK organizers for the numerous events, workshops, excursions and seminars which supported the nice team atmosphere amongst all HEP theorists and experimentalists at KIT. Special thanks go to the ITP secretary Ms. Weiß which supported me with all the paper-work. Furthermore, I would like to thank all my IT admin colleagues, Konstantin Asteriadis, Mustafa Tabet and David Wellmann, for the nice collaboration.

Finally, I wish to thank my family; My parents, Wolfgang & Anke Gabelmann and parents-in-law Birgit Bischoff & Hubert Weiler for their financial support and encouragement throughout my study. I would like to express my deep gratitude to my wife Natascha Gabelmann and my Son Linus Gabelmann for your love, understanding and support in multiple ways which provided me with the power and strength to not only survive but also succeed the journey of a PhD study.